The role of the TLC1 RNA flexible scaffold in yeast telomerase function

By
Kevin J. Lebo

A dissertation submitted to Johns Hopkins University in conformity with the requirements for the degree of Doctor of Philosophy

Baltimore, Maryland
June 2014

ABSTRACT:

In eukaryotic cells, the ends of the chromosomes are capped by structures known as telomeres, comprised of repeated DNA segments bound by proteins. Many organisms employ a ribonucleoprotein (RNP) complex, telomerase, to counteract the telomere DNA shortening that occurs during each cell cycle. Telomerase is minimally composed of a telomerase reverse transcriptase (TERT) and a telomerase RNA component, although other accessory protein subunits are required for telomere maintenance *in vivo*. In the budding yeast *Saccharomyces cerevisiae*, the telomerase RNA is the 1157-nt TLC1. TLC1 forms a Y-shaped overall secondary structure, with three long arms radiating out from a central catalytic core. Yeast TERT (Est2) localizes to the central core, while accessory proteins, including Est1, Ku, and Sm_7, each bind to the tip of a different RNA arm. TLC1 organizes the telomerase RNP by serving as a flexible scaffold, in which accessory protein binding sites can be relocated on the RNA with retention of function.

My research has focused on understanding how the TLC1 flexible scaffold regulates telomerase function. By designing a version of TLC1 with stiffened RNA arms, I have demonstrated that physical flexibility in the RNA is not required for telomerase function. This suggests that rather than allowing the proteins to “flex to position,” TLC1 organizes the RNP as “beads on a string,” without specific orientations required for accessory protein function. Furthermore, I identified a Second Essential Est1-arm Domain (SEED) in the Est1-binding arm of TLC1, which has an essential function independent of Est1 protein. This indicates that portions of the flexible scaffold RNA have roles beyond passive scaffolding. Next, while designing a version of TLC1 that would fold competently for function both *in vivo* and *in vitro*, I uncovered a previously unknown role for the Ku-binding arm RNA in RNA structure and abundance. Finally, I

identified a region of the terminal arm of TLC1 that helps to regulate telomerase RNA levels in the cell. Overall, my research has advanced the flexible scaffold model for telomerase RNA, and suggests that the flexible scaffold RNP may best be viewed as a series of functional modules, which includes both proteins and RNA domains, all tethered together by intervening segments of RNA in non-specific positions within the RNP holoenzyme.

Thesis Advisor: Dr. David Zappulla

Thesis Committee: Dr. Sarah Woodson

Dr. Jeffry Corden

Dr. Karen Beemon

ACKNOWLEDGEMENTS:

I would first like to thank my Ph.D. thesis advisor, Dr. David Zappulla, for all of his guidance throughout my time in his lab. He was always available for advice and support, while still encouraging my independence in my research. David's enthusiasm was always great for my morale; even if an experiment appeared to fail, he was always able to get me excited about the results. I learned so much by working with David.

I would also like to thank my thesis committee members — Dr. Sarah Woodson, Dr. Jeffry Corden, and Dr. Karen Beemon — for taking time from their busy schedules to read my thesis and provide me with helpful guidance for my projects and future career.

Next, I want to acknowledge the other members of the Zappulla lab: Melissa, Rachel, Karen, Evan, and Caitlyn. Between general scientific discussions, brainstorming sessions for projects, advice for protocols, or just venting our frustrations, they made the day-to-day life of a graduate student bearable.

I want to thank the entire CMDB program for providing a helpful and nurturing environment in which to perform my Ph.D. studies.

I'd also like to thank my many friends from Johns Hopkins, especially my classmates Vuong, Lin, Kylie, and Stephanie. They made the entire graduate school experience fun, and their support was important to my success.

Next, I want to thank my family for their support. In particular, I want to thank my Mom for always encouraging me to ask questions, hunt for answers, and to think for myself. Their love and guidance has been essential for me to become the person I am today.

Finally, I want to thank my wife Diane for everything she has done to help me to get to this point. From the time we were high school sweethearts she has encouraged my scientific endeavors, always supporting me along the way. Her advice has been

essential to all of my important career decisions, from picking a graduate program to finding a postdoctoral position. Despite all of the stresses of my Ph.D. thesis research she has remained patient and supportive. For over thirteen years, she has been the most important factor in every facet of my life.

Thank you to everyone who has helped me get to where I am today.

TABLE OF CONTENTS:

LIST OF FIGURES:

Chapter 1:

Introduction: Telomeres, telomerase, and flexible scaffold RNA

Telomeres solve the "end-protection problem" for eukaryotic chromosomes

The ends of linear eukaryotic chromosomes introduce challenges in maintaining genomic integrity in the cell. First, the natural ends of the chromosome are structurally similar to double-stranded DNA breaks; this may cause the ends to be mistakenly "repaired" by non-homologous end joining machinery (Putnam et al., 2009). These end-to-end chromosome fusions create dicentric chromosomes, which will potentially be torn apart during mitosis, introducing new double-stranded DNA breaks. During the next cell cycle, the broken chromosomes can fuse again, creating a breakage-fusion bridge cycle and causing massive genomic instability (McClintock, 1942). This similarity between natural ends and breaks in the DNA is known as the "end-protection problem" (Olovnikov, 1973).

Eukaryotic cells solve the end-protection problem by capping the linear chromosomes with telomeres. Telomeres are repeated tracts of particular DNA sequences, consisting of both double-stranded DNA and a single-stranded 3′ overhang, which create a recognizable natural end to chromosomes. Several different proteins bind specifically to telomeric DNA, preventing the recruitment of DNA repair factors and protecting the DNA from exonucleases (Cervantes and Lundblad, 2002; Grandin and Charbonneau, 2008). The sequence of the telomeric DNA and the specific proteins that bind to the telomere vary between species.

Telomerase solves the chromosome "end-replication problem"

In addition, the canonical DNA replication machinery is unable to fully synthesize the lagging strand at the end of the linear chromosome. Due to this "end replication problem," chromosomes will continue to shorten over successive cell divisions; if left unchecked, this shortening will result in loss of coding regions of the DNA (Levy et al., 1992). While telomeres provide a buffer zone, ensuring that the DNA lost during

synthesis does not code for proteins, they do not fully solve the end replication problem; when the telomeres become critically short, they are recognized by the cell as double-strand breaks, triggering a Rad9-dependent G2/M arrest known as senescence (Abdallah et al., 2009; Lundblad and Szostak, 1989; Weinert and Hartwell, 1988). Senescent cells are metabolically alive, but are unable to undergo cell division.

Most eukaryotic cells use a ribonucleoprotein (RNP) complex known as telomerase to maintain telomere length (Greider and Blackburn, 1985). Telomerase counteracts the end-replication problem by lengthening the shortest telomeres during late S-phase (Bianchi and Shore, 2007; Diede and Gottschling, 1999). The telomerase RNP uses an RNA template to direct extension of the telomeric DNA sequence by reverse transcription, adding iterative repeats of a short nucleotide sequence to the single-stranded DNA overhang (Greider and Blackburn, 1987, 1989; Lingner et al., 1997b; Shippen-Lentz and Blackburn, 1990). Afterwards, canonical DNA replication machinery fills in the second strand of the telomere, leaving only a short overhang (Adams Martin et al., 2000; Chandra et al., 2001; Fan and Price, 1997; Qi and Zakian, 2000). Because not every telomere is lengthened during each cell cycle, telomere length is dynamic and varies even within the same cell.

Telomerase and telomeres are critical for cell proliferation and organism health. Short telomeres have been associated with human aging and other human diseases (Armanios et al., 2005; Garcia et al., 2007; Gomez et al., 2012). In addition, telomerase is upregulated in over 90% of human cancers (Kim et al., 1994; Shay and Bacchetti, 1997). Understanding the molecular mechanisms by which telomerase functions and in regulated will provide important insights to human health.

Telomerase is minimally composed of a telomerase reverse transcriptase (TERT) protein and a telomerase RNA subunit (Greider and Blackburn, 1987). TERT is the enzymatic protein component responsible for reverse transcribing new telomeric DNA

(Lingner et al., 1997b). It is well conserved across eukaryotes, and is one of the earliest eukaryotic reverse transcriptases (Nakamura and Cech, 1998). Telomerase RNA, on the other hand, is poorly conserved across species, making it difficult to identify by sequence alignments. Even the size of the RNA varies greatly, from as small as ~150 nucleotides (nt) in ciliates to ~450 nt in humans to over 2000 nts in some yeast. While the global structure of the RNA is not well conserved, there are conserved structural elements within the catalytic core of the RNA; these include a template for reverse transcription, a template-boundary element, a pseudoknot, and a core-enclosing helix (Lin et al., 2004). This conserved core is important for telomerase enzyme function, providing both the template for reverse transcription, and also a series of base triples that contribute to catalytic function (Qiao and Cech, 2008; Shippen-Lentz and Blackburn, 1990). Many telomerase RNAs also contain a second domain required for TERT function, including the CR4/5 domain in humans, the three-way junction in *S. pombe* and other yeasts, and the stem-terminus element in ciliates (Brown et al., 2007; Mitchell and Collins, 2000; Qi et al., 2013; Tesmer et al., 1999). In addition, the telomerase RNA acts as a scaffold for accessory protein subunits, aiding in assembly of the RNP holoenzyme (Zappulla and Cech, 2004). These accessory subunits vary amongst species, but are important or essential for telomerase function *in vivo*.

Although they share conserved structural elements in the catalytic core, telomerase RNAs vary widely in sequence, structure, and function. In the ciliate *Tetrahymena thermophila*, the telomerase RNA, TER, is 159 nt long (Greider and Blackburn, 1989). The bulk of the RNA is involved in forming structural elements within the catalytic core, including a small pseudoknot, a template boundary element helix, and a core-enclosing helix (Autexier and Greider, 1998; Lai et al., 2002; Lin et al., 2004; McCormick-Graham and Romero, 1995; ten Dam et al., 1991). The ciliate RNA also has a template recognition element that helps TERT locate the template nucleotides (Miller

and Collins, 2002). This template recognition element may also play a role in repeat addition processivity, allowing the template to move back and forth through the TERT active site during telomere elongation (Berman et al., 2011). While TER has relatively few nucleotides outside of the core, it does have a stem-terminus element in loop IV that is required for TERT function (Mason et al., 2003). TER appears to require interactions with telomerase proteins in order to fold into a functionally competent structure (Jiang et al., 2013; Stone et al., 2007). Finally, the *Tetrahymena* telomerase has been shown to be functional as a monomer (Bryan et al., 2003).

The human telomerase RNA, hTR, is larger than the ciliate TER, with 451 nucleotides (Feng et al., 1995). In the catalytic core, hTR has a large pseudoknot with a hinge-like bulge in the middle that is important for the three-dimensional structure of the core (Bachand and Autexier, 2001; Chen et al., 2000; Zhang et al., 2010). It has additional nucleotides outside of the core region, including an essential CR4/5 domain (Bley et al., 2011; Chen et al., 2002; Kim et al., 2010; Mitchell and Collins, 2000). The core and the CR4/5 domain are sufficient for TERT activity *in vitro*, even if expressed as separate RNA components. Human telomerase requires dimerization for function, with both RNP monomers contributing to catalysis (Beattie et al., 2001; Sauerwald et al., 2013; Wenz et al., 2001).

The *Saccharomyces cerevisiae* telomerase ribonucleoprotein complex

The budding yeast *S. cerevisiae* provides a useful model for studying telomerase structure and function, due to the wide array of genetic and biochemical techniques available. The 32 yeast telomeres range from 150−400 bp long, and are comprised of degenerate $G_{2\text{-}3}(TG)_{1\text{-}6}$ repeats (Liti et al., 2009; Szostak and Blackburn, 1982; Wang and Zakian, 1990). Yeast telomeres are bound by a series of proteins. The double-stranded region of the yeast telomere binds to Rap1, which can recruit either Rif1 and

Rif2 or the silencing proteins Sir2, Sir3, and Sir4 (Bourns et al., 1998; Luo et al., 2002; Shi et al., 2013). The Ku-heterodimer, which is normally involved in non-homologous end joining to repair damaged DNA, is thought to bind to the junction between the double- and single-stranded telomeric DNA. The single-stranded region of the telomere is bound by Cdc13, which in turn can bind to Stn1 and Ten1 (Grandin et al., 2001).

The *S. cerevisiae* telomerase RNA is TLC1 (Telomerase Component 1) (Singer and Gottschling, 1994). TLC1 is much larger than the ciliate or human telomerase RNAs; it is initially transcribed by RNA polymerase II as a 1251-nt capped and polyadenylated RNA, before being processed into the mature 1157-nt form (Chapon et al., 1997; Noel et al., 2012). The RNA is poorly conserved even amongst closely related species, with only 43% of nucleotides identical between *S. cerevisiae*, *S. paradoxus*, *S. mikatae*, and *S. bayanus* (compared to over 80% identity for other essential non-coding RNAs; Zappulla and Cech, 2004). In addition, TLC1 expression is very low *in vivo*, with only 29 ± 7 copies of the RNA per haploid cell (Mozdy and Cech, 2006). This is essentially the same as the total number of telomeres in the cell, 32.

TLC1 RNA forms a Y-shaped secondary structure, with three long arms radiating out from the central catalytic core (Figure 1.1; Dandjinou et al., 2004; Zappulla and Cech, 2004). Conservation in the RNA is highest at the core and at the tips of the arms, and lowest in the intervening areas between. The central core contains the 17-nt template, which maintains a degenerate telomere sequence (Forstemann et al., 2000; Singer and Gottschling, 1994). The template boundary element for TLC1 is a helix that forms the base of one of the three long RNA arms, while the core-enclosing helix is the base of another arm (Lin et al., 2004; Seto et al., 2003). The core region also contains the pseudoknot, which has a series of catalytically important base triples (Qiao and Cech, 2008). The pseudoknot, core-enclosing helix, template-boundary element, and template are all functionally coordinated as an area of required

Figure 1.1: The yeast telomerase ribonucleoprotein complex. The TLC1 RNA adopts an overall Y-shaped secondary structure, with three long arms radiating out from the central catalytic core (Dandjinou et al., 2004; Zappulla and Cech, 2004). Yeast TERT, Est2, uses the template region of the RNA core to lengthen the telomeric DNA (Lendvay et al., 1996; Lingner et al., 1997b). Est1 binds to TLC1 at the end of one RNA arm, and is essential for recruitment of telomerase to the telomere through interactions with the DNA-binding protein Cdc13 (Evans and Lundblad, 1999; Seto et al., 2003). The Ku heterodimer and the Sm_7 complex also bind to TLC1 RNA (Peterson et al., 2001; Seto et al., 1999). The Est3 protein does not bind to TLC1, but rather interacts with Est2 (Friedman et al., 2003; Hughes et al., 2000).

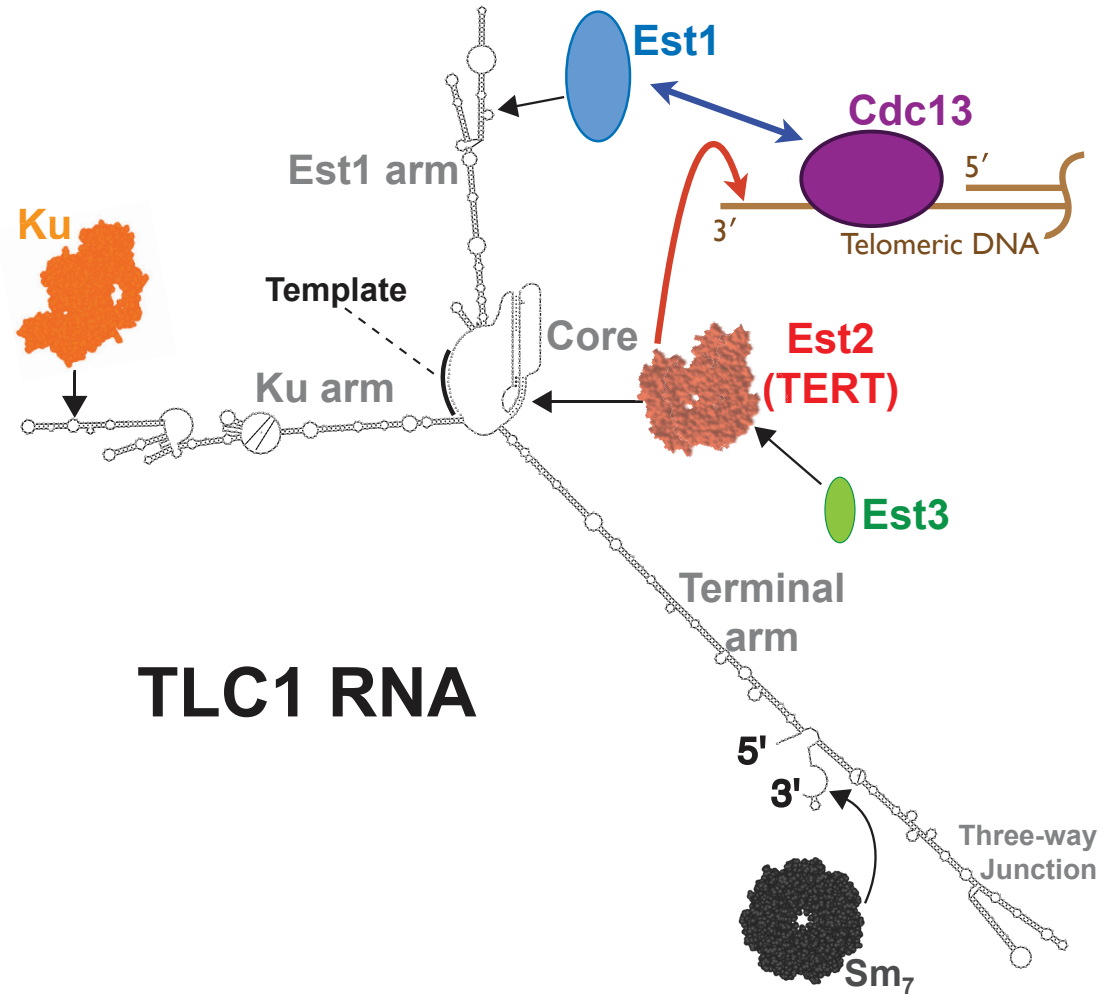

connectivity (Mefford et al., 2013). Although TLC1 has a conserved three-way junction domain near its 3′ end, this region is not essential for function *in vivo* or *in vitro* based on published reports and my own unpublished results, unlike the human CR4/5 or ciliate stem-terminus element domains (Dandjinou et al., 2004; Livengood et al., 2002; Zappulla and Cech, 2004; Zappulla et al., 2005). When expressed *in vitro*, full-length TLC1 RNA is unable to reconstitute robust telomerase activity, likely due to misfolding of the long RNA (Lebo and Zappulla, 2012; Zappulla et al., 2005).

The yeast telomerase TERT catalytic protein subunit is called Est2 (Ever shorter telomeres 2). Est2 binds to the central core of TLC1, and reverse transcribes the RNA template to lengthen the telomeric DNA (Figure 1.1; Lendvay et al., 1996; Lingner et al., 1997b). Together, Est2 and the core of TLC1 are sufficient for telomerase function *in vitro* (Lingner et al., 1997a; Qiao and Cech, 2008; Zappulla et al., 2005). This indicates that a conserved three-way junction element in TLC1, which appears to be homologous to the essential three-way junction in other yeasts and the CR4/5 domain in humans, is not essential for *S. cerevisiae* telomerase activity *in vitro* (Brown et al., 2007; Mitchell and Collins, 2000; Qi et al., 2013; Tesmer et al., 1999). It is important to note that full-length TLC1 is essentially nonfunctional when transcribed *in vitro*, likely due to misfolding of the large RNA (Lebo and Zappulla, 2012; Zappulla et al., 2005).

In vivo, several additional important or essential accessory protein subunits are required for telomerase function. The first of these is the essential Est1 protein. *EST1* was the first yeast telomerase gene identified, and encodes an 82-kDa protein (Lundblad and Szostak, 1989). Est1 binds to the end of one of the TLC1 RNA arms (Figure 1.1); although the precise binding sites are not known, three structural elements are required for Est1-association: a 5-nt bulge, a hinge-like structure, and an internal loop (Lubin et al., 2012; Seto et al., 2002). The primary role for Est1 in telomerase function is recruitment to the telomere through interactions with the telomeric DNA-binding protein

Cdc13 (Evans and Lundblad, 1999). Several mutants of Cdc13 have an ever-shorter telomeres phenotype, and *CDC13* was identified by a senescence screen as *EST4* (Lendvay et al., 1996). Cdc13 binds to single-stranded telomere DNA with high affinity, and has roles in both capping the end of the DNA and in promoting lengthening (Nugent et al., 1996; Zappulla et al., 2009). Through the Est1-Cdc13 interaction, the telomerase holoenzyme is recruited to the telomere. In addition, Est1 has a poorly understood secondary role in "activating" telomerase function (Evans and Lundblad, 2002; Taggart et al., 2002).

The next TLC1-binding accessory protein subunit is the Ku heterodimer, comprised of yKu70 and yKu80, which binds to a 25-nt hairpin at the end of one of the RNA arms of TLC1 (Figure 1.1; Dalby et al., 2013; Peterson et al., 2001). Since Ku is involved in non-homologous end joining — something that should not occur at telomere-capped ends — it is somewhat surprising that Ku binds telomeres. Ku has been shown to interact with telomerase in some other species in addition to *S. cerevisiae*, including humans (Chai et al., 2002; Ting et al., 2005). At the telomere, Ku protects the end from resection by exonucleases, and promotes replication of the second strand after telomerase action (Bertuch and Lundblad, 2003). The exact role for Ku in telomerase function is not known, but it does promote both the lengthening of telomeres natural ends and the *de novo* addition of telomeres at broken ends in budding yeast (Stellwagen et al., 2003). This function requires Ku to bind to TLC1 RNA; loss of Ku-binding to TLC1 results in stably shorter telomeres, without causing senescence, and a reduction in TLC1 RNA abundance (Stellwagen et al., 2003; Zappulla et al., 2011). This indicates that Ku has an important, but non-essential, role in yeast telomerase function. It is thought that Ku acts in a secondary telomerase recruitment pathway (Bertuch and Lundblad, 2003; Fisher et al., 2004; Peterson et al., 2001); however, Ku binding to TLC1 RNA and directly to telomeric DNA is mutually exclusive, suggesting there is an unknown

intermediary protein factor facilitating this Ku-mediated telomerase recruitment (Pfingsten et al., 2012).

The final protein subunit known to bind to TLC1 RNA is the Sm_7 heteroheptameric ring (Figure 1.1). Sm_7 binds near the 3′ end of TLC1, located in the terminal arm of the RNA secondary structure (Seto et al., 1999). Sm_7 is involved in processing the precursor TLC1 transcript, terminated by either non-coding RNA termination factors or a polyadenylation sequence, into the mature TLC1 RNA (Chapon et al., 1997; Noel et al., 2012). By binding to a site at the mature 3′ end of TLC1, Sm_7 blocks the exonuclease that trims the RNA and helps define its final length (Coy et al., 2013). Loss of Sm_7 binding to TLC1 results in very low telomerase RNA abundance, with the precursor form making up most of the remaining population of TLC1 molecules (Seto et al., 1999).

In addition to the RNA-binding subunits, the 21-kDa protein Est3 is also part of the yeast telomerase holoenzyme complex (Hughes et al., 2000). However, Est3 does not appear to bind directly to TLC1. Instead, it is known to bind to Est2, and may have some interactions with Est1 (Figure 1.1; Friedman et al., 2003; Hughes et al., 2000; Lee et al., 2008; Osterhage et al., 2006; Tuzon et al., 2011). Est3 appears to be a structural analog of the human protein TPP1 (Lee et al., 2008; Rao et al., 2014). Although Est3 is essential for telomere maintenance, its role is still not known (Lee et al., 2010; Lendvay et al., 1996).

Unlike ciliate and human telomerase, *S. cerevisiae* telomerase is incapable of significant repeat addition processivity *in vitro*, whether the RNP is reconstituted in transcription-translation systems *in vitro* or immunopurified from cells (Cohn and Blackburn, 1995; Zappulla et al., 2005). Yeast telomerase appears to have low repeat-addition processivity *in vivo* as well, although this has been reported to be increased at short-telomere substrates (Chang et al., 2007; Prescott and Blackburn, 1997). The yeast

telomerase RNP has been shown to function as a monomer *in vitro*, similar to ciliate telomerase, although it is not clear whether it acts as a monomer or a dimer *in vivo* (Shcherbakova et al., 2009).

Yeast telomerase RNA organizes the RNP complex as a flexible scaffold

The yeast telomerase RNA is responsible for tethering the four known TLC1-binding proteins or protein complexes, Est2, Est1, Ku, and Sm_7. These proteins do not appear to bind directly to each other, and they bind to distinct locations on TLC1. Est2 interacts with the central core of the RNA, while the three accessory protein subunits each bind to a different arm in the TLC1 secondary structure, distal from the core (Dandjinou et al., 2004; Livengood et al., 2002; Lubin et al., 2012; Peterson et al., 2001; Seto et al., 1999; Zappulla and Cech, 2004).

Interestingly, TLC1 is very poorly conserved, even amongst closely related species. Other essential non-coding RNAs in budding yeast are much more highly conserved, particularly the ribosomal RNAs. Between four *Saccharomyces* species, the 1800-nt 18S rRNA is 99% conserved, which helps to maintain the highly structured three-dimensional shape required for ribosomal function (Ban et al., 2000; Moore and Steitz, 2002; Verschoor et al., 1998). In TLC1, however, only 43% of the nucleotides are conserved (Zappulla and Cech, 2004). With such high rates of evolution across the telomerase RNA, it is difficult to see how a rigid three-dimensional structure could be maintained between species.

Although TLC1 is generally poorly conserved, the protein binding site regions are better conserved than the intervening RNA arms. In fact, the rapidly evolving RNA within the arms between the apical protein binding sites and the core can be deleted to form a miniaturized TLC1 (Mini-T) that is functional *in vivo* (Zappulla et al., 2005). Furthermore, it has been shown that the Est1-, Ku-, and Sm_7- binding sites on the TLC1 RNA can be

relocated to different positions with retention of accessory-protein function (Mefford et al., 2013; Zappulla and Cech, 2004; Zappulla et al., 2011). These RNA arm truncations or protein-binding site relocations would likely disrupt function of highly structured RNP, and yet telomerase is still able to function. This suggests that the yeast telomerase RNP is not highly ordered. Instead, TLC1 acts as a functionally flexible scaffold for the holoenzyme, tethering protein components in close proximity regardless of specific binding locations (Zappulla and Cech, 2004, 2006).

The extent of "flexibility" in the TLC1 flexible scaffold is not known. The RNA has been shown to be functionally flexible, in that protein-binding modules on the RNA can be repositioned relative to each other (Mefford et al., 2013; Zappulla and Cech, 2004; Zappulla et al., 2011). In addition, it is possible that the RNA is physically flexible, and that the three long RNA arms can bend in three-dimensional space. However, physical flexibility of the RNA arms has not been experimentally proven. There may be other forms of flexibility in the scaffold as well; for example, it is possible that base-pair heterogeneity in the rapidly evolving arms allows for flexibility in secondary structure formation.

The flexibly scaffolded yeast telomerase may represent a new class of RNPs, lacking a highly ordered three-dimensional structure. A growing list of long non-coding RNAs (lncRNAs) have been hypothesized to act as flexible scaffolds, including XIST and HOTAIR (Guttman et al., 2011; Wang and Chang, 2011; Zappulla and Cech, 2006). Like TLC1, these lncRNAs are unlikely to be highly conserved across their entire lengths. Instead, they are most likely evolving rapidly, with patches of nucleotide conservation at protein-binding sites tethered together by the intervening RNA. These flexible-scaffold RNPs likely lack the highly ordered structure found in canonical RNPs such as the ribosome. As the best-studied flexible scaffold RNP, the yeast telomerase long

noncoding RNA provides an important archetype for understanding this new class of RNPs.

My research has focused on understanding how the TLC1 flexible scaffold regulates telomerase function. By removing physical flexibility from the arms of the RNA, I have demonstrated that the telomerase accessory proteins do not need to dock into required positions relative to each other for activity. This suggests that TLC1 organizes the RNP as “beads-on-a-string,” with no required functional orientations for the protein components. In addition, I was able to separate the Est1-protein-binding function of the Est1 arm of TLC1 from other essential roles and discovered a novel second essential domain in the RNA. The presence of this essential domain indicates that the accessory-protein-binding sites of TLC1 can have additional roles in telomere maintenance. This suggests that, rather than merely tethering protein components together, the RNA flexible scaffold may act as a set of individual RNP subunits tethered together by intervening RNA. I also designed a version of TLC1 that folds more stably than wild type with minimal mutations that is able to function both *in vivo* and *in vitro*, and revealed that the Ku-arm RNA may have a previously unknown role in TLC1 structure and function. Finally, I identified a novel RNA-abundance-regulating domain in the terminal arm of TLC1. Taken together, my findings further our understanding of how TLC1 organizes and functions with the rest of the telomerase holoenzyme and, more broadly, the nature of flexible scaffold RNPs.

Chapter 2:

Stiffened yeast telomerase RNA supports RNP function *in vitro* and *in vivo*

Partially adapted from:

Kevin J. Lebo and David C. Zappulla. (2012) Stiffened yeast telomerase RNA supports RNP function *in vitro* and *in vivo*. *RNA* 18, 1666−1678

2.1: ABSTRACT

It has been previously demonstrated that the 1157-nt TLC1 RNA acts as a functionally flexible scaffold, in which protein-binding sites on the RNA can be relocated with retention of function. However, it was not clear what functional role the flexible scaffold played in the telomerase mechanism. In order to differentiate between a “flex-to-position” model, in which physically flexible RNA arms allow proteins to dock into functional positions, and a “beads on a string” model, where the proteins are bound in non-specific orientations to an RNA tether, I designed a version of TLC1 with the three long arms stiffened. This 956-nt “Triple-Stiff Arm TLC1” (TSA-T) is able to reconstitute active telomerase with TERT *in vitro*. In addition, TSA-T is functional *in vivo*, maintaining longer telomeres than wild-type TLC1 on a per-RNA basis. I found that stiffening the Est1 and Ku arms promotes telomere lengthening, while stiffening the terminal arm causes reduced telomerase RNA abundance. This work advances our understanding of the architectural and functional organization of the yeast telomerase RNP and, more broadly, our conception of the world of RNP complexes scaffolded by long noncoding RNAs.

2.2: INTRODUCTION

The yeast telomerase accessory proteins Est1, Ku, and Sm_7 bind to at the ends of each of the different arms of the 1157-nt telomerase RNA, TLC1. These proteins do not appear to bind to any other portion of the RNA, nor to each other or Est2 (TERT). Only 33% of the nucleotides in TLC1 are conserved in 36 sequences from seven *Saccharomyces* species (Mefford et al., 2013); conservation is highest near the proposed protein binding sites in the core and at the periphery of the Y-shaped secondary structure, and lowest in the intervening regions (Dandjinou et al., 2004; Mefford et al., 2013; Zappulla and Cech, 2004). The bulk of the nucleotides in the rapidly evolving arms can be deleted to form a miniature telomerase RNA (Mini-T) that is capable of maintaining telomeres *in vivo* (Zappulla et al., 2005). In addition, the binding sites for the Est1, Ku, and Sm_7 accessory proteins can be relocated to different locations on the RNA while retaining telomerase function (Mefford et al., 2013; Zappulla and Cech, 2004; Zappulla et al., 2011).

The permissiveness of TLC1 to relocation of protein-binding sites and significant truncation of the arms supports the flexible scaffold model of yeast telomerase RNA (Zappulla and Cech, 2004, 2006). TLC1 has been shown to act as a functionally flexible scaffold, in which protein-tethering sites can be relocated on the primary and secondary structure of the RNA scaffold without elimination of activity. This flexible scaffold model contrasts starkly with RNA structure and function in other well-studied RNPs such as the ribosome, where essentially the entire RNA complex, composed of ~5500 nt in *S. cerevisiae*, is highly structured (Ban et al., 2000; Moore and Steitz, 2002; Verschoor et al., 1998). In such highly ordered canonical RNPs, one would expect relocation of protein-binding sites to result in significant functional defects.

While previous research had shown that TLC1 acts as a flexible scaffold for the yeast telomerase RNP, the functional mechanisms by which the RNA organizes the holoenzyme were not clear. It was not known whether the flexible RNA played a role in coordinating the special orientations of the protein subunits. TLC1 may act as a simple scaffold, tethering the accessory proteins together as “beads on a string” with no precise special orientations required for function. Alternatively, the accessory proteins may need to ultimately occupy precise positions in the RNP for function. In this case, physical flexibility in the long arms of TLC1 could allow proteins to dock into their active sites in the holoenzyme, even if the protein-binding sites are relocated on the RNA.

Both the rapid sequence evolution and the many bulges and internal loops in the regions between protein-binding sites on TLC1 suggest that the long RNA arms may be physically flexible, although the importance of this flexibility for telomerase function had not previously been examined. 42% of nucleotides in the Ku arm, 32% in the Est1 arm, and 32% in the terminal arm are predicted to be unpaired; each of these unpaired nucleotides can potentially act as a hinge, allowing the structure to bend and conferring great flexibility to the RNA (Bhattacharyya and Lilley, 1989; Fulle and Gohlke, 2009; Zacharias and Hagerman, 1996). This contrasts with double-stranded RNA (dsRNA), which is quite rigid (Hagerman, 1997). A measure of this physical parameter is “persistence length,” the distance over which the axis of a polymer will tend to continue along a linear trajectory without significant bending. RNA double helices are even more rigid than those formed by DNA, in part due to the wider A-form helical geometry. While the persistence length for B-form dsDNA helix is ~50 nm, or 150 bp (Bustamante et al., 2000), A-form dsRNA has a persistence length of 63 nm, or 225 bp (Abels et al., 2005). It is important to note that nucleic acids shorter than their persistence length are not absolutely rigid and that bends can be induced through protein binding or long-distance interactions (Cloutier and Widom, 2004; Hagerman, 1988; Wiggins and Nelson, 2006;

Wiggins et al., 2006). However, helical RNA has reduced flexibility compared with bulged RNA, and helices greatly shorter than the persistence length tend to remain stiff (Mastroianni et al., 2009).

In this chapter, I describe TLC1 variants engineered with severely constrained physical flexibility in the three RNA arms. I converted the RNA between the central catalytic core and the binding sites for Ku, Est1, and Sm_7 into short, rod-like, uninterrupted helices. I show that this 956-nt "triple-stiff-arm TLC1" (TSA-T) folds stably *in vitro* and reconstitutes telomerase activity with Est2. Furthermore, TSA-T functions *in vivo*, maintaining telomere length 77% that of wild type, despite the RNA being only 15% as abundant. In fact, I demonstrate that the low RNA abundance of TSA-T is responsible for the shortened telomere phenotype, and that, on a per-RNA basis, TSA-T actually produces longer telomeres than wild-type telomerase. Introducing rigidity into the Ku and Est1 arms promotes telomere elongation, while the stiffened terminal arm causes telomere shortening. Finally, I demonstrate that even with a loss of physical flexibility, TSA-T still behaves as a "functionally flexible" scaffold, and retains function when the Est1 and Ku binding sites are relocated. Thus, the telomerase RNP enzyme functions despite all know essential and important RNA-binding accessory proteins being held away from the catalytic core by dsRNA "struts," providing physical evidence for a simple scaffold model for TLC1 RNA function.

2.3: RESULTS

Design of a yeast telomerase RNA with all three arms stiffened

Using the TLC1 secondary structure model (Dandjinou et al., 2004; Zappulla and Cech, 2004) and miniaturized telomerase RNA (Mini-T; Zappulla et al., 2005) as guides, I engineered a highly modified variant of TLC1 with the precise removal of all unpaired nucleotides in bulges and loops in the from the bulk of the RNA arms between protein-binding sites (Figure 2.1). In addition, 22 uracil (U) involved in G•U pairs in these regions were changed to cytosine (C), such that nearly all bases in the stiffened arms would be involved in canonical Watson-Crick base pairs. A few G•U pairs were left near proposed protein-binding sites, and one G•U pair in each arm was left proximal to the core to create a unique restriction site for future subcloning. I used *Mfold* RNA secondary structure prediction software (Zuker, 2003; Zuker and Jacobson, 1998) to help avoid misfolded structures and increase the chance that the RNA would fold as designed (Figure 2.2). The resulting 956-nt "triple-stiff-arm TLC1" (TSA-T) RNA is predicted to form 62 bp of uninterrupted double helix in the Ku arm, 31 bp in the Est1 arm, and 68 bp in the terminal arm. Because each of these paired regions is <30% the persistence length of helical RNA (Abels et al., 2005), the dsRNA regions of the arms should act as semi-rigid rods.

Mfold secondary structure modeling predicts that 72% of the 965 nts in TSA-T will be base paired, compared with 61% paired in the *Mfold* model for 1157-nt wild-type TLC1 and 58% in the 500-nt Mini-T (Figure 2.2). Accordingly, the predicted final secondary structure folding state of TSA-T is more energetically favorable than TLC1 or Mini-T: −458 kcal/mol, compared with −321 kcal/mol for TLC1 and −133 kcal/mol for Mini-T (Figure 2.3).

Figure 2.1: Secondary structure model for Triple-Stiff-Arm TLC1 (TSA-T). The secondary structures of the wild-type TLC1 arms based on the phylogenetic model (Dandjinou et al., 2004; Zappulla and Cech, 2004; Zappulla et al., 2011) are indicated (dashed boxes) next to the stiffened arms (gray cylinders). The length and width of the dsRNA cylinders convey proportions for A-form RNA double helices (Jang et al., 1998) and are drawn approximately to scale with the proteins (Zappulla and Cech, 2006) based on crystal structure models of homologs — *T. castaneum* TERT (Est2; Gillis et al., 2008), human Ku (Walker et al., 2001), and human Sm_7 (Leung et al., 2011). Unpaired nucleotides are indicated in red. G•U pairs are flanked by filled circles (•). The central core displayed is based on published models (Dandjinou et al., 2004; Lin et al., 2004; Qiao and Cech, 2008; Zappulla and Cech, 2004; Zappulla et al., 2011), while the heavily mutated arms are based on the lowest-energy *Mfold* prediction.

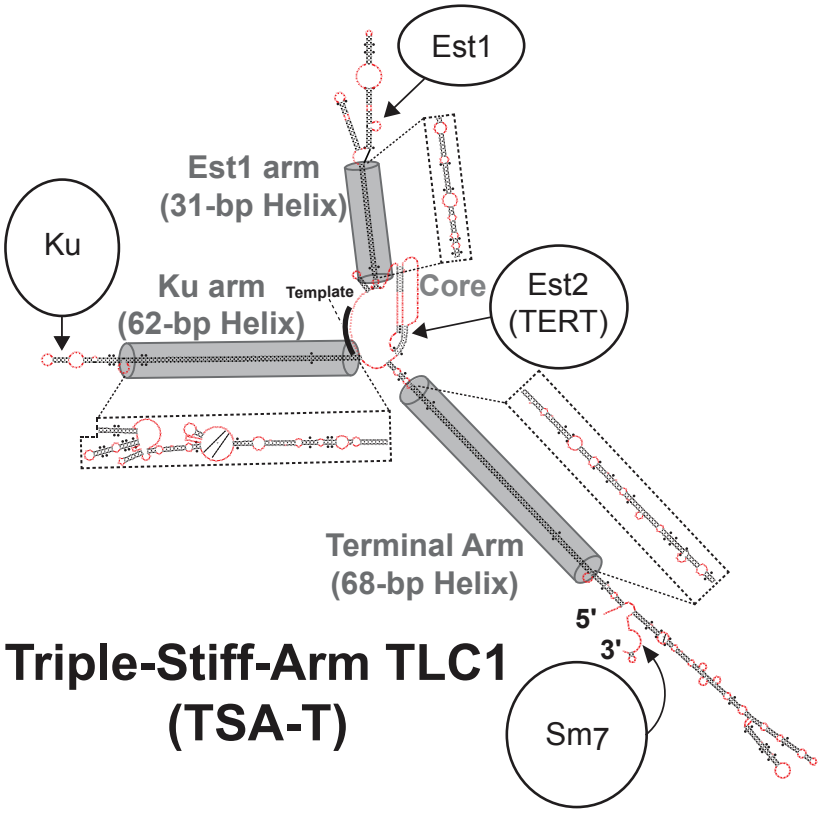

Figure 2.2: Lowest free energy *Mfold* secondary structure predictions for TLC1 and TSA-T. (**A**) *Mfold* prediction for TLC1 structure. The colors are from the *Mfold* "p-num" format, where red indicates areas of most energetically well-determined structure (Zuker and Jacobson, 1998). Note that *Mfold* cannot predict formation of the pseudoknot in the central catalytic core. No constraints based on phylogenetic information were place on the folds. (**B**) *Mfold* prediction for TSA-T structure. The completely paired helical regions of the TSA-T arms are very red, indicating a high likelihood of folding. Stiffened regions are indicated by colored brackets. (**C**) The RNA sequence for TSA-T, with mutated regions underlined to indicate areas stiffened.

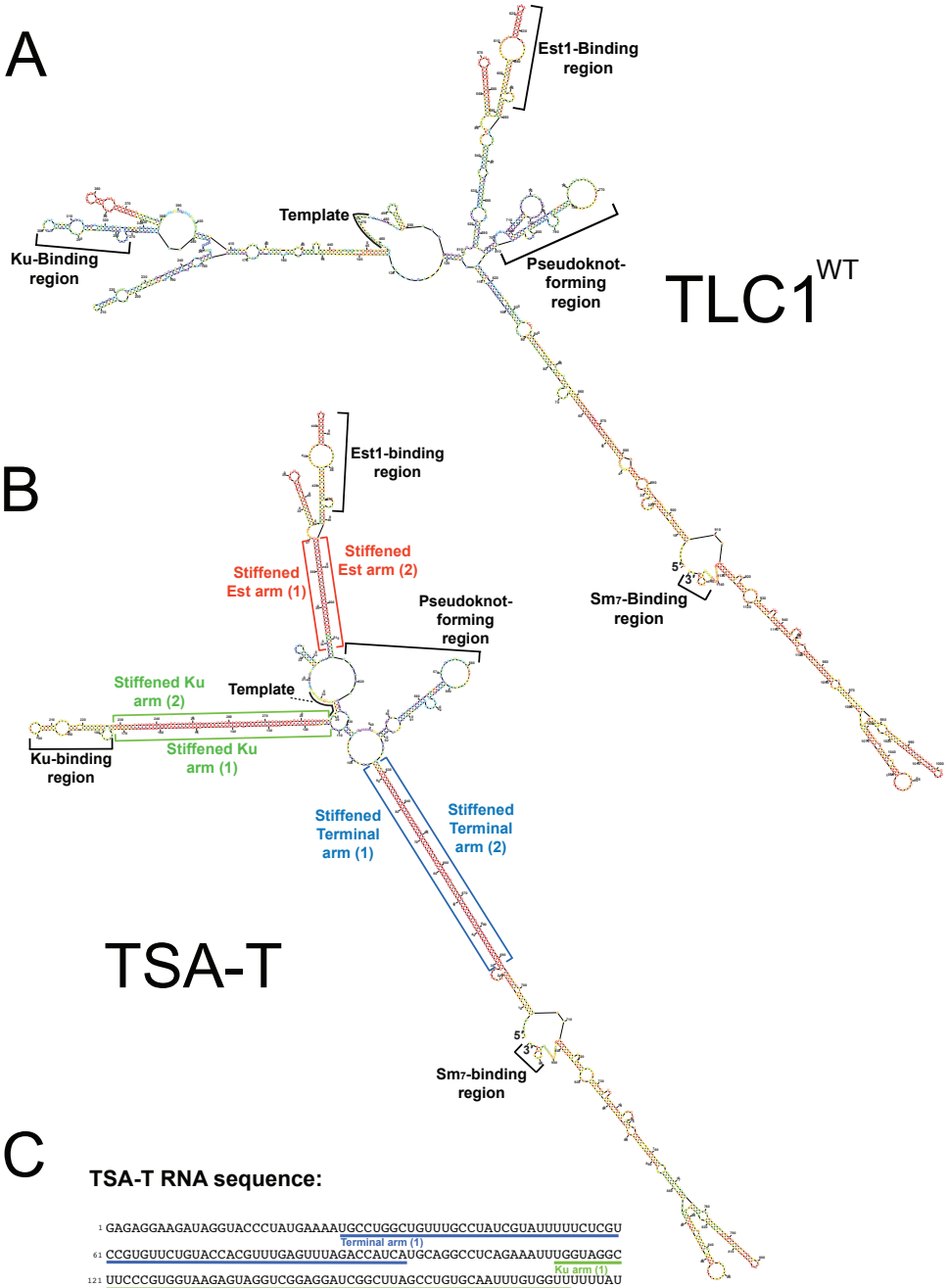

C

TSA-T RNA sequence:

```
1   GAGAGGAAGAUAGGUACCCUAUGAAAAUGCCUGGCUGUUUGCCUAUCGUAUUUUUCUCGU
                                                  Terminal arm (1)
61  CCGUGUUCUGUACCACGUUUGAGUUUAGACCAUCAUGCAGGCCUCAGAAAUUUGGUAGGC
                                                          Ku arm (1)
121 UUCCCGUGGUAAGAGUAGGUCGGAGGAUCGGCUUAGCCUGUGCAAUUUGUGGUUUUUUAU
181 UGUGUUUCUACUUAUAGAUGGCUAAAAUCUGAGUUUAGAAAAUGCAAACCGUAAAUUGCA
                                                          Ku arm (2)
241 CAGGCUAAGCCGAUCCUCCGACCUACUCUUACCAUGGGAAGCCUACCAUCACCACACCCA
301 CACACAAAUGUUACAGCUAAUUGUUUAUUAGCAAAGUUUGAUGCGUUCCUGUCUUUUUCC
                                                  Est1 arm (1)
361 UUUUCUUCCUAGUAUUUUUUCUGACACUGUUUAAGGUGACAGAAAAAAAGGAGUUUAAGU
421 UAGAUUUGCAAACAGACGGUGCUAAGCGCUGUCACUUUAUGUCUAUCUUAUCGUUAACUC
481 UGGAAGAAAAGGAAAAAGACAGGAACGCGUCAUAUAUAGAAAUGGUUUAUUCUAGUUUUU
                                          Est1 arm (2)
541 UCCGUUUUUUCAGUAGAUUUUUGCCUUUAAAAGAAUAAAUCCCACUACAAAAAGGUAAAA
601 UAAAAAAUCUAUUCACUGAACUUACUGAUGGUUUAAACUCAAACGUGGUACAGAACACGG
                                                  Terminal arm (2)
661 ACGAGAAAAAUACGAUAGGUAAACAGCCAGGCAAGGGUGUCCUUUCUUAAGCAUCGGUUA
721 GGUUUGCGGGCGAUCAGUAACUGAACAAUGACACAAGAUCAAGAACGUAAUUUGAGAUUU
781 UUCAAGAUGGUUUUUUUAGGUAUCUAUUAAAACUACUUUGAUGAUCAAUACGGUAUUUUU
861 GUCGCAUUAUUUUCCAAGCGGAAGGAACCGUGUGUUCAUUUUAUGAAUCUUGGUGUUGUA
921 UUCACAGCUACUUCUCCUAAUGCCUUCGAUGCAUUUAGAUAAUUUUUGGAAACAUU
```

Figure 2.3: "Circle structure" plots of TLC1, TSA-T, and Mini-T display the highly paired regions in the stiffened arms. Plots created using the *Mfold* webserver (Zuker, 2003). The RNA sequence is arranged in a circle, clockwise from 5′ to 3′. Colored curved lines within the circle connect predicted paired bases (red indicates G-C pairs, blue A-U pairs, and green G•U pairs). Arm regions are indicated by dashed arc lines outside the circle. Note that *Mfold* does not predict pseudoknots, resulting in a different model within the central core (see Figure 2.2). Unpaired nucleotides in the arms of TLC1 and Mini-T lead to "gaps" appearing between the pairing lines in the arms, whereas completely-paired helical arms of TSA-T lack these gaps and show thick swaths of uninterrupted adjacent lines. Regions stiffened in the Ku, Est1, and terminal arms are indicated by thick colored lines outside of the circle.

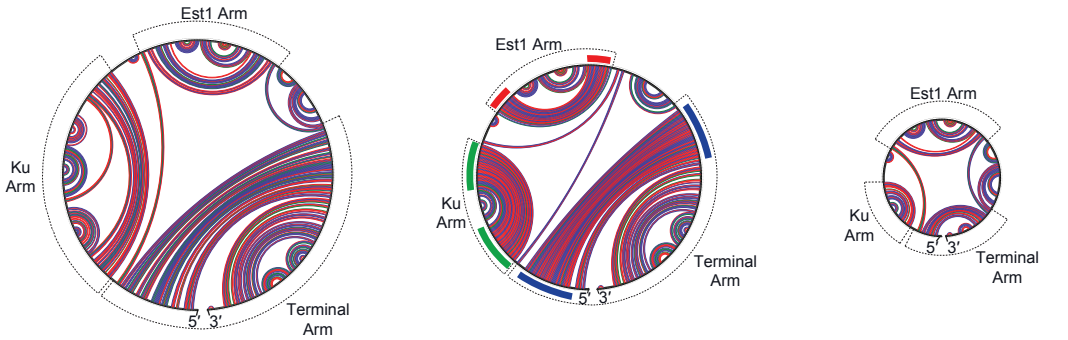

Triple-stiff-arm telomerase RNA folds stably and reconstitutes enzyme activity *in vitro*

TSA-T RNA is predicted to form an extremely stable secondary structure because of its almost entirely double-helical arms. To test if these energetically favored arms form *in vitro*, I synthesized TSA-T using T7 RNA polymerase in the presence of [α-^{32}P]GTP, digested it extensively with single-stranded RNA-digesting nucleases RNase A and RNase T1, and analyzed the protected products by denaturing polyacrylamide-urea gel electrophoresis (Figure 2.4A). Wild-type TLC1 and Mini-T RNAs were also analyzed in parallel by the same method. Unlike TLC1 and Mini-T, the bulk of TSA-T RNA molecules do not migrate into the polyacrylamide gel matrix (Figure 2.4A, lanes 5 and 6). The immobility of TSA-T suggests that the stiffened arms fold sufficiently stably that they are not denatured in the denaturing conditions, and semi-folded RNA (TSA-T*) has an overall topology that does not migrate well through polyacrylamide (e.g., the structure shown in Figure 2.1 with only the stiffened regions remaining paired, trapping the central core as a 178-nt internal loop).

Although treatment with RNases A and T1 essentially completely digests TLC1 and Mini-T (Figure 2.4A, lanes 4 and 10), it does not completely digest TSA-T; a collection of prominent RNase-resistant bands from TSA-T are reproducibly observed over the range of ~20−72 nt (lanes 7 and 8), based on denatured DNA ladders. The two slowest migrating bands are consistent with expected longest dsRNA sections of the terminal and Ku arms of TSA-T (68 and 62 bp, respectively; see the top two arrows in Figure 2.4A). Furthermore, one of the faster-migrating bands is consistent with the expected size for the 31-bp Est1 arm helix (see bottom arrow in Figure 2.4A). Low-intensity bands shorter than the largest protected fragment likely represent partial digestion products.

Figure 2.4: TSA-T telomerase RNA folds stably and functions *in vitro*. (**A**) TSA-T contains RNase-resistant structures *in vitro*. An RNase protection assay was performed on [α-^{32}P]GTP-labeled TSA-T (956 nt), TLC1 (1157 nt), and Mini-T (500 nt) by extensively digesting the T7-transcribed RNAs with RNase A and RNase T1. Digestion reaction products were resolved by polyacrylamide-urea gel electrophoresis. The bulk of full-length TSA-T is reproducibly trapped in the wells, presumably because the long helical regions are resistant to complete denaturation, resulting in a semi-folded RNA conformation (TSA-T*, indicated by * on the gel) that has greatly reduced mobility by PAGE. Arrows indicate bands that likely correspond to protected dsRNA arms of TSA-T. M = Heat-denatured, [γ-^{32}P]-labeled DNA markers; 10-bp marker in lane 1, 50-bp marker in lane 2. (**B**) TSA-T reconstitutes telomerase activity when coexpressed with ProA-Est2 (TERT) in rabbit reticulocyte lysates. Like Mini-T, TSA-T forms an active telomerase RNP, adding 7 nt (+1 through +7) to the telomeric DNA primer. Lanes 3 and 4 show independently generated TSA-Telomerase preparations and assays. IC = 1nM [γ-^{32}P]-labeled primer added before the telomerase reaction serves as an internal control for product recovery and loading onto the gel.

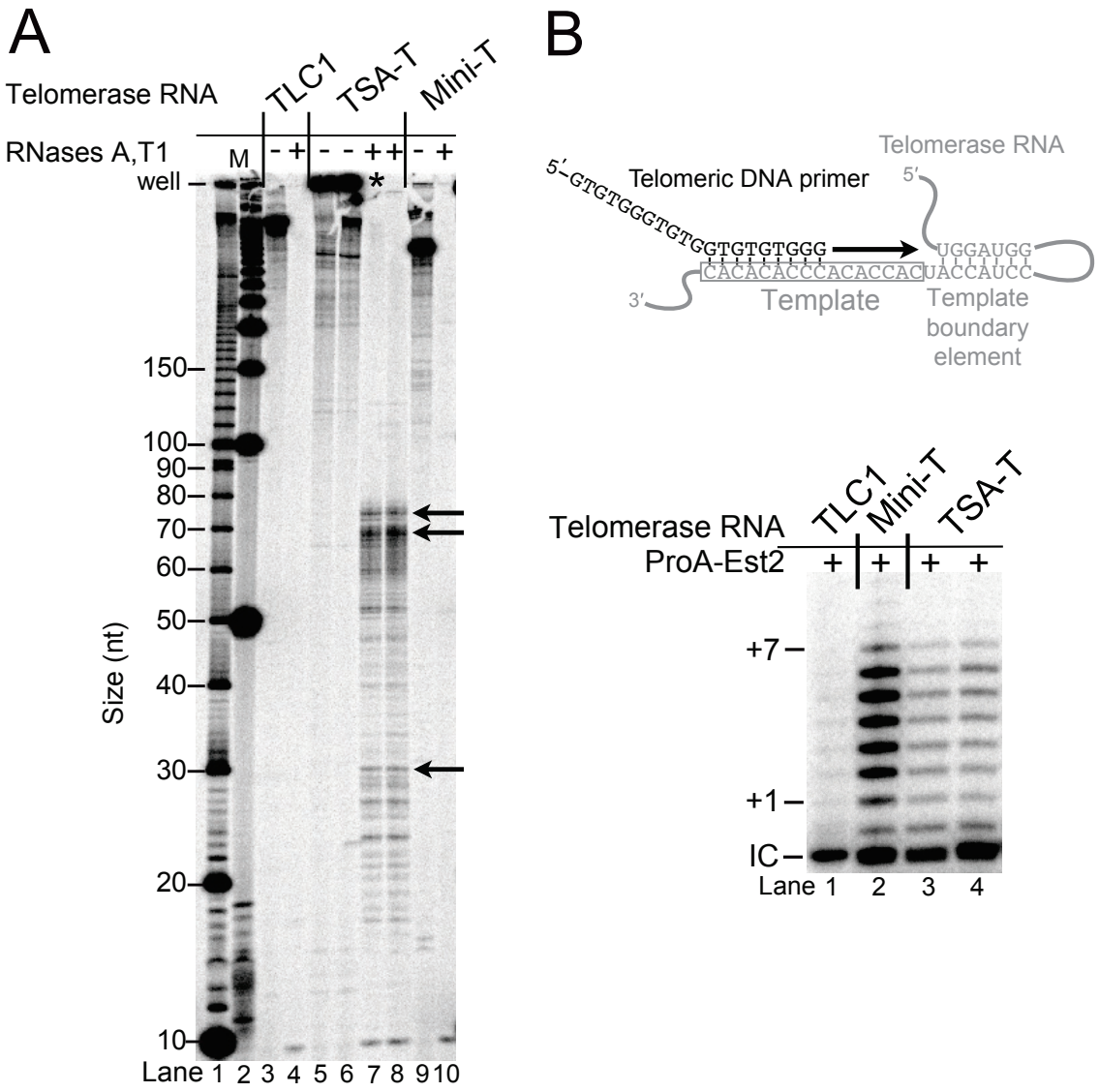
A
Telomerase RNA
TLC1
TSA-T
Mini-T
RNases A,T1
M
- + - - + + - +
well
150
100
90
80
70
60
50
40
30
20
10
Size (nt)
Lane 1 2 3 4 5 6 7 8 9 10
B
Telomerase RNA
5′
Telomeric DNA primer
5′-GTGTGGGTGTGGTGTGTGGG
UGGAUGG
CACACACCCACACCAC
UACCAUCC
3′
Template
Template boundary element
Telomerase RNA
TLC1
Mini-T
TSA-T
ProA-Est2
+ + + +
+7
+1
IC
Lane 1 2 3 4

To analyze TSA-T functionality *in vitro*, I tested if it can form an enzymatically active RNP complex with Est2 using the reconstituted yeast telomerase assay (Zappulla et al., 2005). For *in vitro* function, yeast telomerase RNA must have the ssRNA template (Prescott and Blackburn, 1997), template boundary element formed by long-range pairing (Seto et al., 2003; Tzfati et al., 2000), and the pseudoknot with its embedded base triples (Lin et al., 2004; Qiao and Cech, 2008; Tzfati et al., 2003). TSA-T RNA was coexpressed with a protein A (ProA)-tagged Est2 in a rabbit reticulocyte lysate transcription and translation system, immunopurified, and tested for activity on a telomeric DNA primer. TSA-Telomerase (TSA-T•ProA-Est2 complex) reproducibly lengthens the DNA primer with a pattern similar to Mini-Telomerase (Zappulla et al., 2005), albeit with several fold less activity (Figure 2.4B). The activity reconstituted by TSA-T in the assay is still much greater than that of wild-type TLC1, which, likely due to misfolding, is essentially nonfunctional when synthesized *in vitro* (Zappulla et al., 2005), although I often observe some very weak activity (Figure 2.4B, lane 1). Together, these data indicate that, in addition to the stiffened arms of TLC1 folding as predicted, the catalytic core of TSA-T folds properly *in vitro* to bind Est2 and coordinate with it to successfully reconstitute telomerase activity.

TSA-T RNA supports a highly functional RNP holoenzyme *in vivo*

TSA-T is able to interact with Est2 to form an active catalytic core in vitro. However, in vivo, several accessory protein subunits must interact with telomerase RNA, including the essential Est1 and the important Ku and Sm7 subunits (Peterson et al., 2001; Seto et al., 2002; Seto et al., 1999; Stellwagen et al., 2003). I next tested whether TSA-T could support the formation of a functional holoenzyme in the cell.

A centromere-containing plasmid harboring the *TSA-T* gene (with endogenous *TLC1* upstream and downstream sequences) was transformed into a *tlc1Δ rad52Δ*

pTLC1-LYS2 strain. The *rad52Δ* genetic background prevents initiation of alternative "survivor" pathways for telomere lengthening, providing a clear-cut method for assessing telomerase functionality *in vivo* (Le et al., 1999; Li and Lustig, 1996; Lundblad and Blackburn, 1993; McEachern and Blackburn, 1996). After shuffling out the *LYS2*-marked wild-type *TLC1* cover plasmid by counter-selection on medium containing alpha-aminoadipate, the TSA-T cells were restreaked 10 times (~250 generations). Telomeres in yeast cells without functional telomerase shorten with each cell cycle, eventually resulting in a G2/M arrest known as senescence, by 75–100 generations (Lundblad and Szostak, 1989; Singer and Gottschling, 1994). TSA-T-expressing cells grew like wild type through the entirety of the experiment (Figure 2.5A). Thus, telomerase RNA with the bulk of the three long arms converted to dsRNA functions *in vivo*.

Next, I examined telomere length in cells expressing TSA-T. Southern blotting of *Xho*I-digested genomic DNA using a telomeric probe showed telomeres 76 bp shorter in TSA-T cells than wild type after 250 generations. Average telomere length in TSA-T cells is therefore approximately 248 bp, or 77% of wild-type telomere length for this strain (~320-bp; Figure 2.5B). The statistically significant ($p = 0.0006$) telomere length decrease in TSA-T cells is moderate; other *TLC1* alleles are known to have more dramatically shortened telomeres. For example, *Mini-T(500)* maintains telomeres 231 bp shorter than wild type at generation 250, approximately 28% of estimated wild-type length (Figure 2.5B).

The moderately shortened telomeres observed in TSA-T-expressing cells could be partially or completely explained by a low abundance of the RNA as compared to TLC1-expressing cells. The standard urea-PAGE Northern blots could not be used, due to the impeded migration of TSA-T through polyacrylamide gels (see Figure 2.4A). Instead, total RNA was spotted on a membrane and probed for a 3′ region of TLC1 (nts 906 to 1140), which is also present in TSA-T. Since this region is wild type in TSA-T,

Figure 2.5: TSA-Telomerase maintains functional telomeres *in vivo*. (**A**) *TSA-T* cells grow well and do not senesce after being restreaked for more than 250 generations. (**B**) TSA-T maintains telomeres 76 bp shorter than wild type. A telomere Southern blot is shown for cells at 25, 100, 175, and 250 generations. The weighted average telomere length for the 17 Y′-element-containing telomeric restriction fragments (which cluster below the Chr. IV relative mobility control) from blots of nine biological replicates was measured at 250 generations by the weighted average mobility (WAM) assay (Zappulla et al., 2011). Average length changes are indicated ±SEM. (**C**) TSA-T RNA abundance is 15% of wild-type TLC1 *in vivo*. Shown is a typical result; dot blots are performed instead of Northern blotting because TSA-T does not completely denature in urea, likely due to its extremely stable dsRNA arms. Telomerase RNA abundance was normalized to U1 snRNA control spots.

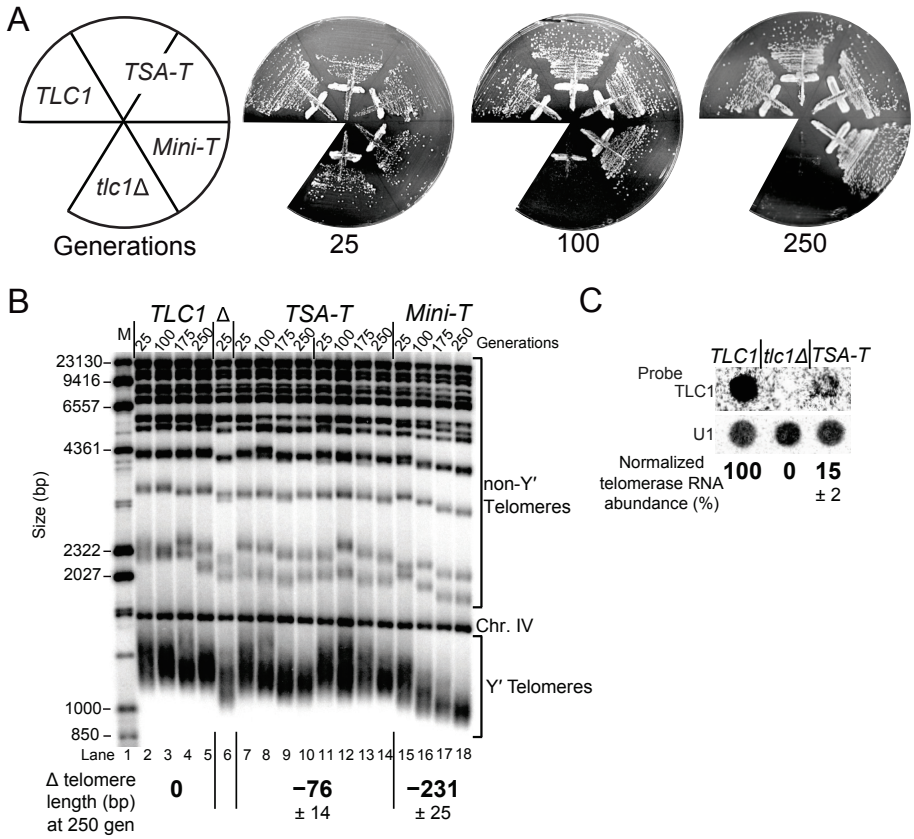

probes are expected to bind equally well to TLC1 and TSA-T. The RNA abundance of TSA-T in cells is approximately 15% of wild-type TLC1 (Figure 2.5C).

It is noteworthy that TSA-T, while only 15% as abundant as TLC1, is able to maintain telomeres only 76 bp shorter. In contrast, although Mini-T(500) RNA abundance is similarly ~16% of wild type (Zappulla et al., 2005), it maintains telomeres that are 231 bp shorter. I hypothesized that the reduced TSA-T RNA abundance contributed to the shorter telomeres in these cells. To compare TSA-T to TLC1 at the same RNA abundance, I expressed *TSA-T* from a high-copy, 2-micron (2μ) plasmid, versus two copies of *TLC1* on a single *CEN* plasmid in a *tlc1Δ* strain. This raised TSA-T abundance to 181% of wild type, and TLC1 levels to 187% (Figure 2.6A). *TSA-T* on a 2μ plasmid maintains telomeres 97 bp longer than wild type, while two copies of *TLC1* on a *CEN* plasmid only increased telomere length by 29 bp, a statistically significant difference ($p = 0.01$, Fig. 4B). Furthermore, telomere length could be rescued by simply expressing two copies of *TSA-T* on a single *CEN* plasmid. This raises TSA-T abundance from 15 to 23%, resulting in telomeres statistically indistinguishable from wild type (Figure 2.6). These data demonstrate that TSA-T maintains longer telomeres in yeast cells than TLC1 when accounting for RNA abundance, and suggest that TSA-T could be viewed as a gain-of-function telomerase RNA allele with respect to telomere lengthening.

The stiffened Ku and Est1 arms of TSA-T promote telomere elongation while the stiffened terminal arm leads to low RNA abundance and short telomeres

To determine how each stiffened arm contributes to TSA-T phenotypes, I made constructs with each individual arm stiffened. Furthermore, I constructed alleles with each pairwise combination of stiffened arms to test their genetic interactions. These TLC1 alleles are named based on the status of the Ku, Est1 and terminal arms,

Figure 2.6: TSA-T supports longer telomeres than wild-type TLC1 when accounting for RNA abundance. (**A**) Dot blot of TLC1 and TSA-T RNAs under different expression conditions. TLC1 was expressed from a single copy of the *TLC1* gene on a *CEN* plasmid (x1), or from a single *CEN* plasmid with two tandem copies of *TLC1* (x2). TSA-T was similarly expressed from a single-copy gene (x1) or two tandem copies of *TSA-T* on a *CEN* plasmid (x2). TSA-T was also expressed from a high-copy 2μ plasmid. Not that the strain background used for this experiment (W303) is different from the strain used to generate the data in Figure 2.5 (S288C). Average relative RNA abundance from four independent isolates after 250 generations of growth is shown ±SEM. (**B**) A telomere Southern blot performed on genomic DNA isolated from cells expressing TLC1 or TSA-T from single (x1) or duplicate-gene (x2) *CEN* plasmids, as well as TSA-T from a 2μ plasmid. Two independent transformants after 250 generations of growth are shown for each condition. Average changes in Y′ telomere length from four independent isolates after 250 generations of growth are indicated ±SEM.

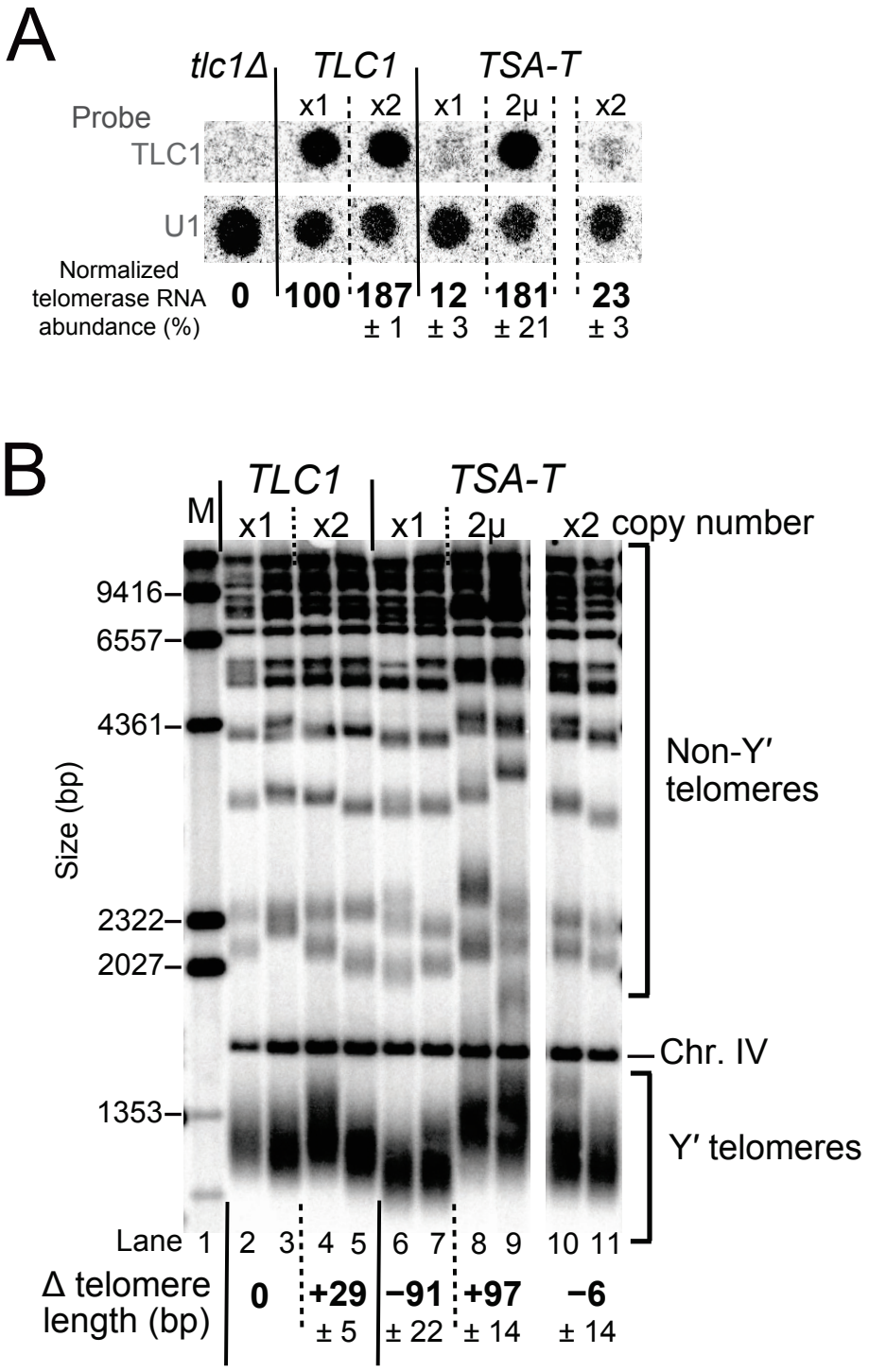
A
tlc1Δ
TLC1
TSA-T
x1
x2
x1
2μ
x2
Probe
TLC1
U1
Normalized telomerase RNA abundance (%)
0
100
187 ± 1
12 ± 3
181 ± 21
23 ± 3
B
TLC1
TSA-T
M
x1
x2
x1
2μ
x2 copy number
9416
6557
4361
2322
2027
1353
Size (bp)
Non-Y′ telomeres
Chr. IV
Y′ telomeres
Lane 1 2 3 4 5 6 7 8 9 10 11
Δ telomere length (bp)
0
+29 ± 5
−91 ± 22
+97 ± 14
−6 ± 14

respectively: "–" indicates the arm is wild type, while "S" indicates it is stiffened (Figure 2.7A). I first tested which combinations of stiffened arms promote reconstituted telomerase activity *in vitro* relative to the 1157-nt wild-type TLC1 RNA. Each TSA-T allele was co-expressed with ProA-Est2, as done previously (Zappulla et al., 2005), and activity was normalized to the level of [^{32}S]-ProA-Est2 recovered. As observed earlier (Figure 2.4B), TSA-Telomerase has roughly 10-fold more activity than wild-type TLC1 (Figure 2.7B, lanes 2 and 3). Alleles with stiffened Ku or terminal arms have greater activity than TLC1 (Figure 2.7B, lane 2 compared to lanes 3, 4, 6, 7, and 8), while stiffening the Est1 arm does not have a significant effect on enzymatic activity (Figure 2.7B, lane 5).

Next, I determined the effects of each stiffened arm on telomerase *in vivo.* I expressed each stiffened-arm telomerase RNA allele from a centromeric plasmid in a *tlc1*Δ strain, and grew cells for 250 generations. All stiffened-arm RNA alleles are able to complement a loss of wild-type *TLC1* (Figure 2.8A). Dot blots analysis showed that stiffening the terminal arm dramatically reduces telomerase RNA abundance in the cell, resulting in levels 10−13% of wild-type TLC1 (Figure 2.8B). The stiffened Ku and Est1 arms also reduce telomerase RNA levels, although to a lesser degree.

I used Southern blots to measure telomere length in cells expressing stiffened-arm TLC1 permutations from *CEN* plasmids, to determine which arm or set of arms is responsible for the increased telomere length maintenance activity for TSA-T. The construct with stiffened Ku and Est1 arms (SS−) maintains telomeres 77 bp longer than wild type ($p = 0.05$; Figure 2.8C, lanes 12 and 13). The stiffened Est1 arm alone (−S−) causes a small increase in telomere length, 23 bp, although with 4 biological replicates, this increase is not quite statistically significant ($p = 0.15$; lanes 8 and 9). Stiffening the Ku arm alone (S−−) also results in no significant change ($p = 0.9$; lanes 6 and 7). Meanwhile, all constructs with a stiffened terminal arm (−−S, S−S, −SS, and SSS)

Figure 2.7: Effects of stiffening particular arms of telomerase RNA on reconstituting active enzyme. (**A**) Variations of yeast telomerase RNA with all possible combinations of wild-type or stiffened arms from TSA-T were made, including one- and two-stiffened-arm RNAs. In the schematics shown, wavy black lines represent wild-type arms, while white cylinders denote stiffening. (**B**) Stiffening the Ku or terminal arms in yeast telomerase RNA promotes activity *in vitro*. Activity levels were normalized to an internal control for recovery and loading (IC, [γ-^{32}P]-labeled primer), and to immunopurified [^{35}S]Met-labeled ProA-Est2 levels. Percent activity relative to TSA-T is shown ±SEM from three replicates.

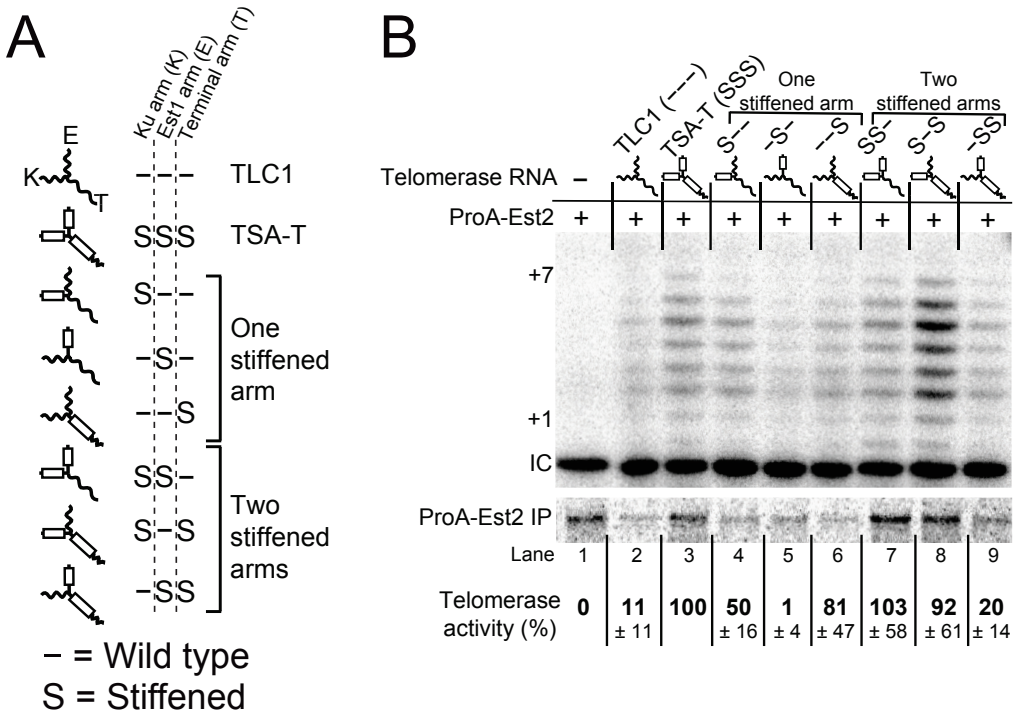

Figure 2.8: Effects of stiffening arms of yeast telomerase RNA individually and in each pair-wise combination on cell growth, RNA abundance and telomere length. (**A**) All stiffened-arm TLC1 constructs are able to support yeast cell proliferation. Each telomerase RNA allele was harbored on a low-copy CEN plasmid in a *tlc1*Δ yeast strain, and restreaked for over 250 generations. (**B**) Stiffening telomerase RNA arms lowers RNA abundance. Telomerase RNA levels from cells expressing stiff-arm TLC1 constructs after 250 generations of growth were determined by dot blot. Average relative RNA abundance is indicated for four biological replicates after 250 generations of growth, ± S.E.M. (**C**) Stiffened Ku and Est1 arms together promote telomere lengthening, whereas a stiffened terminal arm leads to shortening. Telomere lengths from cells expressing stiff-arm TLC1 constructs were examined by Southern blot. Two isolates at 250 generations shown for each sample. Average change in Y′ telomere length is indicated for four biological replicates after 250 generations of growth, ± S.E.M.

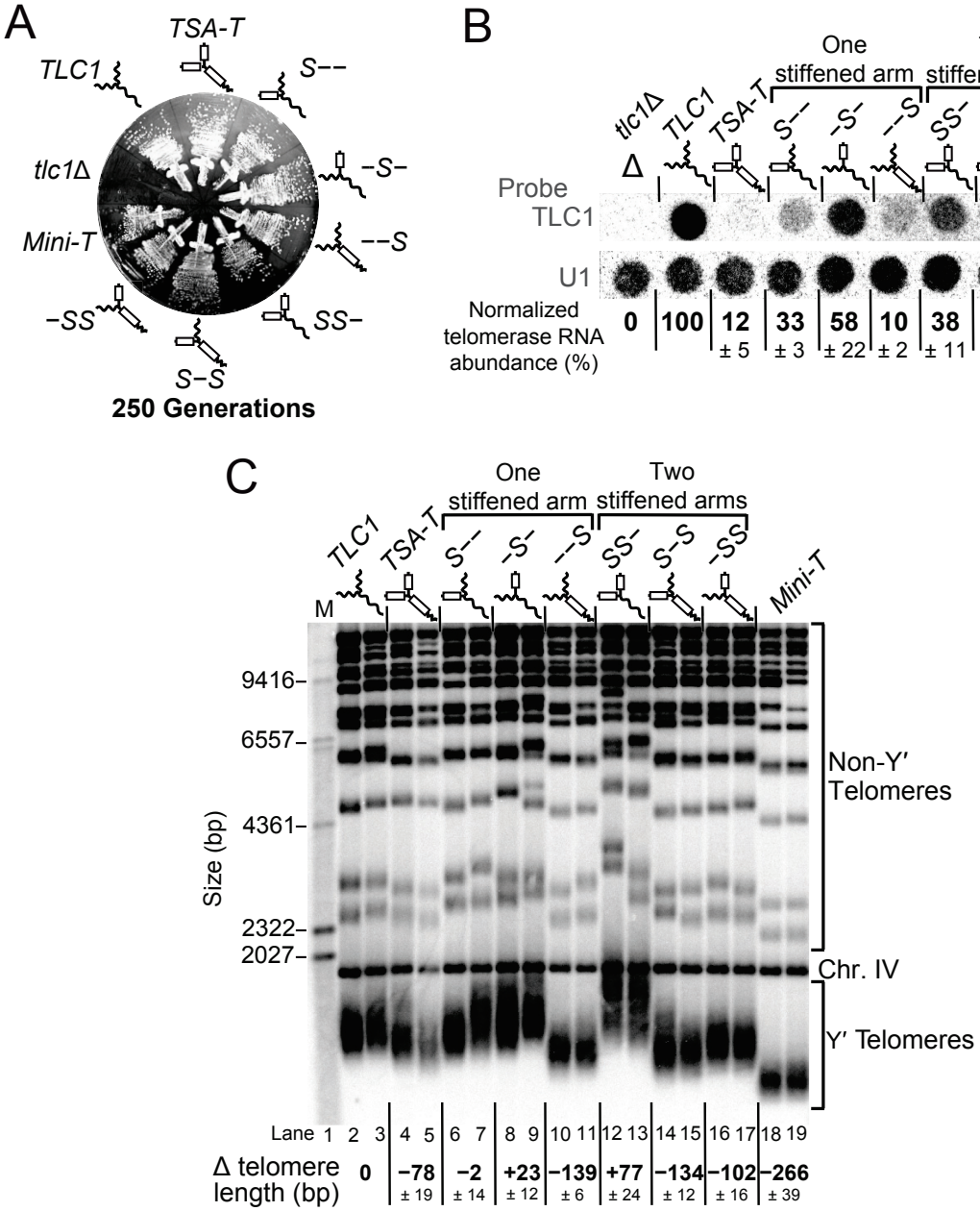
A
TSA-T
TLC1
S−−
tlc1Δ
−S−
Mini-T
−−S
−SS
SS−
S−S
250 Generations
B
One stiffened arm
Two stiffened arms
tlc1Δ
TLC1
TSA-T
S−−
−S−
−−S
SS−
S−S
−SS
Probe TLC1
U1
Normalized telomerase RNA abundance (%)
0
100
12 ± 5
33 ± 3
58 ± 22
10 ± 2
38 ± 11
13 ± 6
12 ± 5
C
One stiffened arm
Two stiffened arms
TLC1
TSA-T
S−−
−S−
−−S
SS−
S−S
−SS
Mini-T
M
9416–
6557–
4361–
2322–
2027–
Size (bp)
Non-Y′ Telomeres
Chr. IV
Y′ Telomeres
Lane 1 2 3 4 5 6 7 8 9 10 11 12 13 14 15 16 17 18 19
Δ telomere length (bp)
0
−78 ± 19
−2 ± 14
+23 ± 12
−139 ± 6
+77 ± 24
−134 ± 12
−102 ± 16
−266 ± 39

maintain telomeres shorter than wild type and stiffening the terminal arm *per se* (−−S) results in telomeres 139 ± 6 bp shorter (p = 0.0002; lanes 10 and 11). These shortened telomeres are likely the result of very low RNA abundance for stiffened terminal arm alleles (Figure 2.8B). All of the stiffened arm constructs, however, maintain telomeres longer than the miniaturized telomerase RNA Mini-T.

An Est1-binding arm "hinge" is essential, but not for flexibility

The Est1 arm is the shortest of the three TLC1 arms, and in TSA-T the stiffened dsRNA helix is only 31 bp long. In addition, the 5′ side of the base of the Est1-binding region at the end of the arm contains a bulge-hairpin domain that could potentially act as a hinge, allowing the Est1 site to orient back towards the core even when the arm is stiffened. I next tested a series of mutants to determine whether this hinge structure was necessary for TSA-T function.

Deleting the hinge-hairpin structure (nts 550−590) from the wild-type Est1 arm did not cause senescence, nor did it result in a significant change in RNA abundance (see TLC1Δ550−590 in Figure 2.9). However, deleting the hinge-hairpin domain from TSA-T to make tsa-tΔHH does cause senescence. Since tsa-tΔHH RNA abundance is comparable to that of TSA-T, it is unlikely that loss of the hinge-hairpin structure is affecting RNA levels in the cell (Figure 2.9). The core of tsa-tΔHH is still functional, an is able to reconstitute telomerase activity *in vitro* (Figure 2.9D) Adding an 8-nt single-stranded bulge of wild-type nucleotide sequence to the hinge site in TSA-T(ssH) restores telomerase function and prevents senescence. Furthermore, an 8-nt hinge of random nucleotide sequence in TSA-T(randH) is sufficient to prevent senescence, suggesting that the function of the hinge is not sequence dependent.

These data suggested that a flexible hinge in the arm might be necessary for function. To test whether a flexible point in the arm was in fact required, I added the 8-nt

Figure 2.9: A "hinge" structure in the Est1 arm is essential, but not for flexibility. (**A**) *Mfold* predicted secondary structures for Est1 arm mutants, with hinge domains boxed, or sites of hinge-hairpin deletion indicated by an arrow: Wild-type Est1 arm; ∆550−590; stiffened Est1 arm in TSA-T or TLC1(−S−); ∆HH; (ssH) with wild-type sequence 8-nt single-stranded hinge restored at the hinge-hairpin locus (UAGUAUAA; see box); (randH) with 8-nt single-stranded hinge of random sequence at the hinge-hairpin locus (CUAGUCAG; see box); (midH), with wild-type 8-nt hinge added into the middle of the stiffened Est1 arm. (**B**) *TLC1* and TSA-T hinge-hairpin mutant alleles expressed from *CEN* plasmids in yeast cells, shown at 250 generations of growth. (**C**) Relative RNA abundance of hinge-hairpin mutants from dot blots, from one or two isolates at 50 generations of growth. (**D**) Deleting the hinge in tsa-t∆HH does not disrupt the catalytic core. *In vitro* reconstituted telomerase activity assay shown, with two replicates for TSA-T and tsa-t∆HH. Internal loading control (IC) is a [γ-^{32}P]-labeled primer.

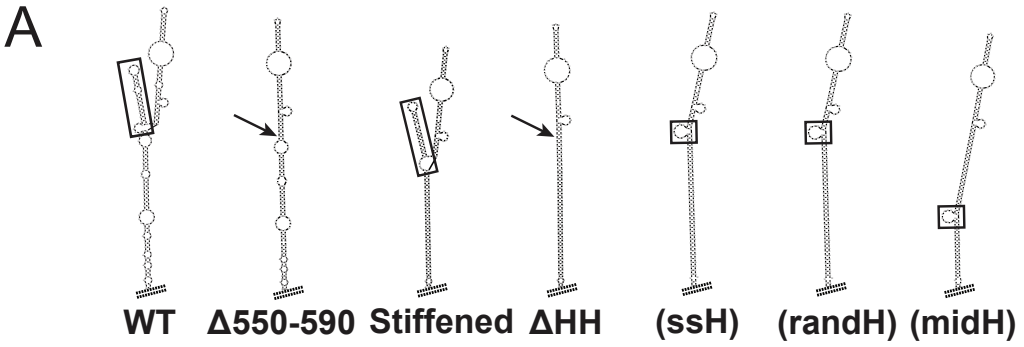
A
WT
Δ550-590
Stiffened
ΔHH
(ssH)
(randH)
(midH)

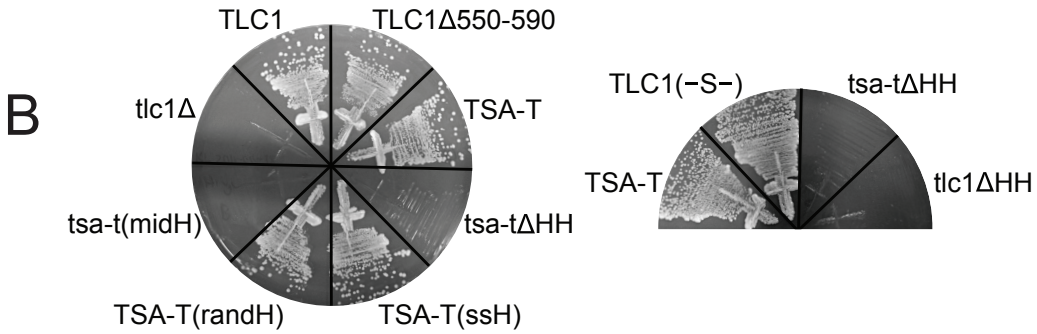
B
TLC1
TLC1Δ550-590
tlc1Δ
TSA-T
tsa-t(midH)
tsa-tΔHH
TSA-T(randH)
TSA-T(ssH)
TLC1(−S−)
tsa-tΔHH
TSA-T
tlc1ΔHH

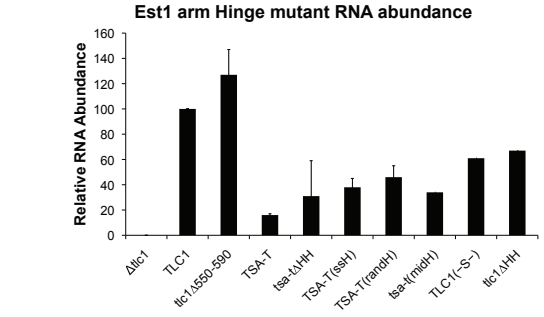
C
Est1 arm Hinge mutant RNA abundance
Relative RNA Abundance
160
140
120
100
80
60
40
20
0
Δtlc1
TLC1
tlc1Δ550-590
TSA-T
tsa-tΔHH
TSA-T(ssH)
TSA-T(randH)
tsa-t(midH)
TLC1(-S-)
tlc1ΔHH

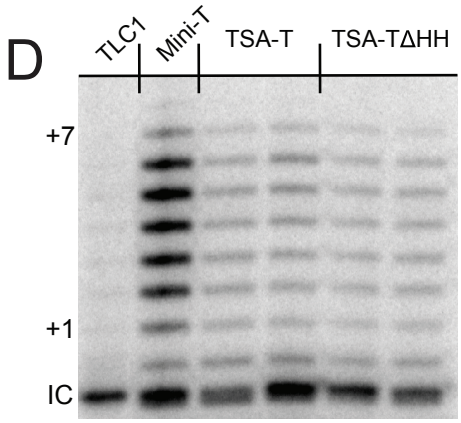
D
TLC1
Mini-T
TSA-T
TSA-TΔHH
+7
+1
IC

wild-type sequence hinge into the middle of the stiffened Est1 arm in tsa-t(midH) (Figure 2.9). This break in the dsRNA helix should add a flexible point in the arm, allowing it to bend. However, cells expressing tsa-t(midH) senesced similarly to tsa-tΔHH, indicating that having a flexible point in the otherwise stiffened Est1 arm is not sufficient for telomerase function.

In addition, I lengthened the helical Est1 arm in TSA-T to 157 bp, which is still shorter than the 225 bp persistence length, and therefore should still act as a stiffened rod (Figure 2.10A). The Est1 arm in this TSA-T(E157) RNA is so long that it is unlikely that Est1 can interact with components of the core *in cis*, even if the hinge structure allows for flexibility. However, TSA-T(E157) did not eliminate telomerase function; cells grew sickly, but did not senesce (Figure 2.10B). However, deleting the hinge-hairpin from TSA-T(E157) caused cells to senesce (See tsa-t(E157ΔHH) in Figure 2.10). Furthermore, adding flexible hinge into the middle of the 157-bp helix in tsa-t(E157midH) did not restore telomerase function.

Together, these data indicate that while the hinge-hairpin structure plays an essential role in TLC1 function, it is not required for physical flexibility. Additionally, it appears that sequence of the hinge is not essential; when the hinge-hairpin is deleted, other unpaired nucleotides in bulges and loops in the wild-type Est1 arm can restore its function. In order to fully eliminate the hinge activity, it was necessary to also delete all of the unpaired nucleotides in the Est1 arm in TLC1 using the stiffened arm from TSA-T (see tlc1ΔHH in Figure 2.9). This data is supported by published findings which showed that the hinge is required for Est1 association with the RNA; deleting the hinge and several other loops and bulges in TLC1 resulted in loss of Est1 binding and shortened telomeres, although not quite senescence (Lubin et al., 2012).

Figure 2.10: TSA-T is functional *in vivo* even when the Est1 arm helix is extended to 157 bp. (**A**) *Mfold* secondary structure models for extended stiffened Est1 arms: TSA-T(E157), tsa-t(E157ΔHH), and tsa-t(E157midH). (**B**) Cells expressing extended Est1 arm variants of TSA-T from *CEN* plasmids, shown at 250 generations. TSA-T(E157) does not cause senescence. Deleting the hinge-hairpin leads to senescence, and cell growth is not rescued by restoring the hinge in the middle of the arm.

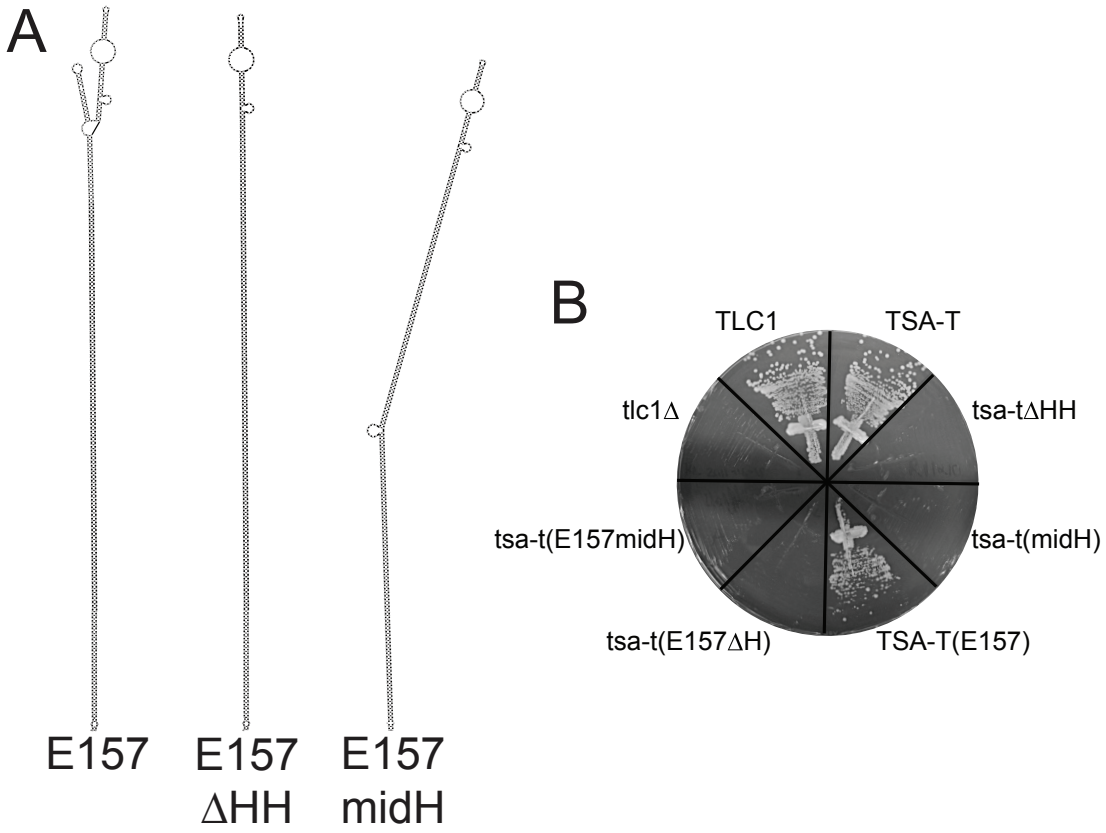

TSA-T still acts as a functionally flexible scaffold

The fact that TSA-T retains function *in vivo* indicates that yeast telomerase tolerates stiffening of the arms of TLC1. This supports a simple flexible scaffold model, in which the accessory proteins do not have specific orientations in the RNP required for function. However, it remained possible that TSA-T had rigidly locked the accessory proteins in functional positions. In order to test whether TSA-T retained functional flexibility, I next relocated the Est1 and Ku arms on the RNA. To avoid relocating them to a flexible region, I simply swapped the binding sites at the end of the two stiffened arms, with the Est1 site relocated to the end of the 62-bp Ku arm, and the Ku site at the end of the 31-bp Est1 arm, in both TSA-T and TLC1(SS−) (Figure 2.11A). Cells expressing TSA-T(K↔E) or TLC1(SS−/K↔E) did not senesce (Figure 2.11B). These swapped-site variants maintained telomeres marginally shorter than TSA-T and TLC1(SS−) (Figure 2.11C); however, a similar telomere-shortening phenotype was observed when the Est1- and Ku-binding sites were simultaneously relocated in wild-type TLC1 (Figure 2.11C, TLC1(Ku@1023/Est1@446) and TLC1(Ku@446/Est1@1023)). These data suggest that Est1 and Ku retained function even when the binding sites were relocated on TSA-T, indicating that the stiffened-arm TLC1 still acts as a functionally flexible scaffold.

Figure 2.11: TSA-T retains function when the Ku and Est1 binding sites are repositioned. (**A**) Secondary structure prediction for TSA-T with the Ku- and Est1-binding site positions swapped on the RNA. Gray cylinders indicate stiffened arms. (**B**) Relocating the Ku and Est1 arms simultaneously does not cause senescence. Cells expressing the following RNA variants are shown at 250 generations of growth: tlc1Δ, TLC1, TSA-T, two isolates of TSA-T(K↔E), TLC1(SS−), TLC1(SS−)(K↔E), TLC1 with Est1 relocated to position 446 and Ku relocated to position 1023, and TLC1 with Ku relocated to position 446 and Est1 relocated to position 1023. (**C**) Relocating the Ku and Est1 sites does not have a significant effect on RNA abundance. Relative RNA abundance from a dot blot of two independent isolates (or four for TSA-T(K↔E)) is indicated ±SD. (**D**) Telomere shortening in TSA-T(K↔E) is similar to when the Ku and Est1 sites are relocated on wild-type TLC1. Telomere lengths from cells expressing stiff-arm TLC1 constructs were examined by Southern blot. Two or four isolates at 250 generations shown for each sample. Average change in Y′ telomere length is indicated for two or four biological replicates after 250 generations of growth, ± SD.

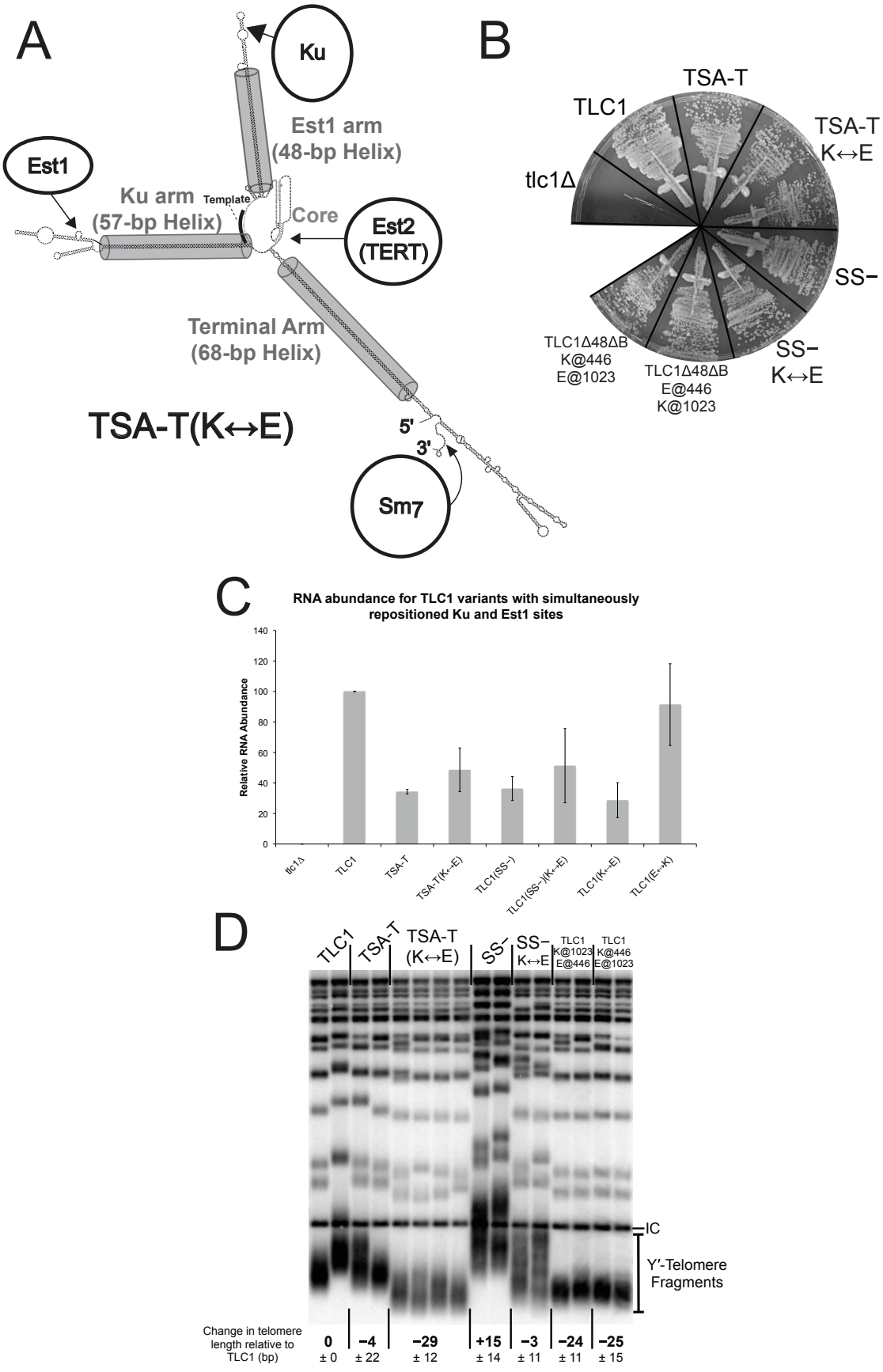
A
Ku
Est1 arm
(48-bp Helix)
Est1
Ku arm
(57-bp Helix)
Template
Core
Est2
(TERT)
Terminal Arm
(68-bp Helix)
TSA-T(K↔E)
5'
3'
Sm7
B
TSA-T
TLC1
TSA-T
K↔E
tlc1Δ
SS−
TLC1Δ48ΔB
K@446
E@1023
TLC1Δ48ΔB
E@446
K@1023
SS−
K↔E
C
RNA abundance for TLC1 variants with simultaneously repositioned Ku and Est1 sites
Relative RNA Abundance
140
120
100
80
60
40
20
0
tlc1Δ
TLC1
TSA-T
TSA-T(K↔E)
TLC1(SS−)
TLC1(SS−)(K↔E)
TLC1(K↔E)
TLC1(E↔K)
D
TLC1
TSA-T
TSA-T
(K↔E)
SS−
SS−
K↔E
TLC1
K@1023
E@446
TLC1
K@446
E@1023
IC
Y′-Telomere
Fragments
Change in telomere
length relative to
TLC1 (bp)
0
± 0
−4
± 22
−29
± 12
+15
± 14
−3
± 11
−24
± 11
−25
± 15

2.4: DISCUSSION

Telomerase RNA contributes far more than a template to the enzymatic functions of the telomerase holoenzyme. *In vitro*, the conserved roles of the telomerase long non-coding RNA (lncRNA) subunit in core enzyme function also include providing a 5′ boundary of the template region for appropriate reverse transcription (Chen and Greider, 2003; Lai et al., 2002; Seto et al., 2003; Tzfati et al., 2000) and binding and coordinating TERT during catalysis (Berman et al., 2011; Bryan et al., 2000; Lai et al., 2003; Stone et al., 2007). Furthermore, *in vivo*, telomerase RNA provides a scaffold for the assembly and function of essential and important holoenzyme protein subunits (Est1, Ku and Sm_7; Blackburn and Collins, 2011; Cech, 2004).

Using the tractable *S. cerevisiae* model organism, it has been shown that the TLC1 telomerase RNA scaffolding has functional and organizational flexibility (Zappulla and Cech, 2006), given that Est1, Ku, and Sm_7 binding sites can be dramatically repositioned in the RNA with significant retention of their essential and important *in vivo* functions, respectively (Mefford et al., 2013; Zappulla and Cech, 2004; Zappulla et al., 2011). Identification of functionally flexible scaffolding by yeast telomerase RNA has provided a prototype for a mechanism that appears to be directly applicable to a rapidly growing list of lncRNAs (Guttman et al., 2011; Wang and Chang, 2011). However, much more remains to be understood about how telomerase RNA contributes to the mechanism of this enzymatic lncRNP. Although the secondary structure model for TLC1 shows many bulges and loops throughout its 1157-nt length (Dandjinou et al., 2004; Zappulla and Cech, 2004), it is not known if the RNA is indeed physically flexible, nor if the potential flexibility, hinging on these loops and bulges, is important. The majority of the 1157-nt wild-type TLC1 RNA molecules do not fold into an active conformation *in vitro* (Figure 2.4), making structural characterization very difficult. Miniaturized telomerase (Mini-T) RNAs reconstitute activity with TERT in rabbit reticulocyte lysates

(Zappulla et al., 2005), but these RNAs range from 57 to 67% (657 to 773 nts) shorter than wild-type TLC1, and are missing the bulk of all three long arms.

In my thesis research, I designed and create a TLC1 allele with significantly stiffened arms, by removing unpaired nucleotides within them, leaving only dsRNA (Figure 2.1), which has been determined to be rigid when shorter than 225 bp (Abels et al., 2005). The data presented in this chapter cannot conclusively prove that the RNA arms of TSA-T are in fact stiff; it remains possible that unknown dsRNA-binding proteins or local RNA structures cause deformation of the helices. In addition, it has been shown that, for DNA, the nucleotide sequence, ionic conditions, or temperature can all affect the persistence length (Geggier et al., 2011; Geggier and Vologodskii, 2010). In fact, DNA helices as short as 67 base pairs have been observed forming loops (Vafabakhsh and Ha, 2012). However, the persistence length for RNA is longer than that of DNA due to RNA adopting an A-form helical structure, which is shorter and wider than the typical B-form DNA (Hagerman, 1988, 1997; Herrero-Galan et al., 2013). Furthermore, each helical arm in TSA-T is less than 30% of the published persistence length for dsRNA; thus, even if local conditions in the cell promoted increased dsRNA flexibility, it is unlikely that the persistence length would decrease so much that these short helices would begin to bend. Therefore, the double-stranded RNA arms of TSA-T are likely to act as stiffened rods, with less potential for physical flexibility than the arms of wild-type TLC1.

Triple-stiff-arm TLC1, TSA-T, differs from Mini-T in that the regions excised to make Mini-T are instead rigidified by removal of bases predicted to be unpaired, and also the distal portion of the terminal arm in TSA-T is left intact. Stiffening the three arms that emanate from the catalytic core significantly constrains the structural freedom within the RNP. Unlike in Mini-T, where the arm tip-binding holoenzyme protein subunits — Est1, Ku and Sm_7 — are moved closer to the catalytic core, these accessory subunits

are predicted to be inhibited from flexing towards the central core by the intervening dsRNA in the arms of TSA-T. While the stiffened arms may still retain some reduced ability to flex, the position of each accessory protein relative to the rest of the RNP is much more constrained than in wild type. Thus, TSA-T is expected to have an unperturbed catalytic core (where Est2 binds) and holoenzyme subunits, Est1, Ku and Sm_7, held at a distance by stiff dsRNA struts.

In many organisms other than *Saccharomyces*, the 31–68-bp tracts of double-stranded RNA in TSA-T would be targeted by the RNA interference (RNAi) degradation pathway and could also alter gene expression. *S. cerevisiae*, however, lacks RNAi, since it does not have a Dicer enzyme homolog, nor some of the other key components of RNAi machinery (Nakayashiki et al., 2006). Furthermore, TSA-T should be spared by the RNase III enzyme in *Saccharomyces*, since Rnt1 recognizes a consensus sequence in terminal loops instead of the RNA double helix (Chanfreau et al., 2000).

With the removal of 201 unpaired nucleotides, TSA-T folding is energetically more favorable than wild-type TLC1: *Mfold* RNA secondary structure prediction software calculates the minimum free energy (ΔG) to be –458 kcal/mol for TSA-T, compared to –321 kcal/mol for TLC1 (Figure 2.3). When normalized for RNA length, this calculated free energy difference (ΔΔG) between TSA-T and TLC1 is 0.20 kcal/mol/nt (–0.48 vs. –0.28 kcal/mol/nt, respectively). *In vitro*, the dsRNA arms of TSA-T drive a highly stable structure that is resistant to denaturation by urea, and that contains regions protected from single-strand-specific RNA nucleases (Figure 2.4A). Furthermore, the energetically favorable structure of TSA-T is functional *in vitro*, reconstituting activity when expressed in a transcription-translation system with TERT (Figure 2.4B). Although TLC1 has been considered to be nonfunctional in reconstituted telomerase assays, I reproducibly detect very low activity from TLC1 when reconstituted in rabbit reticulocyte lysates, thus allowing semi-quantitative comparison to Mini-T and TSA-T (Figures 2.4B and 2.7B).

TSA-Telomerase activity appears to be ≥10-fold more than that supported by wild type TLC1, although still ~5-fold less than that by Mini-Telomerase.

The fact that TSA-T functions well *in vitro* suggests that the energetically favorable folding of its dsRNA arms promotes formation of an active conformation of the central core. However, *in vivo*, where arm-binding subunits are additionally required for telomerase function, it could not be assumed that TSA-T would be functional. Nevertheless, TSA-T complements a *tlc1*Δ mutant and permits cell proliferation (Figure 2.5A). The fact that TSA-T functions despite truncated, strut-like arms connecting Est1, Ku and Sm_7 accessory subunits to the catalytic core provides further evidence that yeast telomerase RNA acts as a simple scaffold for these protein subunits.

The abundance of TSA-T RNA *in vivo* is 15% of wild-type TLC1 (Figure 2.5C). TSA-T abundance was detected by dot blots because it does not migrate appreciably in polyacrylamide-urea gels. This low electrophoretic mobility is ostensibly because its dsRNA arms resist denaturation by urea, consequently trapping the single-stranded 178-nt hub at the intersection of the three arms — this unwieldy topology would not be expected to migrate effectively through a polyacrylamide matrix.

The telomeres supported by TSA-T in yeast cells are 76-bp shorter than wild type. This phenotype contrasts with that of Mini-T cells, which have telomeres that are 231 bp shorter (Figure 2.5B). Thus, despite almost identical RNA abundance in the cell, TSA-T and Mini-T cells have very different telomere lengths. Furthermore, when the TSA-T RNA levels match those of TLC1 (181% TSA-T vs. 187% for TLC1, as compared to TLC1 expressed from a single gene on a *CEN* plasmid), *TSA-T* cells have telomeres 97 bp longer than wild type, while *TLC1* telomeres only increase by 29 bp (Figure 2.6). In addition, telomere length was restored to wild type by increasing TSA-T abundance from 15 to 23% of TLC1. In other words, the telomere shortening phenotype of TSA-T cells appears to be due to the reduction in telomerase RNA subunit abundance and,

when normalized for RNA abundance, TSA-T supports telomeres longer than wild type. It is parsimonious to propose that this is attributable to TSA-Telomerase gain-of-functionality compared to wild type. To our knowledge, the only alleles of yeast telomerase RNA reported to have elongated telomeres are TLC1+Ku RNAs, which have a second Ku-binding site added at a novel position (Zappulla et al., 2011).

When normalizing for telomerase RNA abundance, telomeres are elongated in TSA-T cells compared to those with wild-type TLC1. This appears to be attributable to stiffening both the Ku and Est1 arms in TSA-T. The "SS−" allele has telomeres 77 bp longer than wild type, despite this RNA being only 38% as abundant (Figure 2.8). This effect appears to be a genetic interaction, since neither the stiffened Ku (S−−) nor Est1 (−S−) arm alone shows a significant increase. Intriguingly, the Ku and Est1 arms both function in telomerase recruitment (Bianchi et al., 2004; Chan et al., 2008; Pfingsten et al., 2012; Stellwagen et al., 2003), and it is therefore worth considering how stiffening the Est1 and Ku arms relate to this aspect of telomerase holoenzyme mechanism *in vivo*. In addition, the stiffened Ku arm may affect telomerase specific activity. In reconstituted telomerase assays, the stiffened Ku arm promotes activity in the absence of the Ku protein, implying an effect on telomerase catalytic core formation (Figure 2.7B).

Despite the increased telomere extension caused by stiffened Ku and Est1 arms, TSA-T telomeres are shorter than wild type due to very low telomerase RNA abundance (Figure 2.5C). This is due to stiffening the terminal arm; each allele with the terminal arm stiffened had *in vivo* abundance ranging from 10−13% of wild type (Figure 2.8B). Correspondingly, each stiffened terminal arm allele supported shortened telomeres as well (Figure 2.8C). However, the stiffened-terminal-arm alleles do confer growth to a *tlc1*Δ strain, with telomeres longer than Mini-T cells. The reduced telomerase levels and telomere lengths in stiffened terminal arm alleles may indicate that some flexibility is required in the terminal arm for full function. It is possible that Sm_7 plays a supporting

role in RNP assembly, related to that reported in *Schizosaccharomyces pombe* telomerase (Tang et al., 2012), and that physical RNA flexibility is important for assisting loading or coordinating Est2 and/or Est3. Alternatively, the low RNA abundance may not be due to stiffening *per se*, since previously reported truncations in the terminal arm have resulted in similar RNA and telomere phenotypes (Zappulla and Cech, 2004). It is possible that stiffening the terminal arm introduces mutations in a previously uncharacterized RNA motif within the stiffened region.

TSA-T function is not dependent on flexibility in a hinge-hairpin structure in the Est1 arm. While this structure is essential, restoring flexibility to the arm by adding a flexible hinge in the middle of the stiffened helix of tsa-tΔHH does not rescue telomerase function (Figure 2.9). Furthermore, the arm can be lengthened such that the hinge would not allow Est1 to interact with the core *in cis* without eliminating telomere maintenance (Figure 2.10). Furthermore, even with the stiffened arms TSA-T still behaves as a functionally flexible scaffold, and tolerates repositioning of the Ku and Est1 binding sites on the arms (Figure 2.11).

The fact that telomerase is functional in yeast despite stiffened arm “struts” separating the catalytic core from the holoenzyme subunits (Figure 2.5) advances understanding of the structural nature of the yeast telomerase RNP and its mechanism *in vivo*. There are several possibilities that could explain the architecture and mechanism represented by the flexible scaffold model (Figure 2.12; Zappulla and Cech, 2004; Zappulla et al., 2011). First, like many well-studied RNPs, telomerase may form a highly ordered RNA structure with precise protein subunit positions required for function (Figure 2.12A). However, such a model is inconsistent with previously published data supporting a flexible scaffold (Zappulla and Cech, 2004; Zappulla et al., 2011), since a highly structured RNP with precise active positions would not tolerate subunit repositioning. On the other hand, a second proposed structural model invokes a requirement for precise

Figure 2.12: Possible models for yeast telomerase RNP holoenzyme architecture and function. (**A**) Structured telomerase RNP, with Est1 (E; red) and Ku (K; green) subunits requiring precise positioning by a structured TLC1 RNA (black) for function. Since it has been shown that Est1 and Ku can function when repositioned (arrows; Zappulla and Cech, 2004; Zappulla et al., 2011), this model is not favored. (**B**) Physically flexible telomerase RNA permitting Est1 and Ku subunits to "dock" into hypothetical precise positions (dashed circles) required for function. TLC1 flexibility is indicated by wavy black lines; the arms can bend in three-dimensional space with large accessible volume provided by the wide range of motion. The RNA is a physically flexible tether, allowing Est1 and Ku flex to their active docking positions to function (red and green arrows), even when binding sites on the RNA are repositioned. (**C**) Telomerase RNA as a structured, simple scaffold. In this model, although precisely positioned in the RNA normally, the protein components do not require specific relative positions to function. Therefore, positional and structural rearrangements are tolerated. (**D**) Telomerase as a physically flexible scaffold. In this scenario, yeast telomerase RNP architecture and function can be simply summarized as "beads on a string." The RNA-bound protein components are tethered and do not need to dock into any precise position within the RNP.

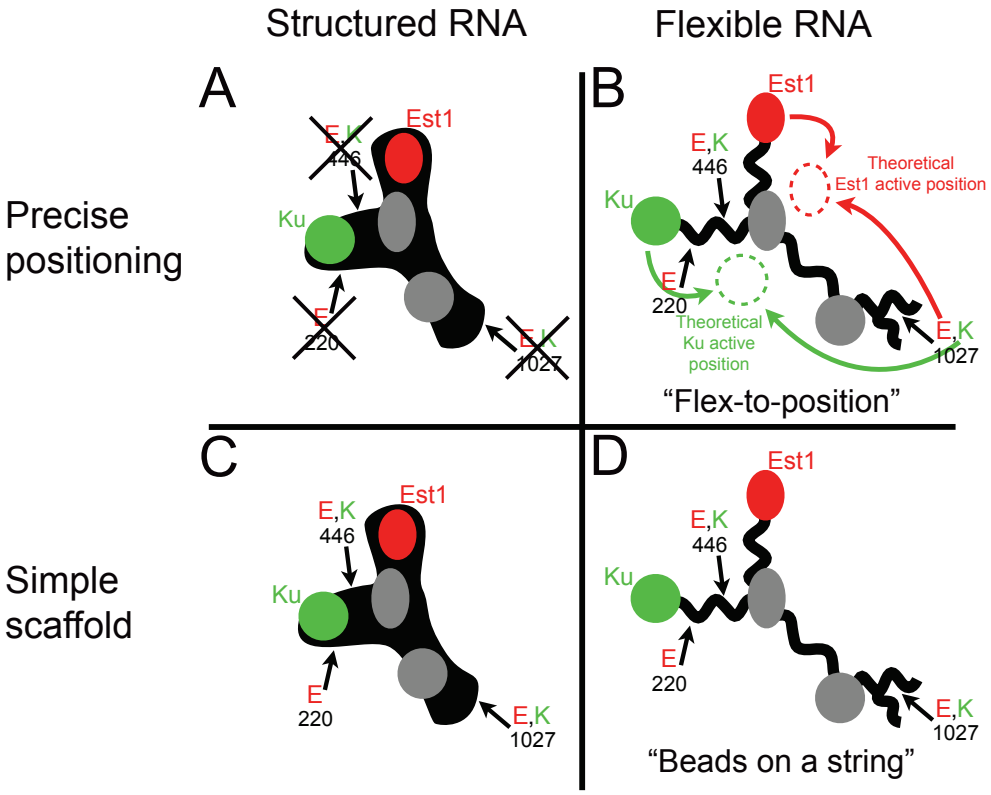
Structured RNA
Flexible RNA
A
B
C
D
Precise positioning
Simple scaffold
Est1
E,K
446
Ku
E
220
E,K
1027
Theoretical Est1 active position
Theoretical Ku active position
"Flex-to-position"
"Beads on a string"

positioning of the protein subunits, as long as the RNA is physically flexible (Figure 2.12B). In this “flex-to-position” model, the physically flexible arms of TLC1 bend in three-dimensional space, allowing the Ku and Est1 subunits to “dock” in their precise functional orientations even when repositioned on the RNA. These “precise positioning” RNA scaffolds stand in contrast to a “simple scaffold” model, in which the protein subunits do not have precise orientations for activity, but rather need only to be held in proximity to each other. In a simple scaffold, TLC1 may be globally structured (Figure 2.12C); since the proteins do not need specific positions, the RNA can tolerate binding-site repositioning, in accordance with the functionally flexible scaffold model. Alternatively, TLC1 may be relatively unstructured and physically flexible (Figure 2.12D); the RNA tethers the proteins together without precise positioning, causing the RNP to behave as “beads on a string,” with protein “beads” held loosely together by RNA “string.”

To test these models, I designed TSA-T with rigidified arms that greatly reduce possible RNA flexibility and act as struts to hold the accessory protein subunits away from the core. The fact that TSA-T functions *in vivo* provides evidence against precise positioning of the proteins within the RNP (Figure 2.12A and B). With physical flexibility essentially eradicated from the arms, the proteins would be unable to achieve the necessary active orientations *in cis*. Instead, functionality of TSA-T supports a simple-scaffold model, in which telomerase RNA holds the protein subunits onto the RNP complex, without conferring precise functional positions (Figure 2.12C and D).

As to whether wild-type TLC1 is physically rigid (Figure 2.12C) or flexible (Figure 2.12D) in the RNP *in vivo*, I favor the latter. Perhaps the strongest evidence favoring this hypothesis is the astonishingly rapid evolution of the arms (Dandjinou et al., 2004; Tzfati et al., 2003; Zappulla and Cech, 2004); nucleotides in the non-protein-binding regions of the arms are only 38% conserved in sequence between *Saccharomyces cerevisiae*,

paradoxus, *mikatae* and *bayanus*, compared to 59% in the other portions of the RNA (Zappulla and Cech, 2004). If a particular structure (or discrete set of structures) existed, there should not be such rapid evolutionary change in sequence, nor so few covarying nucleotides. Flexible RNA, on the other hand, can be generated by a vast array of sequences, consistent with the observed rapid evolution in telomerase RNA sequence and length.

In summary, the fact that TSA-T provides function *in vivo* is additional support for a simple, functionally flexible scaffold model for yeast telomerase RNA (Figure 2.12C and D; Zappulla and Cech, 2004). The strut-like arms of TSA-T holding essential and important accessory subunits away from the core of the RNP enzyme strongly disfavor a "flex-to-position" model for yeast telomerase architecture and mechanism. As to whether wild-type yeast telomerase RNA simple scaffolding is naturally physically flexible or rigid, TSA-T does not necessarily favor one or the other. However, the fact that there are notable phenotypes when arms of TLC1 are stiffened does suggest that there may be some — albeit nonessential — roles for the physical characteristics of telomerase RNA in holoenzyme architecture and function.

2.5: METHODS

Creation of telomerase RNAs with dsRNA arms

I used the secondary structure model of TLC1 (Dandjinou et al., 2004; Zappulla and Cech, 2004) as the basis for engineering modified constructs with tracts of purely double-stranded RNA in the arms. Unpaired nucleotides in the three RNA arms present in regions shown to be dispensable for basic function *in vivo* (Zappulla et al., 2005) were removed from the sequence. For complete TSA-T sequence, see Figure 2.2C. All unpaired nucleotides in the secondary structure model within the following regions of TLC1 were deleted: nucleotides 27−114 and 815−894 in the terminal arm, nucleotides 132− 263 and 334−456 for the Ku arm, and nucleotides 507−548 and 661−701 for the Est1 arm (Figure 2.1). At the core-proximal ends of the Est1 and terminal arms, the wild-type sequence was modified to create useful restriction enzyme sites to facilitate future modifications; an *Mlu*I site was built into the Est1 arm (starting at nucleotide 555 of *TSA-T*), and a *Pme*I site was built into the terminal arm (starting at nucleotide 631 of *TSA-T*). 22 out of 25 uracil residues predicted to be involved in G•U pairing in the regions of the arms to be stiffened were converted to C to promote Watson-Crick base pairing (Figure 2.1). A single G•U pair was added at the core-proximal end of each arm to make engineered palindromic restriction enzyme sites unique. *Mfold* RNA secondary structure predication software was used to model RNA secondary structure (Figure 2.2). The 1003-nt *Bgl*II to *Nsi*I region of the *TSA-T* gene was synthesized, sequence-verified and subcloned (GenScript). The *Bgl*II to *Nsi*I fragment of TSA-T was then subcloned into plasmid pSD107, which had the *Bgl*II to *Nsi*I fragment of TLC1 removed, leaving the upstream and downstream regions of TLC1 intact (pDZ223). To clone the one- and two-stiff-arm *TLC1* variants (Figures 2.7 and 2.8), restriction enzyme sites near the base of each stiffened arm were used to swap wild-type and stiffened arms between *TLC1* in

pSD107 and TSA-T in pDZ223. To determine the percentage of nucleotides paired in TLC1, TSA-T, and Mini-T referred to in the Results, all nucleotides involved in base pairing were counted, and divided by the total nucleotide length of the RNA: 711 paired/ 1157 total for TLC1, 685/956 for TSA-T, and 291/500 for Mini-T. For the percentage of each arm stiffened in TSA-T, the number of nucleotides in the regions of the arms of TLC1 that were converted to dsRNA in TSA-T was divided by the total nucleotides in each arm: 290 in stiffened region/ 325 total in the Ku arm (89%), 121/201 in the Est1 arm (60%), and 190/479 in the whole terminal arm (40%).

Experiments in yeast

To test stiffened arm TLC1 function *in vivo* for Figures 2.5 and 2.8, *TRP1*-marked centromeric (*CEN*) plasmids expressing the desired genes were transformed into strain TCy43 (*MAT-a ura3-53 lys2-801 ade2-101 trp1-Δ1 his3-Δ200 leu2-Δ1 VR::ADE2-TEL adh4::URA3-TEL tlc1Δ::LEU2 rad52Δ::HIS3 [pTLC1-LYS2-CEN]*) (Seto et al., 1999). After shuffling out *TLC1* (*LYS2/CEN*) on solid medium containing α-aminoadipate, colonies were restreaked ten times on synthetic compete media plates lacking tryptophan, with each restreak representing approximately 25 generations of yeast growth. For the increased expression of *TSA-T* for Figure 2.6, the *TSA-T* gene, including 518 bp upstream and 895 bp downstream of the native *TLC1* gene, were cloned into the 2-micron (2μ) expression vector pRS324. To add a second copy of *TLC1* to pSD107, the gene, including the 518 bp upstream and 895 bp downstream regions, was cloned into *Eco*RI and *Xho*I digested pSD107, resulting in a version of the vector harboring two complete *TLC1* genes in tandem. A two-copy *TSA-T* in pDZ223 was made by the same procedure. The plasmids for Figure 2.6 were transformed into strain yVL1009 (*MAT-α tlc1::LEU2 rad52::LYS ura3-52 lys2-801 ade2-101 trp1-Δ1 his3-Δ200 leu2-Δ1 [pTLC1-URA3-CEN]*) (Chappell and Lundblad, 2004), which is capable of maintaining 2μ

vectors. From this strain the plasmid shuffle was performed on 5-fluoroorotic acid (5-FOA), and cells were restreaked 10 times on complete synthetic medium lacking tryptophan.

Southern blots

Southern blots were performed as previously described (Zappulla et al., 2005; Zappulla et al., 2011). Briefly, cell pellets for genomic DNA isolation were prepared from cultures made from serially restreaked plates, with each streak representing ~25 generations. Genomic DNA was isolated (Gentra Puregene system), equal amounts were digested with *Xho*I and electrophoresed through a 1.1% agarose gel at 70 V for 17 h, and transferred to Hybond-N+ Nylon membrane (GE). The blot was then probed for telomeric sequences and a 1627-bp non-telomeric fragment of chromosome IV. Average Y′ telomere fragment length was quantified using the weighted average mobility (WAM) method described previously (Zappulla et al., 2011). To calculate the average length in base pairs of the Y′ telomeres, the average non-telomeric sequence length of Y′ fragments was subtracted from the experimentally determined weighted average motility of the Y′ telomere signal. This length, 1096 bp, was derived by finding the distance, in base pairs, of the nearest *Xho*I site to the start of the telomeric sequence in each Y′ telomere in the *Saccharomyces* Genome Database.

Total RNA dot blots

Total cellular RNA was extracted from late log phase or early stationary phase yeast cultures by a slightly modified version of the hot phenol RNA isolation method (Kohrer and Domdey, 1991). After boiling, 2.5µg of RNA was spotted six times onto Hybond-N+ Nylon Membrane (GE) to provide 3 technical replicates of each biological replicate (a single technical replicated dot for each biological sample for each probe is

shown in Figures 2.5, 2.6, and 2.8). The membrane was cut in half such that three dots of each sample were on each membrane section, air-dried, UV-crosslinked (SpectroLinker XL-1500 UV Crosslinker, "Optimal crosslink" setting), and pre-hybridized in Church buffer at 55°C for 10 minutes. One membrane was probed for the 3′ region of TLC1 shared by TLC1 and TSA-T (nucleotides 906 to 1140 in TLC1), while the other was probed for the U1 snRNA (Friedman and Cech, 1999). The three dots for each sample (i.e., the technical replicates for each biological sample) were averaged for both probes, and telomerase RNA levels were normalized to U1 levels.

RNase protection assay

TLC1, TSA-T, and Mini-T RNAs were transcribed *in vitro* using T7 RNA polymerase in the presence of [α-^{32}P]-GTP. To accomplish this, 2 µg of *Fok*I-linearized plasmid containing a T7 promoter was used as template for T7 polymerase in a reaction containing 10 mM DTT, 40 mM Tris 7.5, 12 mM $MgCl_2$, 2 mM spermidine, yeast inorganic pyrophosphatase (0.4 units; NEB), 25 mM rNTPs, and [α-^{32}P]-GTP (100 µCi), and incubated at 37°C for 1 hour. All 30 µL of reaction products was treated with DNase I (2 units, NEB) for 30 minutes, phenol/chloroform extracted, ethanol precipitated, and resuspended in 24 µL of 0.5xTE. 12 µL of RNA was then refolded by heating to 95°C for 2 minutes, then cooling on ice for 2 minutes. The RNA solution was brought to a volume of 18 µL with a final concentration of 111 mM HEPES (pH 8), 111 mM NaCl, 6.7 µM $MgCl_2$, and incubated at room temperature for 20 minutes. Next, the RNA was digested with RNase A (0.3 µg/µL) and RNase T1 (6 units; Fermentas) in 400µL of RNase digestion buffer (10 mM Tris•Cl pH 7.5, 300 mM NaCl, 5 mM EDTA) and incubated at RT for 45 min (Gilman, 2001). RNase digestion was stopped by adding 10 µL of 20% SDS and 2.5 µL Proteinase K, incubating at 37°C for 15 min, phenol/chloroform extracting, and ethanol precipitating (Gilman, 2001). The RNA products were then electrophoresed

through a 10% polyacrylamide/TBE/urea sequencing gel at 90 W for 75 minutes. The gel was dried, and exposed on a storage phosphor screen, and imaged on a Typhoon 9410 Variable Mode Imager.

Reconstituted telomerase activity assays

Linearized "run off" DNA templates for T7 transcription of telomerase RNAs were made for Figure 2 using *Fok*I-digested plasmids. For Figure 2.6, PCR products of the gene were transcribed using a T7 promoter included at the 5′ end of the forward primer. *In vitro* telomerase activity assays were performed as described previously (Zappulla et al., 2005). Briefly, linear DNA template for telomerase RNA was mixed with plasmid containing T7-ProA-Est2 in an RRL transcription and translation system. Telomerase was immunopurified with IgG-Sephadex beads. Telomerase beads were then incubated with telomeric primer, dNTPs, and [α-^{32}P]-dTTP. Products were electrophoresed through a 10% polyacrylamide/TBE/urea gel, and imaged using phosphor screens and a Typhoon 9410 Variable Mode Imager. As an internal control for product recovery and loading, ~1 nM [γ-^{32}P]-labeled primer was added before the telomerase reaction. Activity levels were normalized to the internal control, and to ProA-Est2 levels. [^{35}S]-Met labeled ProA-Est2 levels were determined by 7.5% SDS-polyacrylamide gel electrophoreses.

Chapter 3:

A second essential function of the Est1-binding arm of yeast telomerase RNA

Partially adapted from:

Kevin J. Lebo, Rachel O. Niederer, and David C. Zappulla. A second essential function of the Est1-binding arm of yeast telomerase RNA. *(Under Review for* Cell Reports*)*

3.1: ABSTRACT

I tested the hypothesis that a lengthy conserved region in the Est1-binding arm of TLC1 contributes more than simply recruiting Est1 to the holoenzyme. By tethering Est1 protein to TLC1 RNA through a heterologous RNA-protein binding module, I separated the Est1-binding role of TLC1 from other essential functions. Tethering rescues telomerase RNA alleles missing nucleotides specifically required for Est1 binding, but not those missing the entire conserved region. Notably, however, telomerase function is restored by expressing the Est1-binding arm of TLC1 *in trans*. Mutational analysis identified a Second Essential Est1-arm Domain (SEED) in the internal loop of the arm, which 3D modeling suggests could be regulated by a conformational change. The SEED functions independently from the Est1 protein. This discovery of a novel essential role for the Est1-binding arm of TLC1 suggests that the telomerase RNA flexible scaffold contributes more to telomerase function than simple tethering of accessory protein subunits.

3.2: INTRODUCTION

Although *EST1* was the first telomerase subunit-encoding gene identified (Lundblad and Szostak, 1989), many details of its function are still unknown. The primary role for Est1 protein is recruitment of telomerase to the telomere through an interaction with Cdc13, which also binds single-stranded telomeric DNA (Evans and Lundblad, 1999; Mitton-Fry et al., 2002; Tucey and Lundblad, 2013; Wu and Zakian, 2011). In addition, Est1 has a poorly understood role in activating telomerase function (Taggart et al., 2002), and deletion of *EST1* results in telomere shortening even when Est1-mediated recruitment is bypassed by fusing Est2 directly to Cdc13 (Evans and Lundblad, 1999, 2002).

Mutations in three discrete sets of nucleotides of the Est1-binding arm of TLC1 RNA have been shown to adversely affect association with Est1 protein *in vivo* (boxes in Figure 1A; Lubin et al., 2012; Seto et al., 2003). The first of these regions comprises 5 nts predicted to form a bulge in the arm (Seto et al., 2002). The second is within an internal loop closer to the tip of the Est1 arm; single-stranded RNA in the loop is critical for Est1 association with TLC1, and the nucleotide sequence is important for full protein association (Lubin et al., 2012). Two phylogenetically supported secondary structure models have been proposed for this internal loop; a single, large loop (Zappulla and Cech, 2004) or two smaller loops separated by three A-U base pairs (Dandjinou et al., 2004). Finally, the third region of TLC1 implicated in Est1 association is a single-stranded junction at the base of the conserved region (see “hinge” in Figure 3.2). TLC1 mutants lacking single-stranded RNA in this region have largely disrupted association with Est1 protein and exhibit short but stable telomeres (Lubin et al., 2012). Deleting all of the unpaired nucleotides in the Est1 arm below the hinge result in full loss of telomerase function (see Figure 2.9). Together, these three structural elements provide

the first essential function of the Est1 arm to be identified; namely, tethering Est1 protein to telomerase RNA.

The TLC1 long noncoding RNA has now been shown to act as a simple flexible scaffold for each of the three known RNA-binding accessory protein subunits, organizing them as “beads on a string” (Zappulla and Cech, 2004; Zappulla et al., 2011) (Lebo and Zappulla, 2012; Mefford et al., 2013; Zappulla and Cech, 2006). This indicates that the yeast telomerase RNP does not require the RNA-tethered subunits to occupy precise positions or orientations in the RNP for them to function (see Chapter 2). However, it remains unclear whether the arms of the RNA function only as tethers for binding the accessory subunits or if they have additional roles in telomerase function.

A recent publication reported an important role for portions of the apical hairpin and internal loop of the Est1-binding arm distinct from Est1-binding function (Laterreur et al., 2013). The reported mutants resulted in stably shorter telomeres, although the cells did not senesce. These alleles did not greatly affect TLC1 RNA levels and the authors found these mutant TLC1 RNAs remained nuclear by fluorescence microscopy, which permitted them to conclude Est1 was still binding. This provided evidence that the region includes a “telomerase-stimulating structure” that plays a non-essential role in telomerase enzyme activity. These findings support the hypothesis that the Est1 arm of TLC1 has additional functions in telomere maintenance beyond simply tethering Est1 to the RNP.

Here I demonstrate that, in addition to tethering Est1 protein to the RNP, the Est1 arm of TLC1 has a second essential function in telomere maintenance *in vivo*. Using a heterologous RNA-protein binding system, I was able to separate the Est1-binding role of the Est1 arm of TLC1 from other functions. I find that a Second Essential Est1-arm Domain (SEED) is located in an internal loop in the Est1-binding arm. SHAPE analysis and mutagenesis suggest that the structure of the internal loop, rather than its sequence,

is required. Overall, these data reveal an additional essential function for the Est1-binding arm of TLC1 and begin to elucidate Est1 arm structural conformations that could regulate telomerase action *in vivo*.

3.3: RESULTS

Although telomerase RNA is evolving very rapidly, the nucleotides and secondary structure in the distal half of the Est1 arm of TLC1 RNA — which includes three regions reported to be required for the essential Est1 association (see Figure 3.1; Lubin et al., 2012; Seto et al., 2002) — is highly conserved among budding yeasts (Dandjinou et al., 2004; Lin et al., 2004; Zappulla and Cech, 2004). To further examine conservation in the Est1-binding region of TLC1, I used an alignment all 36 publically available *Saccharomyces* TLC1 sequences from seven different *Saccharomyces* species (Figure 3.1; Mefford et al., 2013), and mapped sequence and base-pairing conservation onto the secondary structure model of the Est1 arm (Figure 3.2). This analysis revealed that the distal half of the arm is more than twice as conserved as the proximal half, with 54% of nucleotides being identical compared to only 24% in the core-proximal region (Figures 3.1 and 3.2). Additionally, the distal half has 15 nucleotides that covary or vary while maintaining the base pair, while the proximal half has only 4, suggesting higher structural conservation near the tip of the arm. This 108-nt Est1-arm conserved region includes two elements reported to be important for Est1 binding, while the third feature resides just outside of it (Lubin et al., 2012; Seto et al., 2002).

The Est1-binding arm of TLC1 has a second essential function

In order to test if the 108-nt Est1-arm conserved region of TLC1 has additional functions in telomere maintenance, I tethered Est1 to TLC1 using a heterologous protein-RNA interaction domain. I added MS2 coat protein domains to genomic *EST1*, using eight glycines as a linker (Figure 3.3). This *EST1-MS2CP* allele was functional, although it produced telomeres slightly shorter than wild type (see Figure 3.6B). I also used a TLC1 variant with 10 MS2 hairpins inserted just before the 3′ end of the

Figure 3.1: A lengthy conserved region in the Est1-binding arm of TLC1. 36 publically available *TLC1* sequences from seven *Saccharomyces* species (*cerevisiae, paradoxus, pastorianus, cariocanus, kudriavzevii, mikatae,* and *bayanus*) were aligned with the MUSCLE algorithm. Alignment of the Est1 arm (*S. cerevisiae* nts 504−704) is shown, with identical nucleotides highlighted in green. Co-varying nucleotides are highlighted in red, and nucleotides that vary yet retain base pairing are highlighted in blue. The 108-nt Est1-arm conserved region (nts 554−661) is labeled. Subdomains within the conserved region are also labeled (HH = Hinge-Hairpin, IL = Internal Loop, AH = Apical Hairpin, B = Bulge). Percent conservation for regions of the RNA is shown in black for nucleotides with 100% conservation, co-variation, or variation while retaining base pairing. Green numbers indicate percent of nucleotides with 100% conservation.

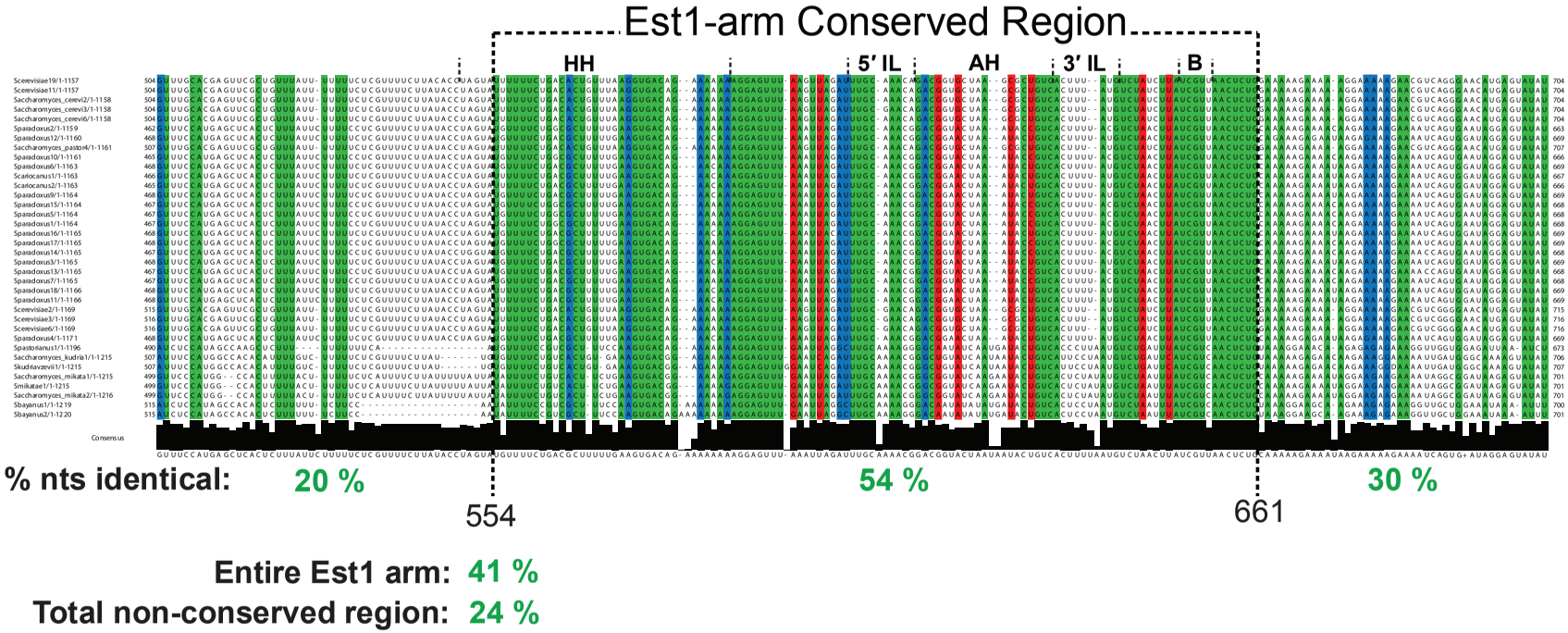
Est1-arm Conserved Region
HH
5′ IL
AH
3′ IL
B
% nts identical:
20 %
54 %
30 %
554
661
Entire Est1 arm: 41 %
Total non-conserved region: 24 %

Figure 3.2: The Est1-arm conserved region maps to the end of the Est1-binding arm secondary structure. Left, phylogenetically-supported secondary structure for TLC1 (Zappulla and Cech, 2004), with protein-binding sites indicated. Right, the phylogenetically-supported secondary structure of the *S. cerevisiae* Est1-binding arm of TLC1, with nucleotides highlighted based on the sequence alignment in Figure 3.1. Gray nucleotides are absent in one or more sequences. Gray arrows indicate locus of ≥1 nt insertion in one or more sequences. Dashed line indicates 108-nt Est1-arm conserved region (nts 554−661). Solid black boxes indicate elements proposed to be required for Est1 association.

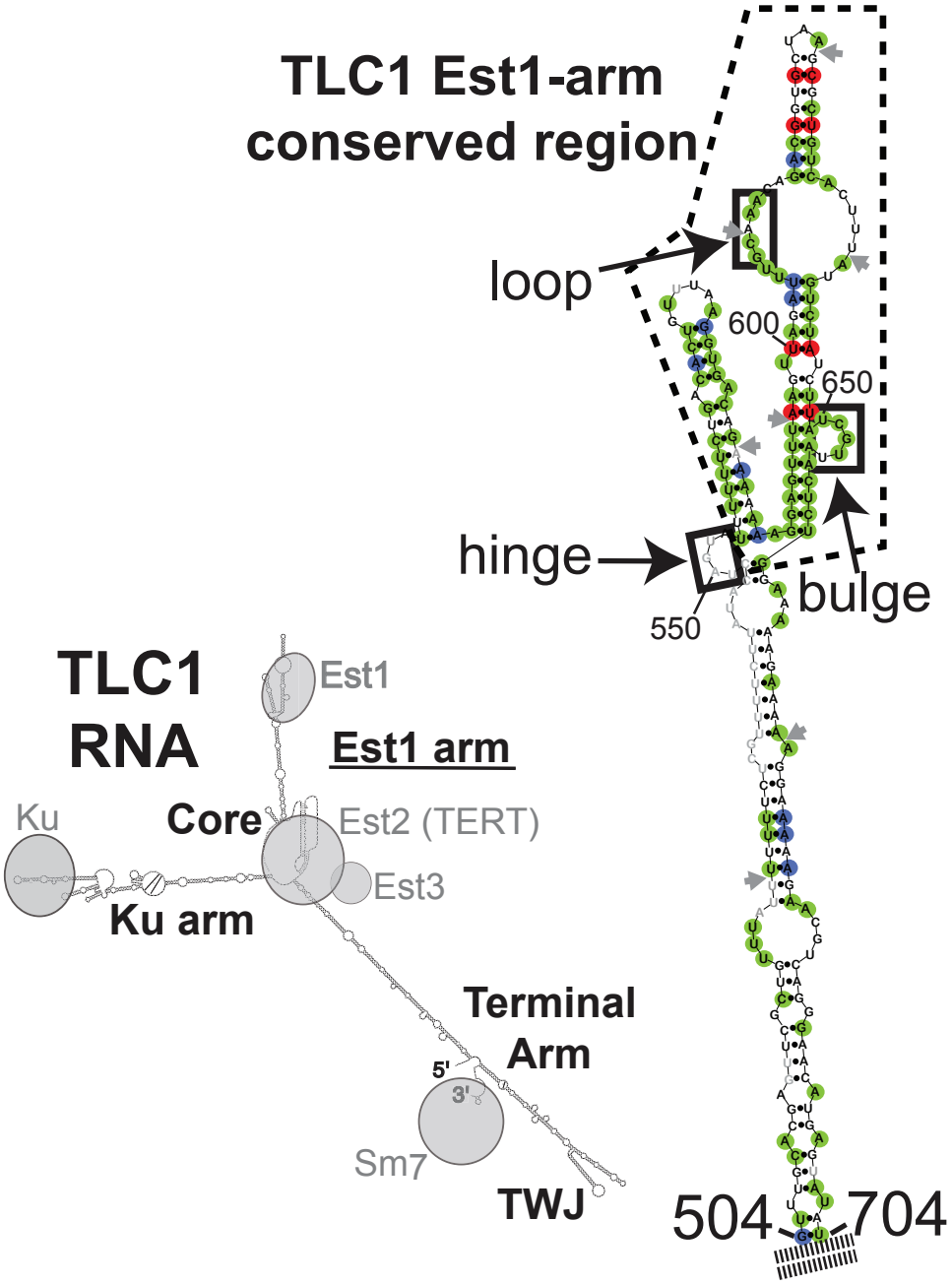
TLC1 Est1-arm
conserved region
loop
600
650
hinge
bulge
550
TLC1
RNA
Est1
Est1 arm
Ku
Core
Est2 (TERT)
Est3
Ku arm
Terminal
Arm
5'
3'
Sm7
TWJ
504
704

Figure 3.3: Gene and protein sequences of the Est1-MS2CP fusion. *Gly_8-$MS2CP_2$* was integrated in place of the stop codon of *EST1* at its endogenous chromosomal locus. *EST1* gene and protein sequences are highlighted in blue, Gly_8 linker in brown, and *MS2CP* sequences are in purple.

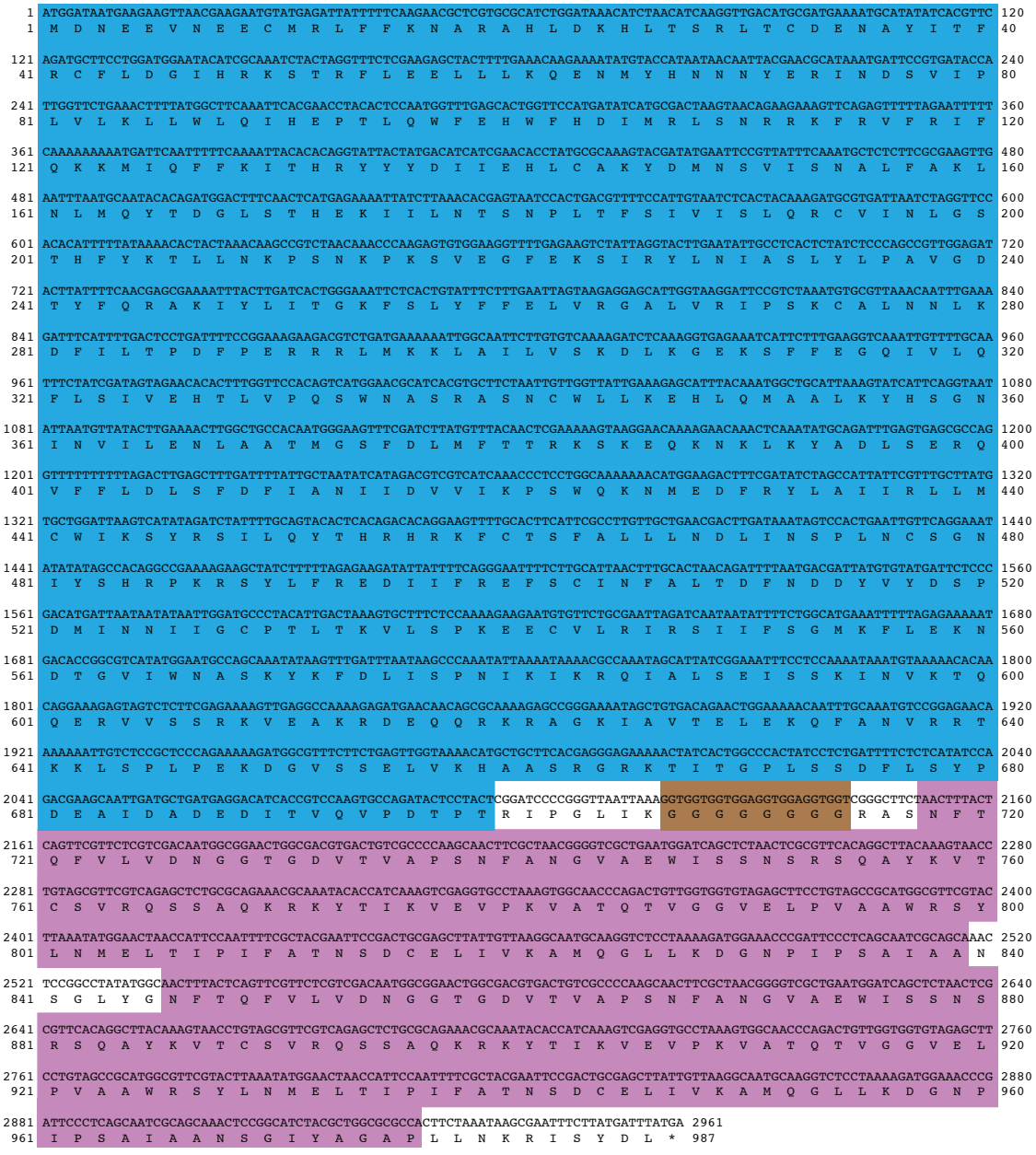

RNA, upstream of the Sm_7-binding site (Figures 3.4 and 3.5). This TLC1-MS2 construct has been shown to function similarly to wild-type TLC1 *in vivo* (Gallardo et al., 2011), although I observed moderately reduced RNA abundance and slightly shorter telomeres (Figure 3.6). With this experimental design, the MS2CP tag on Est1 should bind to the MS2 RNA hairpins in TLC1, thereby tethering Est1 to TLC1 even if the endogenous Est1-TLC1 binding interaction is disrupted (Figure 3.7A).

Tethering Est1-MS2CP protein to TLC1-MS2 RNA resulted in telomere length indistinguishable from wild type, a net increase compared to either individual fusion construct (Figure 3.6B). I next MS2-tethered Est1 to two different mutant TLC1 RNAs: (1) tlc1∆bulge, which lacks the 5-nt bulge in the Est1 arm and has greatly reduced binding to Est1 protein and loss of telomere maintenance (Lubin et al., 2012; Seto et al., 2002) or (2) tlc1∆ecr, which is missing the entire 108-nt Est1-arm conserved region of TLC1 (see Figures 3.2 and 3.5). The tlc1∆bulge and tlc1∆ecr RNAs without MS2 hairpins did not functionally complement a *tlc1*∆ strain, and failed to maintain telomeres, leading to senescence (Figure 3.7B). However, MS2-tethering tlc1∆bulge to Est1 restored telomere maintenance, allowing cells to grow without senescing (Figure 3.7B) and supporting stably shorter telomeres (Figure 3.6B). This indicates that the loss of telomerase function caused by the ∆bulge mutation is primarily a failure of Est1 to physically associate with the RNP, and that establishing direct binding through the MS2 tether is sufficient to rescue function. Furthermore, these results extend the flexible scaffold model for TLC1 by demonstrating that an essential Est1-binding interface in TLC1 can be functionally replaced with a heterologous RNA-protein direct-binding system.

In contrast, MS2-tethering tlc1∆ecr RNA to Est1 did not rescue telomerase-mediated telomere maintenance, and cells senesced by 125 generations (Figure 3.7B). Senescence was confirmed by telomere Southern blots, which showed that the few

Figure 3.4: RNA nucleotide sequence for TLC1-MS2. TLC1 is highlighted in gray, and the ten MS2 hairpins highlighted in yellow (Gallardo et al., 2011).

GAGAGGAAGAUAGGUACCCUAUGAAAAUGUCAAUGGCUGUUGCGUUUGCUUAAUCGUAUUUUUUUUUUUUUUCA
GUCCGUGUUUUUUGUACAUUCUACGUUUGAGUUUUCCAUCAUGCAGGCCUCAGAAAUUUGGUAGGCACUCGAU
GGUGAAGAGAUAGUGUCGGAUUUCGGAUUGAUCUUUCAGUUGAUAGCCUGCUGCUCUUUUCUUUUCCAAAGAA
UUUCGAGUAUGCUGGUGUCAGUGUAGAUGCUUGUGUGUGCGCAAUUUGUGGUUUUUUAUUGUGUUUCUACUUA
UAGAUGGCUAAAAUCUGAGUUUAGAAAAUGCAAACCGUAAAUUCUUAAACACUGCUAUUGCAUUUAGUUGCUA
AAGCAGUGUUUUUGAACUUAUUCCUGUUAUUCCUUCUUCGUACCGAUCCUCUUCUCGACCUAACCUUUUAAUU
ACCAUGGGAAGCCUACCAUCACCACACCCACACACAAAUGUUACAGCUAAUUGUUUAUUAGCAAAGUUUGCAC
GAGUUCGCUGUUUAUUUUUUUCUCGUUUUCUUAUACCUAGUAUUUUUUCUGACACUGUUUAAGGUGACAGAAA
AAAAGGAGUUUAAGUUAGAUUUGCAAACAGACGGUGCUAAGCGCUGUCACUUUAUGUCUAUCUUAUCGUUAAC
UCUGGAAAAAGAAAAAGGAAAAAGAACGUCAGGGAACAUGAGUAUAUAUAGAAAUGGUUUAUUCUAGUUUUUU
CCGUUUUUUCAGUAGAUUUUUGCCUUUAAAAGAAUAAAUCCCACUACAAAAAGGUAAAAUAAAAAAUCUAUUC
ACUGAACUUACUGAUGAAAUUUCCAAAUGUGCCCCGUACAUCGAACGAUGUGACAGAGAAAAAUACGAGUAGG
UAAAUAAGCCAAAAGGCAAGGGUGUCCUUUCUUAAGCAUCGGUUAGGUUUGCGGGCGAUCAGUAACUGAACAA
UGACACAAGAUCAAGAACGUAAUUUGAGAUUUUUCAAGAUGGUUUUUUUAGGUAUCUAUUAAAACUACUUUGA
UGAUCAAUACGGUAUUUUUGUCGCAUUAUUUUCCAAGCGGAAGGAACCGUGUGUUCAUUUUAUGAAUCUUGGU
GUUGUAUUCACAGCUACUUCUCCUAAUGCCUUCGAUGCAGAAACAUGAGGAUCACCCAUGUCUGCACGUCGAC
UCUAGAAAACAUGAGGAUCACCCAUGUAUGCAGAAACAUGAGGAUCACCCAUGUCUGCACGUCGACUCUAGAA
AACAUGAGGAUCACCCAUGUAUGCAGAAACAUGAGGAUCACCCAUGUCUGCACGUCGACUCUAGAAAACAUGA
GGAUCACCCAUGUAUGCAGAAACAUGAGGAUCACCCAUGUCUGCACGUCGACUCUAGAAAACAUGAGGAUCAC
CCAUGUAUGCAGAAACAUGAGGAUCACCCAUGUCUGCACGUCGACUCUAGAAAACAUGAGGAUCACCCAUGUA
UGCAUUUAGAUAAUUUUUGGAAACAUU

Figure 3.5: TLC1-MS2 variant secondary structures. Lowest-free-energy *Mfold* secondary structure predictions for TLC1 Est1-arm mutants: TLC1-MS2 with wild-type Est1 arm, Est1 arms from tlc1Δbulge, tlc1Δecr, TLC1ΔAH, tlc1ΔHH, tlc1ΔIL, TLC1(3-1), tlc1(5-1), tlc1(5-2), tlc1(5-3). Colors are in *Mfold* "p-num" format, where the red end of the color spectrum indicates most energetically well-determined structures (Zuker and Jacobson, 1998). The Est1 arm for each mutant is shown, after folding in the context of the entire RNA. Each Est1 arm mutation had similar overall secondary structures, suggesting that the mutations do not disrupt global RNA folding. Note that the central core region of tlc1ΔHH is predicted to fold differently due to the stiffened Est1 arm; the *Mfold* structure in the core is similar to that of Triple-Stiff-Arm TLC1, which is functional *in vivo* and *in vitro* (see Chapter 2 and (Lebo and Zappulla, 2012).

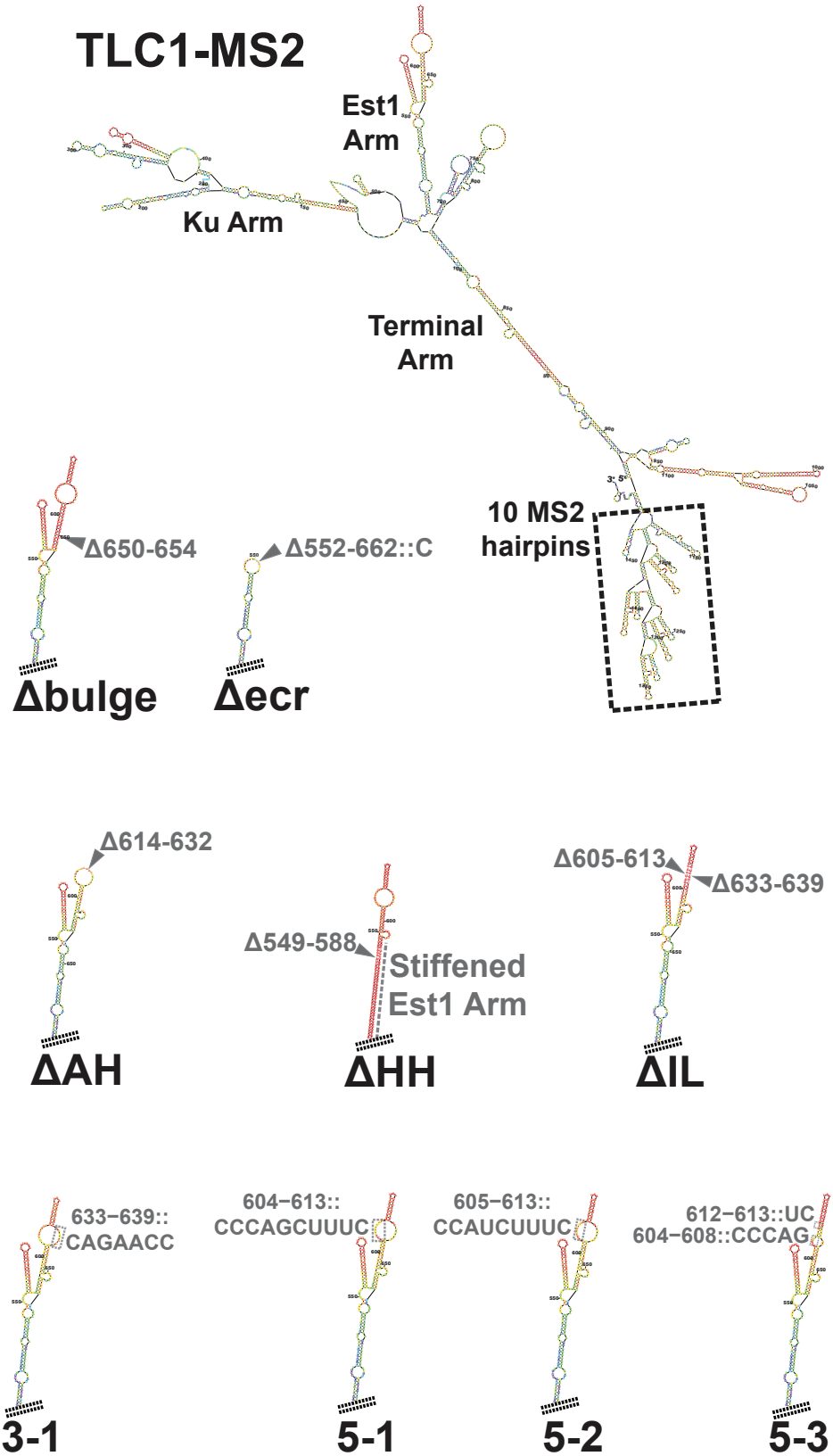
TLC1-MS2
Est1
Arm
Ku Arm
Terminal
Arm
10 MS2
hairpins
Δ650-654
Δbulge
Δ552-662::C
Δecr
Δ614-632
ΔAH
Δ549-588
Stiffened
Est1 Arm
ΔHH
Δ605-613
Δ633-639
ΔIL
633−639::
CAGAACC
3-1
604−613::
CCCAGCUUUC
5-1
605−613::
CCAUCUUUC
5-2
612−613::UC
604−608::CCCAG
5-3

Figure 3.6: Effects of Est1-arm conserved region mutants on telomere length and RNA abundance. (**A**) Northern blot of Est1 arm mutants in an *EST1* strain. TLC1 RNAs were probed for the shared 3′ end, and normalized to U1 RNA. Average relative RNA abundance from two independent isolates at 25 generations of growth are indicated ± SD. *Note that tlc1ΔHH migration is impeded in urea-PAGE due to the stiffened arm, and the RNA abundance is likely underestimated (see Chapter 2 and (Lebo and Zappulla, 2012). (**B**) Telomere Southern blot for Est1-binding arm mutants in *EST1* and *EST1-MS2CP* strains. Colonies were picked at 250 generations of growth. Red mutant names indicate survivor colonies that arose from senescent samples. A telomere pattern typical of Type I survivors can be observed in the senescent sample lanes (red asterisk; Teng and Zakian, 1999), confirming that telomerase-mediated telomere lengthening was disrupted. Average change in Y′ telomere length ± sample SD is shown relative to wild type (TLC1 in *EST1*) from two independent isolates, or relative to TLC1-MS2 in the specific strain (from two isolates for *EST1*, and three for *EST1-MS2CP*). IC = Internal control, a non-telomeric *Xho*I fragment from chromosome IV.

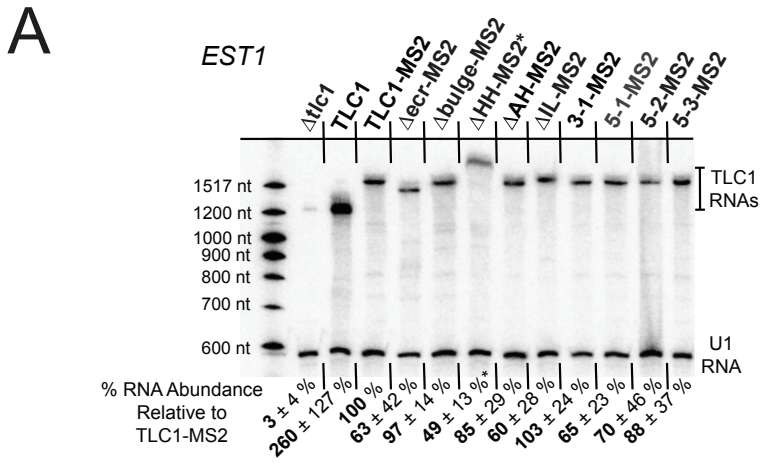

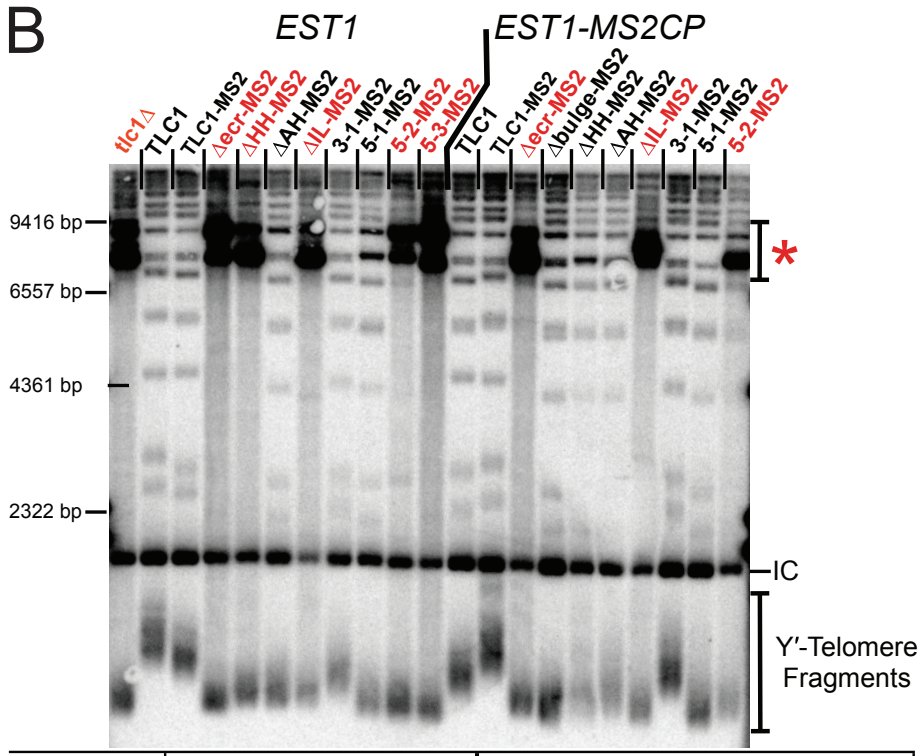

Strain:	*EST1*					*EST1-MS2CP*						
RNA:	TLC1	TLC1-MS2	ΔAH-MS2	3-1-MS2	5-1-MS2	TLC1	TLC1-MS2	Δbulge-MS2	ΔHH-MS2	ΔAH-MS2	3-1-MS2	5-1-MS2
Difference from WT telomere length (bp):	0 ± 0	−52 ± 16	−172 ± 1	−131 ± 3	−217 ± 36	−91 ± 26	−10 ± 52	−180 ± 4	−132 ± 33	−125 ± 1	−46 ± 28	−163 ± 28
Difference from TLC1-MS2 telomere length by strain (bp):	+52 ± 16	0 ± 0	−120 ± 17	−79 ± 18	−166 ± 52	−81 ± 78	0 ± 0	−134 ± 74	−135 ± 32	−115 ± 36	−43 ± 58	−149 ± 57

Figure 3.7: The Est1-binding arm of TLC1 has a second essential function in telomere maintenance. (**A**) Schematic of MS2-tethered Est1 mediating telomerase RNP recruitment to the telomere. (**B**) MS2-tethering Est1 to tlc1Δbulge, but not tlc1Δecr, is sufficient for telomerase function. *TLC1* alleles with or without MS2 hairpins were expressed in *EST1-MS2CP* cells. Streaks are shown at 125 generations of growth.

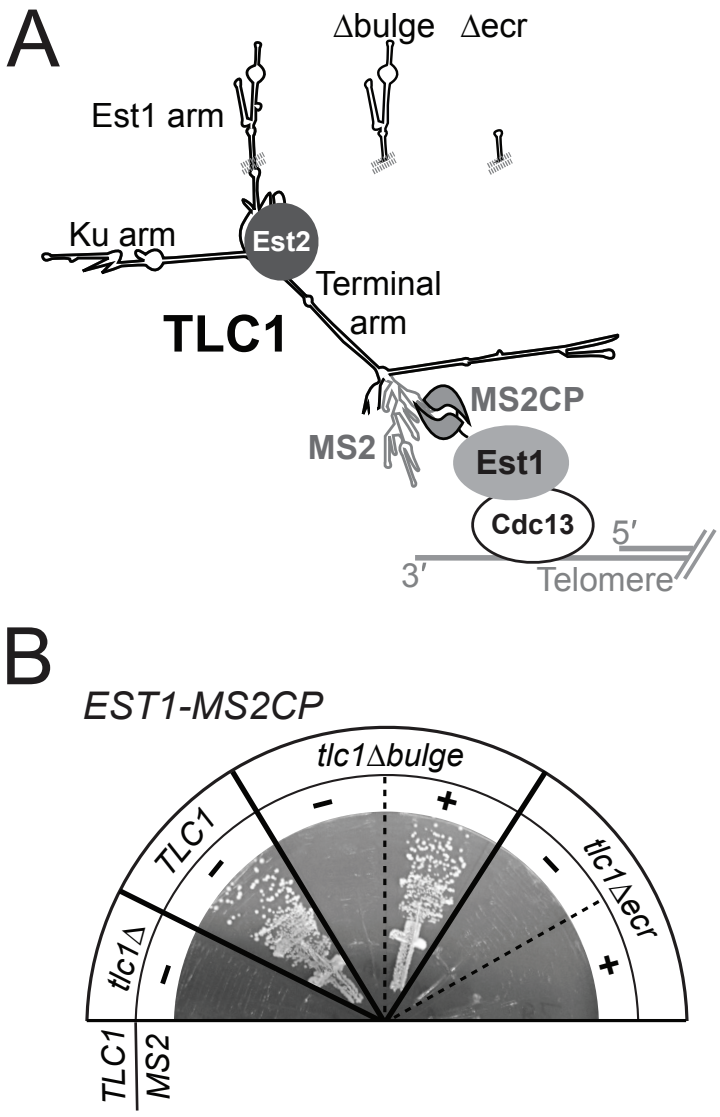

cells that occasionally survived were Type-I post-senescence survivors, which maintain telomeres telomerase-independently via recombination (Figure 3.6B; Lundblad and Blackburn, 1993; Teng and Zakian, 1999). The abundance of tlc1∆ecr-MS2 RNA was approximately 60% of TLC1-MS2 RNA levels (Figure 3.6A), showing that RNA abundance is not responsible for abolished telomerase function. The fact that MS2-tethering Est1 to tlc1∆ecr does not allow telomerase function strongly suggests that a portion of the conserved region of the Est1-binding arm (Figure 3.2) retained in tlc1∆bulge, but missing in tlc1∆ecr, is essential for an Est1-binding-independent telomerase process. I therefore propose that this region contains a Second Essential Est1-arm Domain (SEED) functionally distinct from the reported Est1-binding sites.

In parallel with the MS2-tethering system, I also tested a system in which Est1 is covalently bound to Est2. By integrating the *EST2* coding sequence in place of the *EST1* stop codon in its genomic locus, connected by an eight-glycine linker, I was able to ensure that Est1 would be part the telomerase RNP even when Est1-binding sites on TLC1 were disrupted (Figure 3.8). Like MS2-tethering Est1 to TLC1, the Est1-Est2 fusion protein was able to function with tlc1∆bulge; cells did not senesce, and telomeres were maintained stably shorter than wild type (Figure 3.9). However, the Est1-Est2 fusion did not rescue telomerase function in tlc1∆ecr cells. These results strongly support the findings from the MS2-tethering experiments: heterologously tethering Est1 to the telomerase RNP can restore telomere maintenance to cells expressing Est1-binding-deficient variants of TLC1, but not to those lacking the SEED.

The SEED can function as part of an Est1 arm RNA expressed *in trans*

If the second essential function of the Est1 arm is distinct from binding Est1 protein to tether it to the telomerase RNP, then the SEED could perhaps even function *in trans*. I tested this by expressing the Est1 arm from a constitutive *TEF2* promoter harbored

Figure 3.8: Gene and protein sequence for *EST1-EST2*. *Gly_8-EST2* was integrated in place of the stop codon of *EST1* at its endogenous chromosomal locus. *EST1* gene and protein sequences are highlighted in blue, Gly_8 linker in brown, and *EST2* sequence is in green.

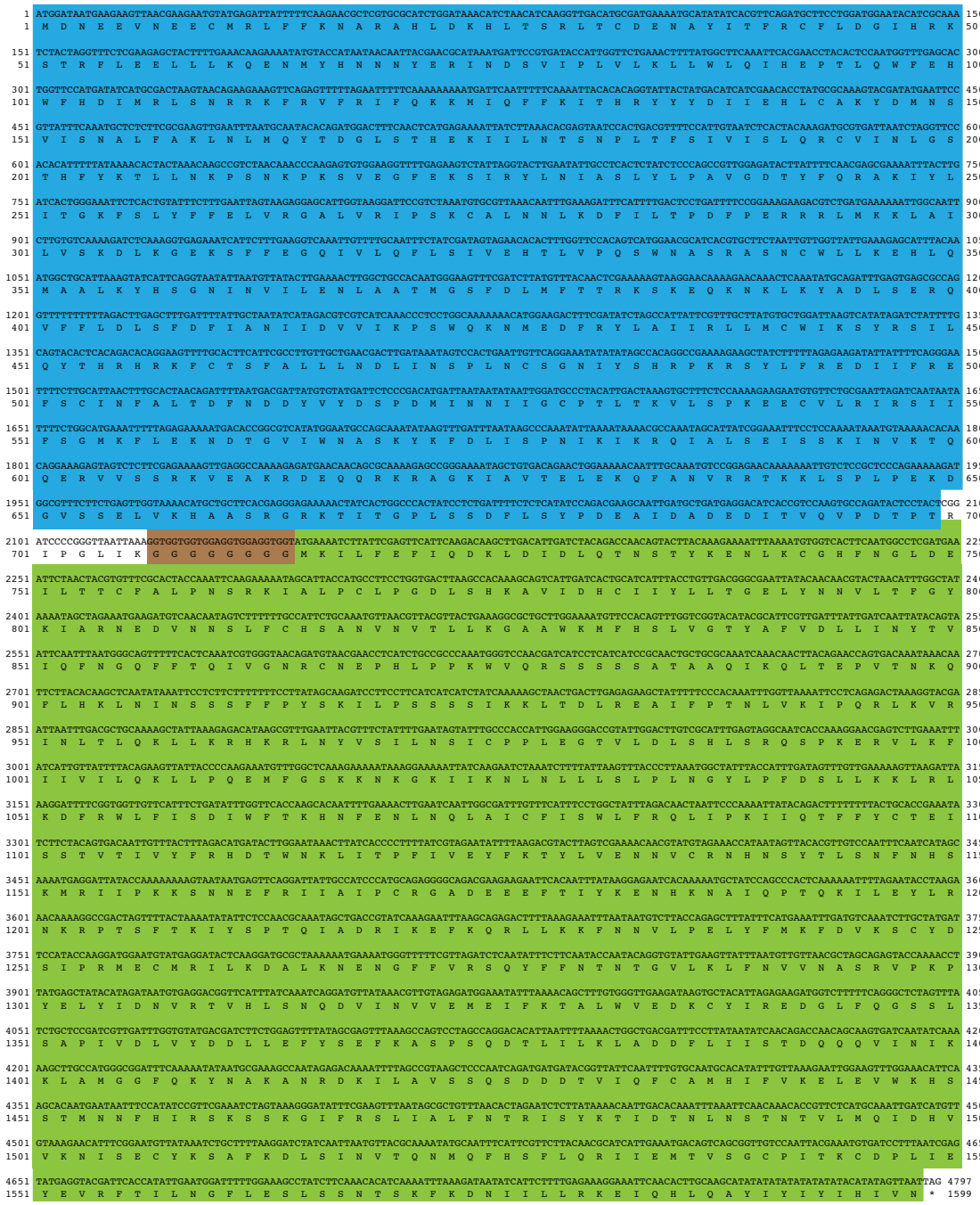

Figure 3.9: Covalently attaching the Est1 and Est2 proteins behaves similarly to MS2-tethering Est1 to TLC1 RNA. (**A**) *EST1-EST2* rescues Est1-binding deficient TLC1 mutants from senescence, but does not rescue mutants lacking the second essential domain. Plate showing *EST1-EST2* cells expressing TLC1 variants is shown at 125 generations of growth: tlc1Δ; wild-type TLC1; tlc1Δecr, which lacks the second essential domain; tlc1Δbulge, which disrupts Est1 association to TLC1; tlc1Δ606−639::GAAA, which lacks the internal loop and apical hairpin; and tlc1ΔHH, which disrupts Est1 association. (**B**) Telomere Southern blot for Est1-binding arm mutants in the *EST1-EST2* strain. Two independent isolates for each condition at 250 generations of growth are shown. IC = Internal control, a non-telomeric *Xho*I fragment from chromosome IV.

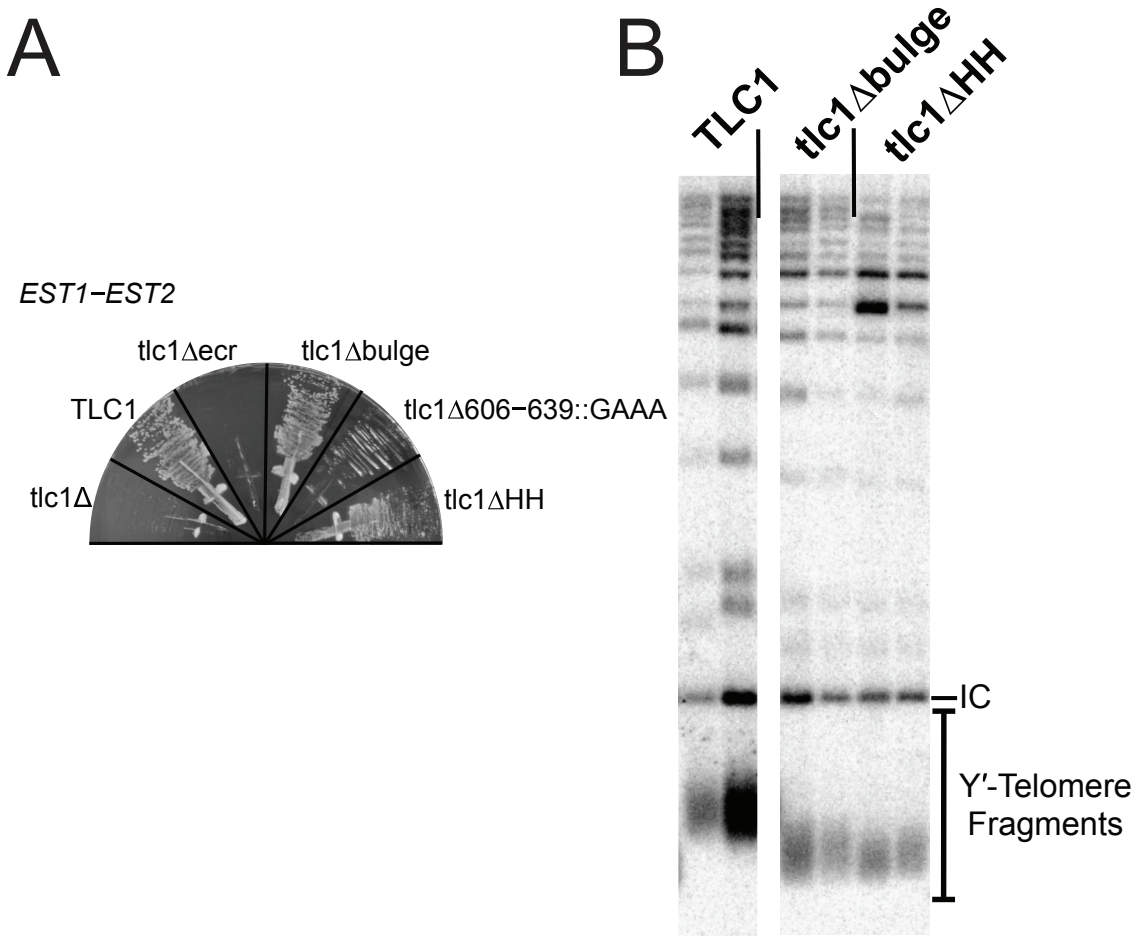

on a multiple-copy 2μ plasmid (Figure 3.10; Mumberg et al., 1995). Although the Est1 arm expressed *in trans* is expected to bind to Est1 protein, it should not help tether Est1 to the telomerase RNP since it is a separate RNA molecule. Expressing the arm *in trans* with wild-type TLC1 did not have a significant effect on telomere length (Figure 3.11).

Expression of the Est1 arm of TLC1 *in trans* while Est1 protein was MS2-tethered to the tlc1Δecr RNA rescued cells from senescence (Figure 3.11A), indicating that the SEED can function in telomere maintenance as a separate RNA molecule. However, in the absence of MS2-tethering Est1 to tlc1Δecr RNA, the *in trans* Est1 arm did not prevent senescence (Figure 3.11A). This confirms that Est1 protein binding to full-length TLC1 is still required for the ectopic arm to provide its other function. In summary, these results show that the SEED can function *in trans* when Est1 is MS2-tethered to the telomerase RNA, indicating that the Est1 arm of TLC1 has a second essential function beyond simply scaffolding proteins in the telomerase RNP.

Interestingly, certain Est1-binding arm mutants are unable to restore SEED function *in trans*. Like the wild-type *in trans* Est1 arm, the stiffened Est1 arm from TSA-T (see Chapter 2), without mutations in the Est1-arm conserved region, restored telomere maintenance when Est1 protein is MS2-tethered to tlc1Δecr (Figure 3.11D). However, variants with mutations known to disrupt Est1 protein association to the Est1-binding arm, including deletions of the bulge and hinge-hairpin domains, were unable to rescue cells from senescence (Figure 3.11D). This suggests that, although it can function when expressed as a separate RNA *in trans* in the cell, the *in trans* Est1 arm still needs to be able to bind to Est1 protein for proper SEED function when Est1 is tethered to tlc1Δecr. I hypothesize that this is not a requirement for Est1-binding *per se*, but rather that the SEED must be recruited to the telomerase RNP in order to function.

Figure 3.10: Design of an *in trans* Est1 arm transcript. (**A**) Predicted RNA sequence of the *in trans* Est1 arm transcript. The Est1 arm (TLC1 nts 514−694) is highlighted in gray. Five G or C nucleotides were added to either side (highlighted in brown), to form G-C pairs to aid in proper folding. The rest of the RNA is predicted to be transcribed due to the *TEF2* promoter (Mumberg et al., 1995) and *CYC1* terminator (Russo and Sherman, 1989). Like wild-type TLC1, the *in trans* RNA is a Pol II transcript, and is expected to be polyadenylated. (**B**) Lowest energy *Mfold* secondary structure prediction for the *in trans* Est1 arm RNA transcript. Colors are in *Mfold* "p-num" format (Zuker and Jacobson, 1998), where the red end of the color spectrum indicates most energetically well-determined structures. The Est1 arm is predicted to fold as in TLC1. A GC "clamp" at the base of the Est1 arm helps to ensure proper folding.

A

UCUAGAACUAGUGGCCGGUUCGCUGUUUAUUUU
UUUCUCGUUUUCUUAUACCUAGUAUUUUUUCUG
ACACUGUUUAAGGUGACAGAAAAAAAGGAGUUU
AAGUUAGAUUUGCAAACAGACGGUGCUAAGCGC
UGUCACUUUAUGUCUAUCUUAUCGUUAACUCUG
GAAAAAGAAAAAGGAAAAAGAACGUCAGGGAAC
CGGCCCUCGAGUCAUGUAAUUAGUUAUGUCACG
CUUACAUUCACGCCCUCCCCCCACAUCCGCUCU
AACCGAAAAGGAAGGAGUUAGACAACCUGAAGU
CUAGGUCCCUAUUUAUUUUUUUAUAGUUAUGUU
AGUAUUAAGAACGUUAUUUAUAUUUCAAA...

Poly-A tail

B

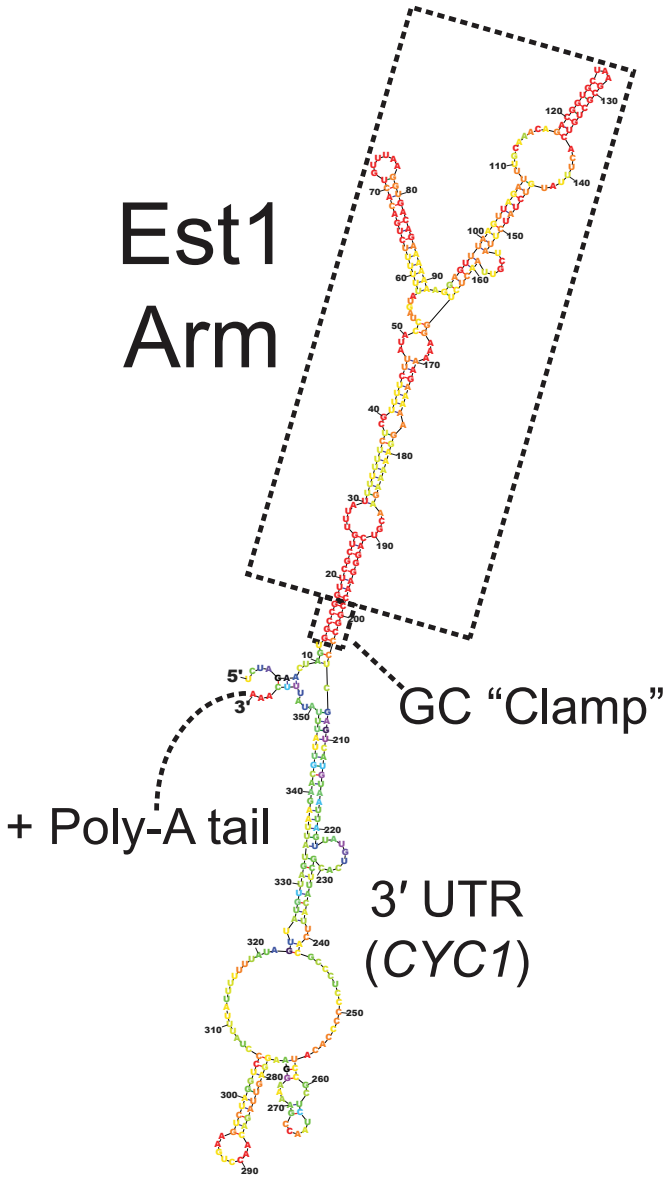

Figure 3.11: The second essential Est1 arm domain can function when expressed as part of a separate RNA *in trans*. (**A**) Expression of the Est1 arm *in trans* restores telomerase activity when Est1 is MS2-tethered to tlc1∆ecr. *TLC1* alleles with or without MS2 hairpins expressed in *EST1-MS2CP* cells along with the Est1 arm *in trans*. Streaks shown at 125 generations of growth. (**B**) Northern blot for probed for Est1 arm expression in Est1-MS2CP cells. The two Est1-arm bands correspond to predicted sizes for a non-polyadenylated arm (~389 nt; lower band) and a polyadenylated arm (~400−450 nts; upper band). (**C**) Telomere Southern blot for Est1-MS2CP cells with or without the *in trans* Est1 arm. Two or four independent transformants are shown for each condition after 250 generations of growth. Average changes in Y′ telomere length relative to TLC1 are indicated ± SD. Internal control = non-telomeric *Xho*I fragment from chromosome IV. (**D**) Est1 arm variants lacking Est1-association domains cannot restore the second essential function when expressed *in trans*. ∆IL+AH arm lacks TLC1 nucleotides 603−644. Streaks shown at 125 generations of growth.

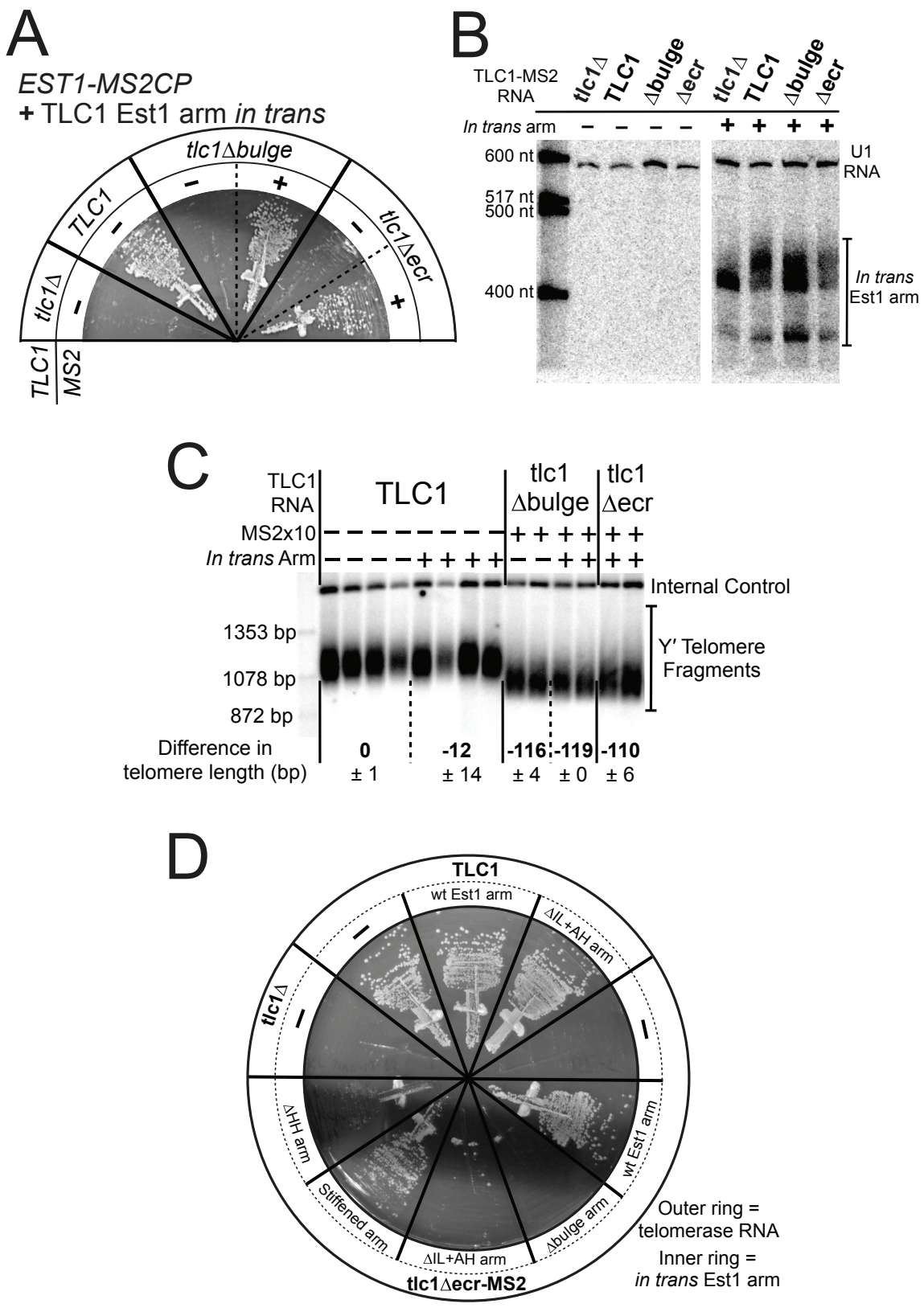
A
EST1-MS2CP
+ TLC1 Est1 arm in trans
tlc1Δbulge
TLC1
tlc1Δ
tlc1Δecr
TLC1
MS2
B
TLC1-MS2 RNA
tlc1Δ
TLC1
Δbulge
Δecr
tlc1Δ
TLC1
Δbulge
Δecr
In trans arm
600 nt
517 nt
500 nt
400 nt
U1 RNA
In trans Est1 arm
C
TLC1 RNA
TLC1
tlc1 Δbulge
tlc1 Δecr
MS2x10
In trans Arm
Internal Control
1353 bp
1078 bp
872 bp
Y′ Telomere Fragments
Difference in telomere length (bp)
0 ± 1
-12 ± 14
-116 ± 4
-119 ± 0
-110 ± 6
D
TLC1
wt Est1 arm
ΔIL+AH arm
tlc1Δ
ΔHH arm
wt Est1 arm
Stiffened arm
Δbulge arm
ΔIL+AH arm
tlc1Δecr-MS2
Outer ring = telomerase RNA
Inner ring = in trans Est1 arm

A conserved internal loop of the TLC1 Est1 arm is required for SEED function

To determine more precisely the region containing the SEED, I designed a series of deletions in the Est1 arm of TLC1 to test specific RNA elements. To accurately target these elements, I used a secondary structure model of the Est1 arm conserved region that was supported by selective 2′-hydroxyl acylation analyzed by primer extension (SHAPE), performed by Rachel O. Niederer (Figure 3.12A; Lebo *et al.*, *submitted*). Based on SHAPE analysis, I designed deletions of the apical hairpin (AH), the hinge-hairpin structure (HH), and the internal loop (IL) (Figures 3.5 and 3.12A). Deleting the 19-nt AH from the Est1 arm did not cause senescence (Figure 3.12B), in agreement with previously reported deletions in the apical hairpin (Laterreur et al., 2013; Lubin et al., 2012).

Next, I tested deletions of the hinge-hairpin (HH) domain (Figures 3.5 and 3.12A). To help ensure that no unpaired nucleotides remained at the base of the conserved region to provide surrogate hinge-like flexibility in the deletion mutant, tlc1ΔHH also has all bulges and loops from the core-proximal portion of the Est1 conserved region deleted (see Chapter 2 and Figure 2.9). This tlc1ΔHH RNA was unable to maintain telomeres, resulting in senescence (Figure 3.12B). This phenotype was not due to decreased RNA abundance, since northern blots showed this RNA (as well as each of the other TLC1 Est1-arm mutants) was substantially above the threshold for function (Figure 3.6A; Mefford et al., 2013; Seto et al., 1999). Consistent with tlc1ΔHH having a defect in Est1 binding, MS2-tethering Est1 to the RNA rescued tlc1ΔHH and cells did not senesce (Figure 3.12B). After being propagated for 250 generations to reach equilibrium, telomeres from these cells were 135 bp shorter than TLC1-MS2, similar to the 134-bp shortening for the condition with Est1 tethered to tlc1Δbulge (Figure 3.6B). This suggests that, like the 5-nt bulge, the hinge-hairpin element in the Est1 arm is important for proper Est1 protein association with TLC1, and not for SEED function.

Figure 3.12: The Second Essential Est1-arm Domain (SEED) maps to a large internal loop of the Est1 arm. (A) Secondary structure of the Est1-binding arm conserved region, colored based on SHAPE analysis (Lebo *et al.*, *submitted*). Red nucleotides are highly reactive, orange are moderately reactive, and black lines have low reactivity. Structural elements of the Est1 arm are boxed: HH = Hinge-Hairpin (nts 549−588), AH = Apical Hairpin (nts 614−632), IL = Internal loop (nts 605−613 and 633−639). Black lines in the internal loop highlight nts 609−611 and 635−637, which have been proposed to form base pairs. (B) MS2-tethering Est1 to TLC1 alleles with deletions of structural elements of the Est1 arm maps the second function to the internal loop. All *TLC1* alleles are tagged with MS2 hairpins, and expressed in cells with *EST1* (top) or *EST1-MS2CP* (bottom). Streaks shown represent 150 generations of growth.

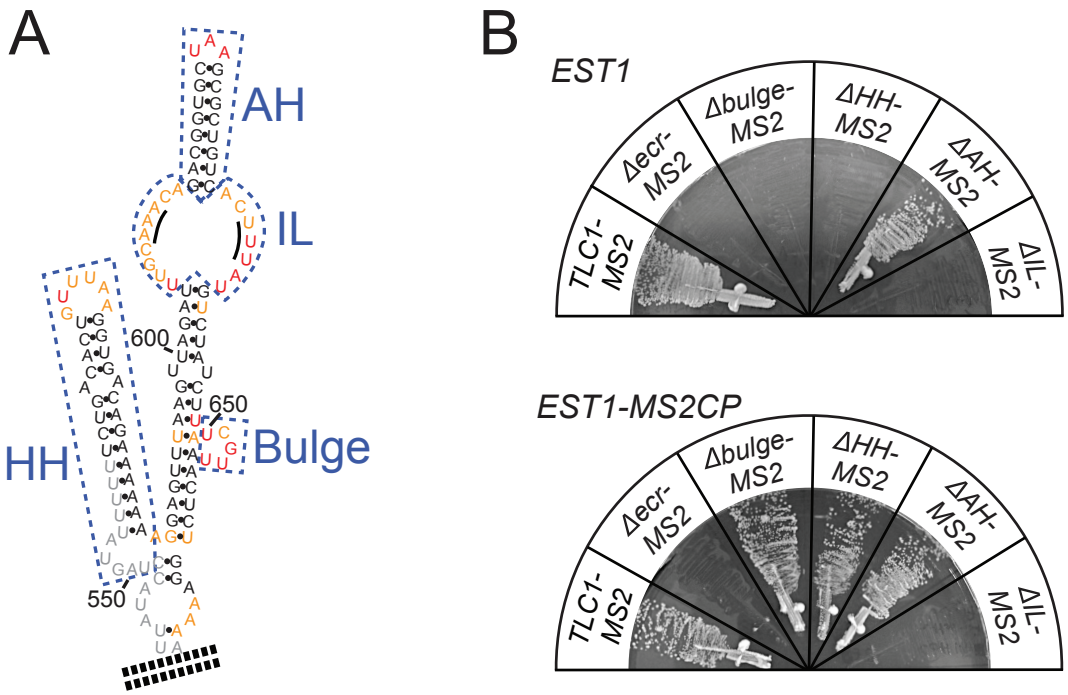

Finally, I deleted the Est1 arm internal loop (IL) (Figures 3.5 and 3.12A) and found that it caused senescence. However, in contrast to the ∆bulge and ∆HH deletion mutants, MS2-tethering Est1 to tlc1∆IL did not rescue telomerase function (Figure 3.12B). This unique result provides compelling evidence that the Second Essential Est1-arm Domain of TLC1 is located within this internal loop.

Mutations that disrupt structure of the internal loop also disrupt SEED function

To understand how structure of the internal loop relates to SEED function, I made a series of nucleotide substitution mutations within the internal loop. We first altered the sequence of the entire 3′ side of the loop, while maintaining internal loop secondary structure based on *Mfold* predictions (Figures 3.5 and 3.13A). Mutant TLC1(3-1) did not exhibit senescence, maintaining telomeres slightly shorter than wild type (Figures 3.13C and 3.6B), and indicating that the sequence of the 3′ side of the internal loop is not essential for binding Est1 or for SEED function.

I next made sequence mutations in the 5′ side of the internal loop. Mutant tlc1(5-1) has all 5′-side nucleotides substituted as shown in Figure 3.13A, and is still predicted by *Mfold* to form a single internal loop (Figure 3.5). SHAPE analysis demonstrated that there is a moderate reduction in nucleotide reactivity in the internal loop compared to wild type, demonstrating a loss of flexibility in portions of the structure, whereas the lower half of the 3′ side of the loop remained highly reactive (Figure 3.13B; Lebo *et al.*, *submitted*). Cells expressing tlc1(5-1) grew poorly and occasionally displayed a delayed senescence phenotype in the absence of tethering (Figure 3.13C), which is consistent with this allele exhibiting extremely short telomeres (Figure 3.6B).

MS2-tethering Est1 protein to tlc1(5-1) prevented senescence and restored telomere maintenance to levels similar to the condition of Est1 MS2-tethered to tlc1∆bulge (Figures 3.13C and 3.6B). Since tethering Est1 to tlc1(5-1) suppresses its

Figure 3.13: The structure of the internal loop is required for SEED function. (**A**) Schematic of nucleotide substitution mutants in the large internal loop of the Est1-arm conserved region. Mutant nucleotides are boldface. Arrowheads indicate nucleotides that differ from mutant 5-1. (**B**) Secondary structures of internal loop nucleotide sequence substitution mutants, colored based on SHAPE analysis (Lebo *et al.*, *submitted*) Asterisks indicate non-wild-type nucleotides in the mutants. Orange arrow indicates residue U604, with high SHAPE reactivity in mutant 5-2. Dotted lines indicate base pairs predicted to form by *Mfold* in mutant 5-3. (**C**) Mutants tlc1(5-2) and tlc1(5-3) have lost SEED function since they cannot be rescued by MS2-tethering Est1. All *TLC1* alleles were tagged with MS2 hairpins, and expressed in cells expressing *EST1* (top) or *EST1-MS2CP* (bottom). Streaks shown represent 150 generations of growth.

A

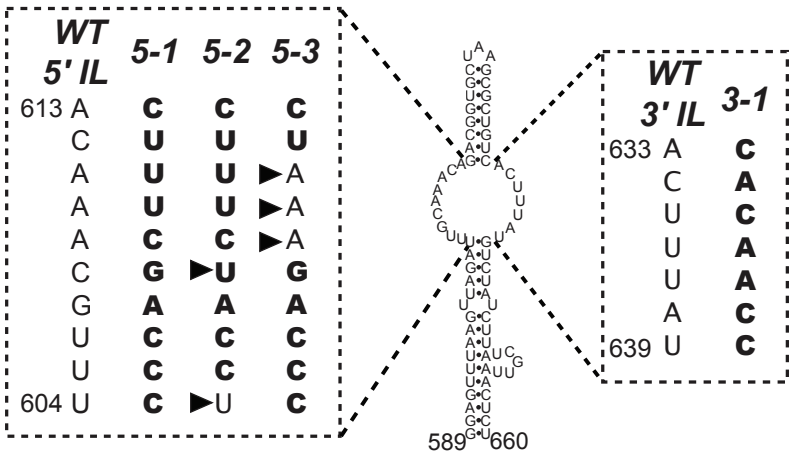
WT 5′ IL
5-1
5-2
5-3
613 A C A A A C G U U 604 U
C U U U C G A C C C
C U U U C U G A C C
C U A A A G A C C U
WT 3′ IL
3-1
633 A C U U U A 639 U
C A C A A C C
589
660

B

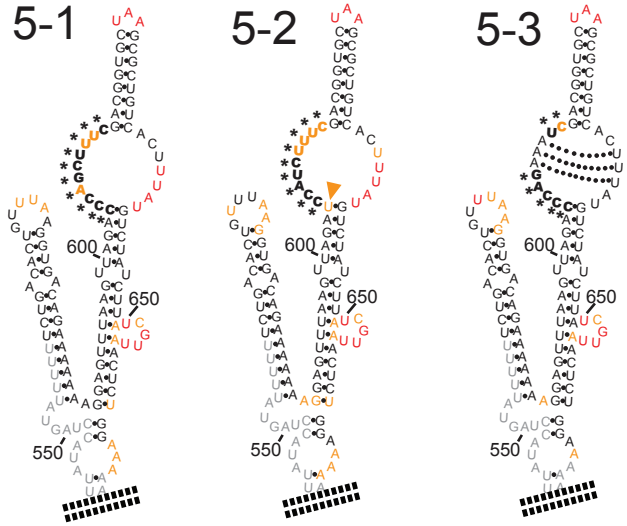
5-1
5-2
5-3
600
650
550

C

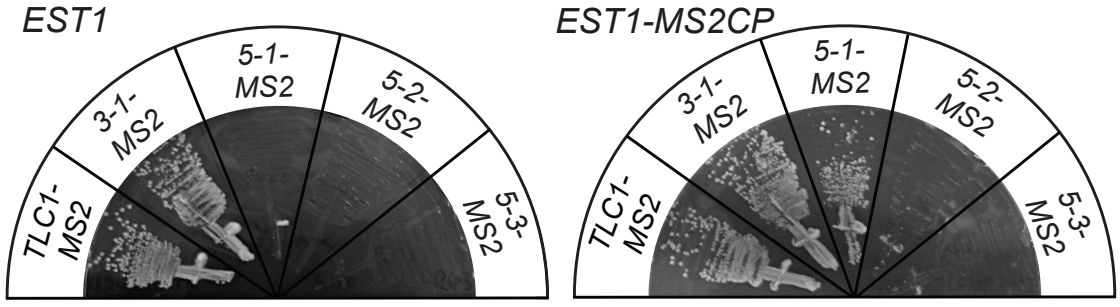
EST1
EST1-MS2CP
TLC1-MS2
3-1-MS2
5-1-MS2
5-2-MS2
5-3-MS2

phenotype, I conclude that mutations in the 5′ side of the internal loop cause a loss of Est1 association with the RNA, similar to previously reported internal loop mutants (Lubin et al., 2012), and do not abolish SEED function.

While nucleotide substitutions in the internal loop are tolerated, mutants that alter the structure of the loop disrupt SEED function. I designed a second IL 5′-side mutant, tlc1(5-2), with two different nucleotide substitutions than 5-1 (indicated by black arrows in Figure 3.13A), including restoring nucleotide 604 to the wild-type U. Tlc1(5-2) resulted in a senescence phenotype not suppressible by MS2-tethering Est1 protein, indicating lost SEED function (Figure 3.13C). It is unlikely that the sequence of tlc1(5-2) *per se* is responsible for disruption of the SEED, given that tlc1(5-1) — which has all nucleotides in the 5′ side of the internal loop changed — retains SEED function.

SHAPE reactivity was similar for both 5-1 and 5-2 in the 3′-most quadrant of the internal loop (Figure 3.13B), but there was alternate folding in the basal part of the internal loop exclusively in 5-2 (Lebo *et al.*, *submitted*). In particular, U604, which is essentially unreactive in wild-type TLC1, is strongly reactive in tlc1(5-2), suggesting it is not forming the wild-type base pair (see orange arrow in Figure 3.13B). Phylogenetic analysis indicates that this base pair forms in all *Saccharomyces* yeast species (Figure 3.2). A possible explanation for the SHAPE results for 5-2 is G640 pairing with C606 or C605, in turn causing U604 to be unpaired and significantly changing the structure in the base of the internal loop. The SHAPE analysis suggests an altered internal loop structure in tlc1(5-2) results in SEED dysfunction.

To test the hypothesis that the structure of the internal loop is more important than its sequence for SEED function, I designed a modification to tlc1(5-1) that disrupts the structure with fewer mutated residues. This mutant, 5-3, has 7 of the same 10 nucleotide substitutions as 5-1, but retains the wild-type AAA sequence at positions 609 to 611 (Figure 3.13A). *Mfold* predicts that the internal loop of mutant 5-3 will contain

three A-U base pairs, resulting in the formation of two small loops separated by this 3-bp helix (Figures 3.5 and 3.13B). This structure may be biologically relevant and has been suggested previously to form in wild-type TLC1 (Dandjinou et al., 2004). SHAPE analysis of tlc1(5-3) indicated a clear reduction in reactivity of essentially all nucleotides in the internal loop (Figure 3.13B; Lebo *et al.*, *submitted*), consistent with the expected increase in base pairing between the two sides. The greatest reduction in reactivity was in the 3′-most quadrant of the loop, a region highly reactive by SHAPE in wild-type TLC1 and the 5-1 allele with its functional SEED (Figures 3.12A and 3.13B). Cells expressing tlc1(5-3) exhibited loss of telomere maintenance leading to senescence, which could not be bypassed by MS2-tethering Est1 (Figure 3.13C), thus demonstrating that disrupting the structure of the internal loop results in loss of SEED function.

Overall, SHAPE and functional analyses of the three 5′ IL mutants and wild-type TLC1 suggests that the base of the internal loop is of particular structural importance to the second essential function of the Est1 arm, and therefore comprises the SEED.

Computational modeling suggests that the 3D structure of the internal loop may regulate SEED function

Previously reported phylogenetic models predicted two possible structures for the internal loop: one large loop (Zappulla and Cech, 2004) or two smaller loops separated by a 3-bp helix (Figure 3.14A; Dandjinou et al., 2004). SHAPE analysis on purified Est1-arm RNA suggests the former conformation dominates *in vitro* in the absence of protein (Figure 3.8A; Lebo *et al.*, *submitted*). In addition, phylogenetic analysis showed that just two of the A residues, and none of the pair-partnering U residues, were conserved among TLC1 sequences, and there is no covariation evident that would suggest conserved base pairing (Figure 3.2). Together, these data support a single, large internal loop secondary structure as the most favorable conformation for the naked RNA.

Figure 3.14: 3D computational modeling of the TLC1 Est1-arm conserved region. (**A**) TLC1 Est1-arm conserved region secondary structure, with sub-elements colored. Blue = 5′ side of the Internal Loop, orange = Apical Hairpin, green = 3′ side of Internal Loop, yellow = Hinge-Hairpin, and red = Bulge. Open circles indicate the potential A-U pairs across the internal loop. (**B**) 3D structure prediction by RNAComposer of the Est1-arm conserved region with unpaired internal loop. Inset shows internal loop secondary structure, with the three unpaired A and U residues boxed. The structure of the entire 193-nt Est1 arm (nts 508−700) was modeled. (**C**) Predictions for the Est1 arm with three A-U base pairs in the internal loop have a very different tertiary structure with coaxially stacked RNA helices. Inset shows the corresponding secondary structure, with the A-U pairs boxed.

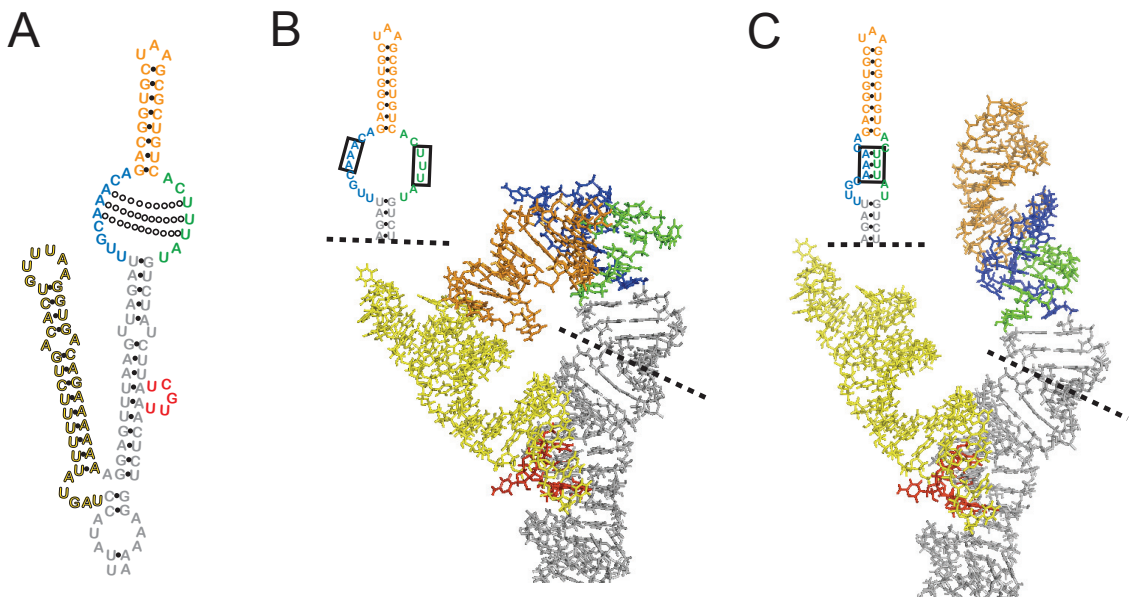

However, it remains quite possible that limited pairing across this internal loop occurs in the ribonucleoprotein complex, either transiently or in equilibrium with the unpaired loop in the cell. Consistent with this, pairing across the internal loop can have potent effects on telomerase function (Figure 3.13; Laterreur et al., 2013; Lubin et al., 2012).

The seemingly small secondary structure difference between the two possible internal loop folding states may have a large effect on the tertiary RNA structure in the region. I used RNAComposer bioinformatic software to model the 3D structure of the 193-bp Est1 arm (Figure 3.14; Popenda et al., 2012). I used the secondary structure model for the wild-type TLC1 Est1 arm with the large, single internal loop (Figure 3.14B). The 3D structure prediction shows that the bulge and hinge domains come into close proximity. Since both of these domains have been implicated in Est1 association with the RNA, this tertiary structure may represent an important Est1-binding site. As for the internal loop containing the SEED, it is predicted to bend sharply, forming a kink that imparts a large-scale conformational change, orienting the apical hairpin back towards the hinge-hairpin and exposing nucleotides along the internal loop required for SEED function.

Next, based on the results with tlc1(5-3) (Figure 3.13) and the slightly different secondary structure previously proposed for this region (Dandjinou et al., 2004), I modeled the same wild-type Est1-arm conserved region, but this time with the three A-U pairs across the internal loop (Figure 3.14C). The modeling shows the three base pairs in the internal loop dramatically switching the overall 3D conformation of the Est1-arm conserved region; it is no longer predicted to be bent, but rather the apical hairpin coaxially stacks with the helix between the internal loop and the bulge, thus projecting away from the catalytic core. This tertiary structure is consistent with SHAPE results that showed the internal loop nucleotides being less exposed in this conformation (Figure 3.13B; Lebo *et al.*, *submitted*). This 3D modeling suggests that the secondary structure

of the internal loop may play a role in large-scale conformational changes in the tertiary structure of the Est1 arm of TLC1.

The SEED has an Est1-independent function in telomerase mechanism

To explore the mechanism of SEED function in telomerase, I further examined the functional relationships between TLC1 and Est1 *in vivo*. The essential role of Est1 protein in recruiting telomerase to the telomere can be bypassed by fusing the telomere-binding protein Cdc13 to the telomerase catalytic subunit Est2 (Evans and Lundblad, 1999). I employed this *CDC13-EST2* system to test (1) if the TLC1 SEED function is separable from Est1-mediated telomerase recruitment and (2) if SEED function is dependent on the presence of Est1 protein. I integrated a DNA sequence of 8 glycine-encoding codons followed by the *EST2* gene in place of the stop codon of *CDC13* to generate *CDC13-Gly$_8$-EST2* (Figure 3.15). In an *EST1* genetic background, by 250 generations of passaging cells, the Cdc13-Est2 fusion protein caused extensive hyperlengthening of telomeres (Figure 3.16B, lanes 5 and 6), as observed for the originally reported Cdc13-Est2 fusion (Evans and Lundblad, 1999). Due to the highly elongated telomeres, cells were able to grow for over 600 generations after *TLC1* was deleted before senescing (~6 times longer than wild-type cells survive without telomerase). The decrease in telomere length in *tlc1*Δ cells was apparent by Southern blotting; as telomeres shortened, distinct bands became apparent on the Southern blot due to differences in the size of subtelomeric regions in the *Xho*I-digestion products (Figure 3.16B, lanes 1 and 2). As previously reported, deletion of *EST1* in the *CDC13-EST2* fusion strain caused relative telomere shortening, but not senescence (Evans and Lundblad, 1999). Although telomeres in the *est1*Δ *CDC13-EST2* strain (lanes 7 and 8) became shorter, even after 500 generations they appeared stably longer than standard wild-type telomeres.

Figure 3.15: Gene and protein sequences of Cdc13-Est2 fusion. *Gly_8-EST2* was integrated into the stop codon of genomic *CDC13*. *CDC13* gene and protein sequence are highlighted in orange, *Gly_8* in brown, and *EST2* in green.

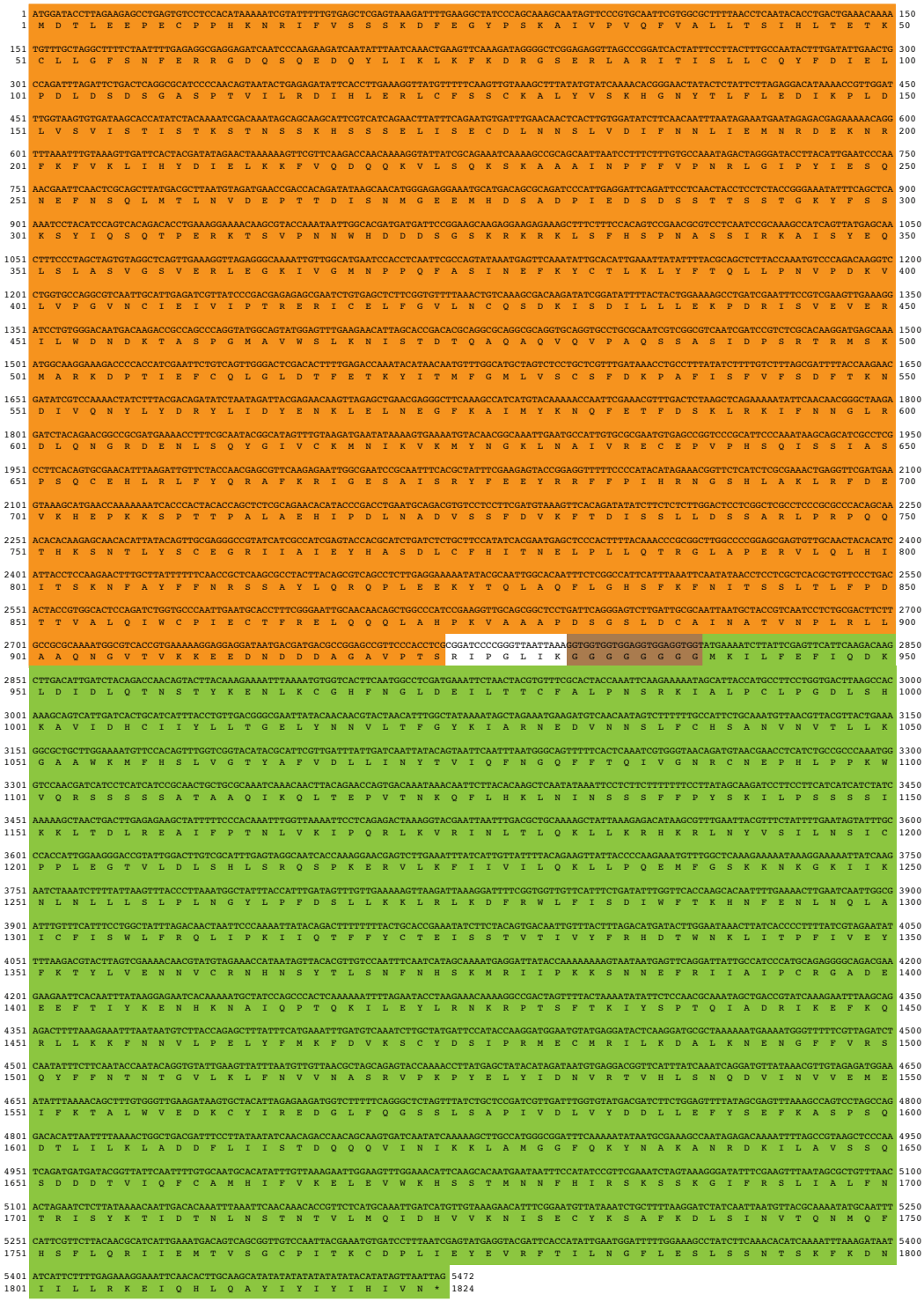

Figure 3.16: The SEED is essential in a Cdc13-Est2 fusion-protein strain. (A) Schematic showing Est1-bypassing recruitment of telomerase to the telomere in a Cdc13-Est2 protein fusion strain. *CDC13-Gly$_8$-EST2* is genomically encoded in either an *EST1* or *est1*Δ background. *TLC1* alleles are expressed from centromeric plasmids. (B) Telomere Southern blot from *CDC13-EST2* cells expressing TLC1 mutants with or without Est1 protein at 250 and 500 generations. Conditions with hyperlengthened telomeres (lanes 5 and 6) are indicated by a blue line, conditions with stably shorter telomeres (lanes 7−12) are indicated by a green line, and senescent conditions (lanes 1−4 and 13−16) are indicated by red lines. Marker sizes are based on [γ-^{32}P]-labeled λ*Hind*III DNA ladder. Internal control, a non-telomeric *Xho*I fragment from chromosome IV.

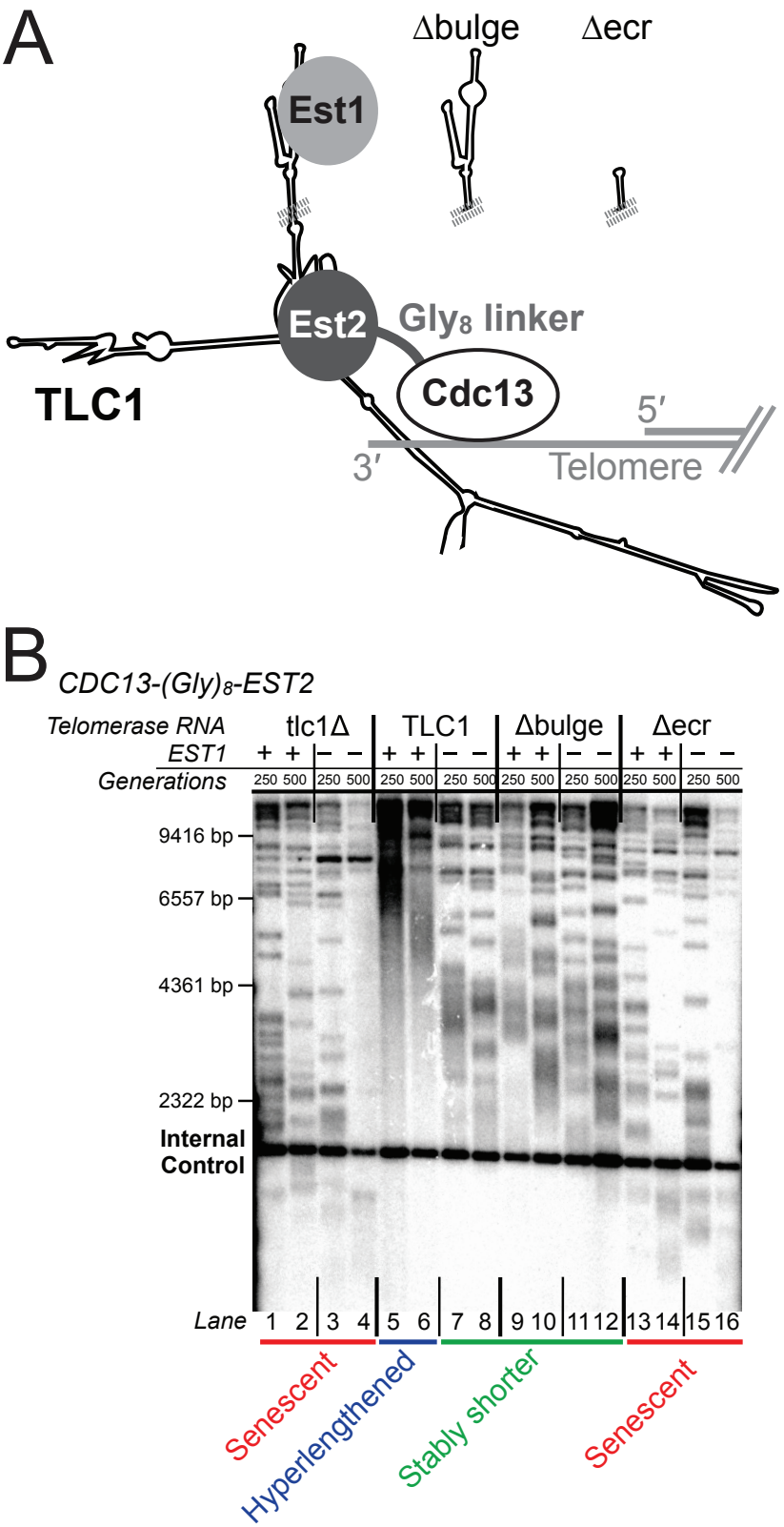
A
Δbulge
Δecr
Est1
Est2
Gly8 linker
Cdc13
TLC1
5′
3′
Telomere
B
CDC13-(Gly)8-EST2
Telomerase RNA
tlc1Δ
TLC1
Δbulge
Δecr
EST1
+ + – – + + – – + + – – + + – –
Generations
250 500 250 500 250 500 250 500 250 500 250 500 250 500 250 500
9416 bp
6557 bp
4361 bp
2322 bp
Internal Control
Lane
1 2 3 4 5 6 7 8 9 10 11 12 13 14 15 16
Senescent
Hyperlengthened
Stably shorter
Senescent

I next examined TLC1 alleles with Est1-arm mutations in the *CDC13-EST2* strain to test if the Est1-binding or SEED functions are required after recruitment of telomerase to the telomere (see Figure 3.16A). Expressing tlc1∆bulge (which disrupts Est1 binding to the RNA but not SEED function) in the *CDC13-EST2 EST1* strain resulted in telomere length similar to *TLC1 est1∆ CDC13-EST2* cells (Figure 3.16B; lanes 9 and 10 versus 7 and 8), consistent with the reported activation function of Est1 in telomerase requiring TLC1 binding (Taggart et al., 2002). Furthermore, simultaneous loss of *EST1* and the bulge from TLC1 in *tlc1∆bulge est1∆ CDC13-EST2* cells resulted in a very similar telomere length phenotype (lanes 11 and 12). This lack of a genetic interaction provides evidence that these mutations are epistatic, disrupting the same non-essential secondary function of Est1 protein.

Having demonstrated that disrupting the Est1-tethering function of the TLC1 Est1 arm results in moderate telomere shortening, I next tested whether the SEED plays a role in telomere maintenance when telomerase recruitment to telomeres via Est1 is bypassed. I expressed tlc1∆ecr — which lacks the Est1-binding sites as well as the SEED — in *CDC13-EST2* cells, and found that it resulted in loss of telomere maintenance in both *EST1* and *est1∆* strains (Figure 3.16B, lanes 13–16). Telomeres shortened similarly to those of *tlc1∆ CDC13-EST2* cells (lanes 1–4), and eventually cells senesced. These data indicate that the SEED is essential even when Est2 is covalently fused to Cdc13, suggesting that SEED function is required after recruitment of telomerase to the telomere. In addition, the results indicate that the SEED mechanism is independent of Est1 protein once telomerase has been recruited to the telomere.

3.4: DISCUSSION

The 1157-nt yeast telomerase RNA TLC1 acts as a flexible scaffold that tethers essential and important accessory subunits to the RNP complex (Lebo and Zappulla, 2012; Zappulla and Cech, 2004, 2006; Zappulla et al., 2011) (Mefford et al., 2013). As additional long non-coding RNAs (lncRNAs) have subsequently been proposed to function through flexible scaffold mechanisms like TLC1 (Chu et al., 2011; Guttman et al., 2011; Wang et al., 2011), this class of RNPs defined by TLC1 (Zappulla and Cech, 2004) is being increasingly recognized as an important archetype (Wang and Chang, 2011; Zappulla and Cech, 2006). While TLC1 has been shown to tether each of the three known accessory subunits — Est1, Ku, and Sm_7 — to the telomerase RNP without fixing the subunits into precise positions in the RNP (Lebo and Zappulla, 2012; Mefford et al., 2013; Zappulla and Cech, 2004; Zappulla et al., 2011), it was not known if any of these protein-binding sites on TLC1 RNA had additional roles in RNP function. Although only 33% of TLC1 nucleotides are conserved overall amongst species of the same genus, conservation is clearly highest around proposed protein-interacting regions in the catalytic core and at the ends of the three long arms (Dandjinou et al., 2004; Mefford et al., 2013; Zappulla and Cech, 2004). In this regard, I have been intrigued by alignments of TLC1 from known *Saccharomyces* sequences in the Est1-interacting region of TLC1 which show that it is an expansive 108-nt stretch of highly conserved nucleotides (Figures 3.1 and 3.2). This contrasts markedly with the conserved 25 nts shown to bind the ~152-kDa Ku complex (Dalby et al., 2013; Peterson et al., 2001) and 13-nt conserved nucleotides that bind the ~91-kDa Sm_7 complex (Jones and Guthrie, 1990; Mefford et al., 2013; Seto et al., 1999; Zappulla and Cech, 2004). The expansive conservation in the Est1-arm of TLC1 and reports of mutations in different positions over this region that disrupt Est1 binding led me to hypothesize that the Est1-arm conserved

region comprises a domain with sophisticated structure that is important for functions beyond simply binding Est1 to tether it to the RNP.

Using the MS2 bacteriophage-based RNA-protein interaction system allowed me to separate the primary essential function of the Est1-binding arm — recruitment of Est1 to the RNP (Lundblad and Szostak, 1989) — from other roles essential for telomere maintenance (Figure 3.7A). This allowed testing TLC1 mutants that would otherwise disrupt Est1 binding, while still promoting Est1 recruitment to the telomerase RNP and led to identification and structural mapping of the Second Essential Est1-arm Domain (SEED).

My findings expand the flexible scaffold model for yeast telomerase RNA. MS2-tethering Est1 to the tlc1Δbulge RNA rescues telomere maintenance, demonstrating that an essential Est1-binding interface in TLC1 can be functionally replaced with a heterologous RNA-protein direct-binding system (Figure 3.7B). Furthermore, like the protein-binding sites on TLC1, the SEED appears to be flexibly scaffolded in the RNP; it retains function when relocated on TLC1 (Zappulla and Cech, 2004), and even functions *in trans* as a separate RNA (Figure 3.11A). This *in trans* functionality strongly suggests that the SEED does not function in recruiting protein subunits to the RNA scaffold. The presence of the SEED indicates that the accessory-protein binding arms of TLC1 can have roles in telomere maintenance in addition to flexibly scaffolding the holoenzyme protein components.

My results indicate that the SEED mechanism is Est1-independent, and does not require Est1 protein once telomerase has been recruited to the telomere-binding protein Cdc13. I hypothesize that Est1 first binds to TLC1 to promote telomerase recruitment to the telomere by also binding Cdc13, and then the SEED functions as part of the recruited telomerase RNP•telomere complex (Figure 3.17).

Figure 3.17: Schematic of the SEED in telomerase function. Telomerase is recruited to the telomere through the interaction between Est1 and Cdc13. I hypothesize that the SEED functions downstream of recruitment to the telomere, and allows for telomere lengthening by Est2.

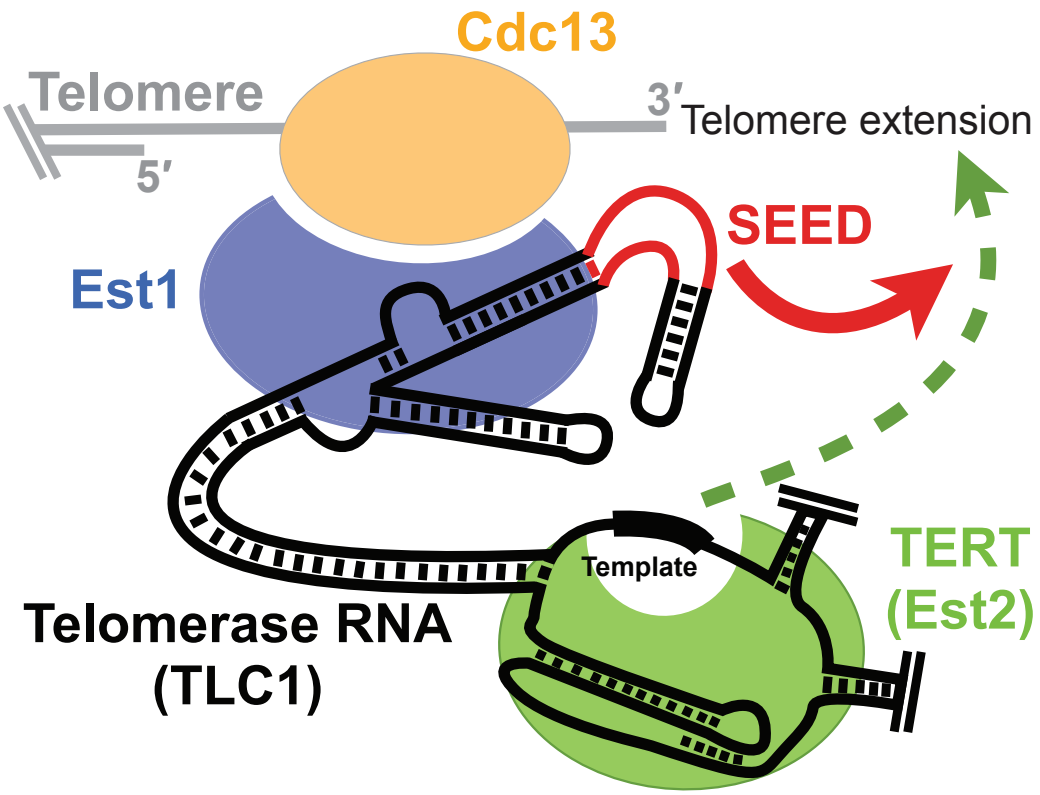

I find it interesting that Est1 association with the RNA and SEED function are each dependent on the internal loop in the Est1-binding arm, despite being at least partially functionally independent. The existence of an internal loop below the apical hairpin is structurally conserved across many species of yeast within the *Saccharomyces*, *Kluyveromyces*, and *Candida* genera (Gunisova et al., 2009). Even reported models for the distantly related fission yeast *S. pombe* appears to have a large internal loop in the Est1-binding arm, although nucleotide sequence in the region is not conserved (Webb and Zakian, 2012). In fact, the 5′ side of the internal loop is even more conserved amongst budding yeast than the essential bulge region, with relatively high conservation even through the *Candida* genus (Gunisova et al., 2009).

Previous phylogenetic models predicted that the internal loop could either form as a single, large loop (Zappulla and Cech, 2004), or as two smaller loops separated by a 3-bp helix (Dandjinou et al., 2004). While SHAPE analysis supports the single large loop (Lebo *et al.*, *submitted*), and phylogenetic analysis of 36 TLC1 sequences from seven *Saccharomyces* species provides no evidence indicating pairing across the loop (Figure 3.2), it remains possible that both structures exist in an equilibrium *in vivo*. Bioinformatic modeling of the Est1-binding arm suggests that switching between the two possible secondary structures for the internal loop may cause large-scale changes in the tertiary structure of the region (Figure 3.14).

I hypothesize that modulating the secondary structure of the internal loop may act as a regulatory mechanism, switching the 3D structure between active and inactive SEED states. It is not yet known precisely where Est1 protein binds the internal loop, although binding does require at least some unpaired nucleotides in the internal loop and is also at least partially affected nucleotide substitutions in the 5′ part of the loop (Lubin et al., 2012). The SEED, however, appears to be inactive in the partially paired internal loop conformation (see mutant 5-3 in Figure 3.13). Instead, the SEED is

functional when the internal loop is more flexible (see mutant 5-1 in Figure 3.13), which may allow for a tertiary structure that exposes nucleotides along the loop (Figure 3.14B). Although the essential SEED function is Est1 independent, it remains possible that Est1 protein binding has a role in modulating the conformational state of the SEED. Since both Est1-binding and SEED nucleotides are essential, future studies to understand the relationship of these functions will be facilitated by identification of more conditional and partial loss-of-function alleles that individually affect these processes. These studies will extend my results based on MS2-tethering Est1 to telomerase as a means to parse Est1-binding and SEED functions of the Est1 arm.

The *trans* functionality is evidence that the SEED does not function in RNP assembly or recruiting protein components, but rather affects telomerase action in a different way. Furthermore, the fact that Est1-association mutations in the *in trans* Est1 arm RNA, such as ∆bulge or ∆HH, prevents the SEED from functioning from a separate RNA molecule suggests that the SEED itself must be part of the RNP complex to function (Figure 3.11D). I do not favor the hypothesis that the SEED activates the yeast telomerase reverse transcriptase (TERT), Est2. Although in organisms other than *Saccharomyces* it has been shown that telomerase activity *in vivo* and *in vitro* requires a portion of telomerase RNA in addition to the central core that can function *in trans* (Mason et al., 2003; Mitchell and Collins, 2000; Qi et al., 2013; Tesmer et al., 1999), simply the central core of TLC1 — entirely without the Est1 arm — is sufficient to reconstitute robust yeast telomerase activity with Est2 *in vitro* (Mefford et al., 2013; Qiao and Cech, 2008). This suggests the SEED is not analogous to the human CR4/5, the ciliate stem-terminus element, or the three-way junction in other yeasts (Brown et al., 2007; Mitchell and Collins, 2000; Tesmer et al., 1999; Theimer and Feigon, 2006). Instead, I favor the hypothesis that SEED mechanism involves a telomerase-regulating protein such as Cdc13 or the also-essential telomerase RNP component Est3. Since the

SEED appears to function after telomerase has been recruited to the telomere by way of Est1-Cdc13 interaction, it is more likely that it promotes the telomerase-extendible state of the telomere and/or permits multiple rounds of template-directed telomerase activity, through either activation or derepression of a protein function.

A recent publication reported a “telomerase-stimulating structure” (TeSS) in the conserved region of Est1 (Laterreur et al., 2013), mapping to the apical hairpin/upper portion of the internal loop of the Est1-binding arm. The mutants analyzed showed a non-essential function for this region, causing shortened telomeres but not senescence. The TeSS and SEED reported here may represent distinct functional domains. Alternatively, the TeSS mutants may be altering the structure of the internal loop, partially disrupting the SEED without fully abolishing SEED function.

In summary, I have demonstrated that a second essential function exists for the Est1-binding arm of yeast telomerase RNA, in addition to tethering the protein to the RNP. This Second Essential Est1-arm Domain is located in the base of the internal loop of the Est1-arm conserved region. Despite also mapping to a region of TLC1 implicated in binding Est1 protein, the SEED can function *in trans* and its role in telomere synthesis does not require Est1. Dynamic tertiary structural conformations of the Est1 arm may regulate SEED function. I hypothesize the SEED represents a key, non-scaffolding domain of TLC1 RNA required for telomerase-mediated telomere extension.

3.5: METHODS

Phylogenetic analysis of *TLC1*

To analyze the Est1-binding arm in the context of an alignment of entire *TLC1* sequences, 36 unique *TLC1* sequences from NCBI ascribed to seven *Saccharomyces* species (*cerevisiae, paradoxus, pastorianus, cariocanus, kudriavzevii, mikatae,* and *bayanus*) were aligned. The alignment was viewed using Jalview (Waterhouse et al., 2009) to generate what is shown in Figure 3.1. Percent conservation values were calculated by comparing the number of 100% conserved residues (green in Figures 3.1 and 3.2) or total number of conserved and covarying nucleotides (green, red, and blue) by the length of the alignment for each section.

Creation of a heterologous binding interaction system for tethering Est1 protein to TLC1 RNA *in vivo*

The MS2 bacteriophage coat protein-RNA interaction system was used to tether Est1 to TLC1 RNA. For the MS2 hairpin-tagged TLC1 RNA, a version of the gene with 10 MS2 hairpins inserted at position 1135 was used (Gallardo et al., 2011). In order to tag various *TLC1* alleles with the MS2 hairpins in the same vector backbones, the *Bcl*I to *Nsi*I fragment, including the MS2 sites, was cloned into a pRS314-based centromere-containing (*CEN*) vector harboring *TLC1*, including approximately 518 bp of genomic sequence upstream and 795 bp of genomic sequence downstream of *TLC1* (pSD107), to make pDZ641. This fragment was also cloned into *tlc1*Δ*bulge* vector pAS558 (Seto et al., 2002) to make *tlc1*Δ*bulge-MS2* (pDZ353) and *tlc1*Δ*ecr* vector pDZ428 to make *tlc1*Δ*ecr-MS2* (pDZ432). See Figure 3.3 for TLC1-MS2 *Mfold*-predicted secondary structure.

In order to C-terminally tag Est1 with two tandem copies of the bacteriophage MS2 coat protein domain (MS2CP), the *MS2CP*$_2$ coding region was PCR amplified using an MS2CP-containing plasmid, pRS426-TAP-MS2CP$_2$ (Gallardo et al., 2011), using primers that insert 8 glycine residues (Gly_8) upstream, which has been shown to maintain function of C-terminally-tagged Est1 (Sabourin et al., 2007). This fragment was cloned into *Pac*I/*Asc*I-digested pFA6a-3HA-His3MX6 vector (Longtine et al., 1998). Next, Gly_8-MS2CP::His3MX6 was PCR amplified and integrated it in place of the stop codon of *EST1* in the strain TCy127 (*MATa, ADE2, his3Δ, leu2Δ0, lys2Δ0, trp1Δ63, ura3Δ0, RAD52, tlc1::Kan*^{R}*, pTLC1-URA3*) (Mozdy and Cech, 2006) to make *EST1-Gly*$_8$*-MS2CP*$_2$ strain yDZ385 (Figure 3.2). Correct integration was confirmed by colony PCR.

For creation of the *EST1-EST2* fusion protein strain (Figure 3.8), *EST2* was amplified from the genome by PCR using primers to add eight glycine residues (Gly_8) to the 5′ end of the open reading frame. The product was cloned into *Pac*I/*Asc*I-digested pFA6a-3HA-His3MX6 (Longtine et al., 1998) to make pDZ699. *Gly*$_8$*-EST2::HIS3* was PCR-amplified off of the plasmid using primers containing 50 bp of homology to the 3′ end of *EST1* on both sites of the product. The insertion cassette was transformed into TCy127 for integration in place of the *EST1* stop codon, and was confirmed by PCR to have created *EST1-Gly*$_8$*-EST2* (yDZ455).

In trans Est1 arm expression in yeast

The Est1 arm of *TLC1* (nucleotides 514 to 694) or Est1-arm mutant variants of *TLC1* was amplified using PCR primers that add a 5 C or G residues to either side, respectively, designed to form G-C base pairs at the base of the RNA's secondary structure to help promote proper folding. The product was cloned into *Spe*I/*Xho*I-digested 2μ vector p425TEF, harboring the *TEF2* promoter and a *CYC1* terminator (Mumberg et al., 1995; Russo and Sherman, 1989). The *in trans* Est1 arm transcript is

predicted to include additional nucleotides from the promoter and terminator regions; *Mfold* predicts proper folding of the Est1 arm in the transcript. See Figure 3.10 for complete *in trans* Est1 arm transcript sequence and *Mfold* predicted secondary structure.

Est1 arm mutants

The TLC1 Est1-arm conserved region was deleted by ligating two PCR products, resulting in *tlc1*∆*ecr* (*TLC1(552−662::C)*; pDZ428 without MS2s, pDZ432 with MS2s). Est1-arm conserved region sub-element deletions TLC1∆AH (∆614−632; pDZ767 without MS2s, pDZ760 with MS2s) and tlc1∆IL (∆605−613, 633−639; pDZ768 without MS2s, pDZ761 with MS2s) were also made using PCR fragments. For tlc1∆HH, deletion of the hinge-hairpin domain alone was insufficient for fully disrupting hinge function, presumably due to remaining unpaired nucleotides that still can provide flexibility (Figure 2.9). Therefore, the stiffened Est1 arm was used, with all unpaired nucleotides deleted (see Chapter 2; Lebo and Zappulla, 2012). *Nco*I−*Hpa*I and *Hpa*I−*Mlu*I gene fragments were synthesized, sequence-verified, and subcloned by GenScript (Piscataway, New Jersey). Then, the two fragments were cloned into *Nco*I/*Mlu*I-digested vector pDZ386 (harboring *TLC1* with a stiffened Est1 arm; Lebo and Zappulla, 2012), creating *tlc1*∆*HH* (pDZ389 without MS2s, pDZ794 with MS2s). We created the internal loop sequence mutations in TLC1-MS2 using PCR fragments (3-1 = pDZ766, 5-1 = pDZ791, 5-2 = pDZ765, 5-3 = pDZ788). All Est1-arm mutants were cloned into *CEN* plasmids expressing TLC1 from its endogenous promoter, either in pSD107 (TLC1) or pDZ641 (TLC1-MS2). *Mfold* software secondary structure predictions were used to guide the creation of all mutants, to reduce the likelihood of off-target effects on folding (Zuker, 2003; Zuker and Jacobson, 1998). See Figure 3.5 for *Mfold* lowest-free-energy structure models of each mutant.

Senescence experiments in yeast

TRP1-marked *CEN* plasmids harboring *TLC1* alleles were transformed into haploid *S. cerevisiae* strain TCy127 (Mozdy and Cech, 2006) for testing in the absence of MS2-tethering, or yDZ385 (*MAT**a**, ADE2, his3*Δ*, leu2*Δ*0, lys2*Δ*0, trp1*Δ*63, ura3*Δ*0, RAD52, tlc1::Kan*^{R}*, pTLC1-URA3, EST1-Gly*$_{8}$*-MS2CP*$_{2}$*::HIS3)* for testing in the presence of Est1-MS2CP. The p*TLC1-URA3* cover plasmid was shuffled out using counter-selection on 5-fluoroacetic acid (5-FOA), and colonies were restreaked sequentially 10 times on synthetic-complete medium lacking tryptophan. Each colony-forming unit was estimated to represent 25 generations. Colonies were visually monitored for signs of senescence. Due to the presence of *RAD52* in the strains, "survivor" colonies sometimes occur; these cells maintain telomeres through a telomerase-independent recombination-based pathway (Lundblad and Blackburn, 1993). Senescence was indicated by an obvious decrease in colony viability before the onset of any survivors. Additionally, telomeric Southern blotting was used to verify telomerase-independent survivorship by the characteristic telomeric restriction fragment patterns (see Figure 3.6B; Lundblad and Blackburn, 1993; Teng and Zakian, 1999). Cells were restreaked a minimum of 10 times (~250 generations) to test for late-senescence phenotypes.

For the *in trans* Est1 arm tests (Figure 3.11), *LEU2*-marked 2μ plasmid were co-transformed into cells along with the *TRP1*-marked *TLC1*-allele-harboring plasmids. After shuffling out p*TLC1*^{WT}*-URA3* using 5-FOA-containing medium, cells were restreaked on synthetic complete medium lacking tryptophan and leucine, while carefully monitoring for senescence.

All *in vivo* experiments were performed multiple times.

Cdc13-Est2 fusion protein experiments

A strain expressing *CDC13-Gly$_8$-EST2* from the genomic *CDC13* locus was created. To do this, *EST2* was amplified from the genome by PCR using primers to add eight glycine residues (Gly_8) to the 5′ end of the open reading frame. The product was cloned into *Pac*I/*Asc*I-digested pFA6a-3HA-His3MX6 (Longtine et al., 1998) to make pDZ699. *Gly$_8$-EST2::HIS3* was PCR-amplified off of the plasmid using primers containing 50 bp of homology to the 3′ end of *CDC13* on both sites of the product. The insertion cassette was transformed into TCy127 for integration in place of the *CDC13* stop codon, and was confirmed by PCR to have created *CDC13-Gly$_8$-EST2* (yDZ453). The *est1*Δ *CDC13-EST2* strain was made by knocking out *EST1* in yDZ453. This was achieved using *Candida glabrata LEU2*, PCR-amplified with primers adding 50 bp of homology upstream and downstream of *EST1*. The product was transformed into yDZ453 cells and the *est1*Δ genotype was then confirmed by PCR (yDZ485). Telomeres in the *CDC13-EST2* and *est1*Δ *CDC13-EST2* strains were longer than previously reported (Evans and Lundblad, 1999); this is likely due to genomic expression of Cdc13-Est2, instead of plasmid-based expression.

Est1-arm mutants on *TRP1-CEN* plasmids were transformed into yDZ453 or yDZ485 cells. After p*TLC1-URA3* was shuffled out on solid synthetic medium containing 5-FOA, cells were restreaked on solid synthetic complete media lacking tryptophan for 30 restreaks (approximately 750 generations).

Southern Blots

Southern blots were performed as previously described (Zappulla and Cech, 2004; Zappulla et al., 2011). Cell pellets were prepared from liquid cultures grown from serially restreaked plates, and genomic DNA was isolated (Gentra Puregene system). Equal amounts of DNA were digested with *Xho*I, and electrophoresed through a 1.1%

agarose gel for 17 h at 70 V. DNA was transferred by capillary action to a Hybond-N+ Nylon membrane (GE), and probed for telomeric sequence. A non-telomeric 1627-bp fragment probe of chromosome IV was also included as an internal control. Average Y′ telomere fragment length was quantified using the weighted average mobility (WAM) assay (Zappulla et al., 2011).

Northern Blots

Northern blots were performed as previously described (Zappulla et al., 2005). Briefly, total cellular RNA was isolated from yeast cultures using a modified hot-phenol RNA isolation method (Kohrer and Domdey, 1991). After boiling, ~10µg of total RNA was separated by Urea-PAGE, transferred to a Hybond-N+ Nylon Membrane (GE), UV-crosslinked (Spectrolinker XL-1500 UV Crosslinker, "Optimal Crosslink" setting), and pre-hybridized in Church buffer for 10 min at 55°C. The membrane was then probed for the 3′ end of TLC1 (nts 906−1140; Lebo and Zappulla, 2012) or for the Est1 arm (nts 504−704), and for the U1 snRNA (Friedman and Cech, 1999). Relative abundances were determined by normalized TLC1 or Est1 arm levels to U1 snRNA. Since U1 is far more abundant, 100-fold less U1 probe was used relative to TLC1 probe.

RNA three-dimensional structure modeling

Dot-bracket notations were generated for the phylogenetically supported Est1 arm secondary structure model (i.e., nts 508–700). Modified version of the dot-bracket structure were also made, with three A-U pairs in the internal loop, formed between nts 609−611 and 635−637. The wild-type Est1 arm sequence was submitted alongside each dot-bracket structure to the RNAComposer Automated RNA Structure 3D Modeling Server (Popenda et al., 2012).

Chapter 4:

Synthetic design of a more stably folding TLC1 RNA that functions *in vivo* and *in vitro*

4.1: ABSTRACT

Full-length, wild-type TLC1 does not support robust telomerase activity when telomerase is reconstituted in an *in vitro* transcription and translation system, whereas a miniaturized TLC1 containing just the catalytic core does. This suggests that the 1157-nt RNA is prone to misfolding, and requires other cellular factors to promote proper structure formation. So far only extensively truncated or mutated variants of TLC1have been used for *in vitro* studies. In order make a TLC1 allele that folds stably *in vitro* into the phylogenetically supported secondary structure, I designed a version of TLC1 with the fewest sequence changes possible predicted to energetically favor this conformation. I used *Mfold* RNA secondary structure prediction software to guide the design of this "determined arm TLC1" (DA-TLC1) while planning point mutations to promote a more energetically determined predicted final structure. I found that unlike wild-type TLC1, DA-TLC1 reconstitutes robust telomerase activity *in vitro*, and is also able to prevent cellular senescence *in vivo*. However, DA-TLC1 RNA abundance is very low in cells, resulting in very short telomeres. This defect maps to the determined Ku-binding arm. These findings suggest that RNA structure in the Ku arm of TLC1 may play a previously unknown, important role in telomerase function.

4.2: INTRODUCTION

Although several telomerase accessory protein subunits are required for telomere maintenance *in vivo*, the RNA and telomerase reverse transcriptase (TERT) components are sufficient to reconstitute enzymatic activity *in vitro* (Cohn and Blackburn, 1995; Lingner et al., 1997a; Weinrich et al., 1997). For the budding yeast *Saccharomyces cerevisiae*, this minimal telomerase RNP requires the TLC1 RNA and yeast TERT, Est2. However, full-length TLC1 only shows robust *in vitro* function when it has been co-immunopurified from yeast cells (Cohn and Blackburn, 1995; Zappulla et al., 2005). When yeast telomerase is reconstituted in an *in vitro* rabbit reticulocyte lysate transcription and translation system, wild-type TLC1 is essentially nonfunctional, although I have reproducibly seen trace amounts of activity (see Figures 2.4, 2.7 and 2.9; Lebo and Zappulla, 2012). Instead, several mutant variants of TLC1 have been developed for use in reconstituted *in vitro* telomerase assays. These include a series of miniaturized telomerase RNAs, which involve extensive deletions of the TLC1 arms to make “Mini-T” and “Micro-T” variants (Mefford et al., 2013; Qiao and Cech, 2008; Zappulla et al., 2005), or telomerase RNAs with significant structural modifications in the arms, such as triple-stiff arm TLC1 (TSA-T) (see Chapter 2; Lebo and Zappulla, 2012).

Micro-T RNAs lack the accessory protein-binding arms, and are therefore nonfunctional *in vivo* (Mefford et al., 2013; Qiao and Cech, 2008). Mini-T and TSA-T are able to support telomere maintenance in cells, and therefore can be used to study the RNA both *in vivo* and *in vitro* (Lebo and Zappulla, 2012; Zappulla et al., 2005). However, these TLC1 variants are highly mutated; Mini-T(500) has 657 nucleotides deleted from the three RNA arms, while TSA-T has 201 nts deleted from the arms, and several other nucleotide substitutions. Furthermore, both Mini-T and TSA-T have dramatic structural changes from wild-type TLC1; the truncated arms of Mini-T bring the accessory proteins

in closer to the central catalytic core, while the stiffened arms in TSA-T hold the accessory proteins away from the core on dsRNA struts. These mutations limit the about of information that Mini-T and TSA-T can provide about the relationships between structure and function in yeast telomerase RNA. Therefore, I sought to engineer a version of TLC1 with fewer mutations that would be highly functional both *in vivo* and *in vitro*.

To design a TLC1 variant with a more energetically stable final folded state, I employed the *Mfold* RNA secondary structure prediction software (Zuker, 2003). *Mfold* is able to model both the secondary structure and the ∆G of folding for TLC1. In addition, it can provide information on how well determined the RNA structure is, based on a P-num scale. P-num describes the number of base pairs a particular nucleotide is able to make in the iterative folding predictions (Zuker and Jacobson, 1998). A high P-num value indicates that nucleotide is able to pair with many other nucleotides, while a low P-num value indicates pairing with few other nucleotides. *Mfold* uses a color scale to annotate the P-num values of each nucleotide, red representing nucleotides with a low P-num value, and purple or black representing nucleotides with a high value. Red nucleotides in *Mfold* structures have a high probability of folding as predicted; RNA domains with many red nucleotides are therefore considered to be "well determined," with a relatively high confidence in the secondary structure model.

Here I describe my progress on generating a version of TLC1 with the accessory-protein-binding arms engineered to fold into well-determined structures based on the phylogenetically predicted secondary structure model (Zappulla and Cech, 2004). Unlike wild-type TLC1, this "Determined Arm TLC1" (DA-TLC1) is functional *in vitro*, indicating that the catalytic core folds into an enzymatically active state. However, although cells expressing DA-TLC1 do not senesce, telomeres are very short, and DA-TLC1 RNA abundance is low *in vivo*. I show that the determined Ku arm is responsible for both the

increase in telomerase function *in vitro*, and the low RNA abundance *in vivo*. Although DA-TLC1 is not fully functional *in vivo*, my data suggest a previously unknown role for the Ku arm in TLC1 folding and abundance.

4.3: RESULTS

Design of a "determined arm" TLC1

In order to design a TLC1 variant that would function both *in vivo* and *in vitro*, I made a series of single nucleotide substitutions in the RNA to drive the secondary structure into a more energetically favorable final folded state. I used the *Mfold* software to guide the design for two purposes: to promote folding into the phylogenetically derived secondary structure (Zappulla and Cech, 2004), and to find the mutations that would create the most "well-determined" arms (Zuker and Jacobson, 1998). It is important to note that the *Mfold* secondary structure prediction for wild-type TLC1 varies from the phylogenetic model in several ways (Zappulla and Cech, 2004). First, *Mfold* does not predict pseudoknots. Second, some portions of the arms are predicted to fold differently; in particular, the region of the Ku arm distal to the core is very different between the phylogenetically derived and *Mfold* models.

The final "Determined Arm TLC1" (DA-TLC1) has 110 substituted nucleotides across the 1157-nt RNA (Figure 4.1). The majority of the nucleotide substitutions are in the Ku arm, which has 62, compared to 33 substitutions in the Est1 arm, and 15 in the terminal arm. All of these mutations were made in the regions of the arms between the core and the predicted accessory-protein binding sites. These areas of TLC1 are not known to bind any proteins, and have been previously deleted in Mini-T (Zappulla et al., 2005) or stiffened in TSA-T (see Chapter 2; Lebo and Zappulla, 2012) without abolishing telomerase holoenzyme function.

The lowest-free-energy *Mfold* secondary structure model for DA-TLC1 (Figure 4.2) closely matches the secondary structure of the phylogenetically-derived structure for wild-type TLC1 (Zappulla and Cech, 2004). However, the *Mfold* prediction for DA-TLC1 differs from the *Mfold* prediction for wild-type TLC1 in two major ways. First, the

Figure 4.1: RNA nucleotide sequence of a "Determined Arm" TLC1 (DA-TLC1). Nucleotide substitution mutations were made in TLC1, without deletions or insertions, in non-essential regions previously deleted in Mini-T (Zappulla et al., 2005) or stiffened in TSA-T (Lebo and Zappulla, 2012). 9.5% of the 1157 nts were substituted. The 110 mutated nucleotides are indicated in red. The terminal arm is highlighted in green (with 15 nucleotide substitutions), the Ku arm in orange (with 62 substitutions), the Est1 arm in blue (with 33 substitutions), and the template in gray.

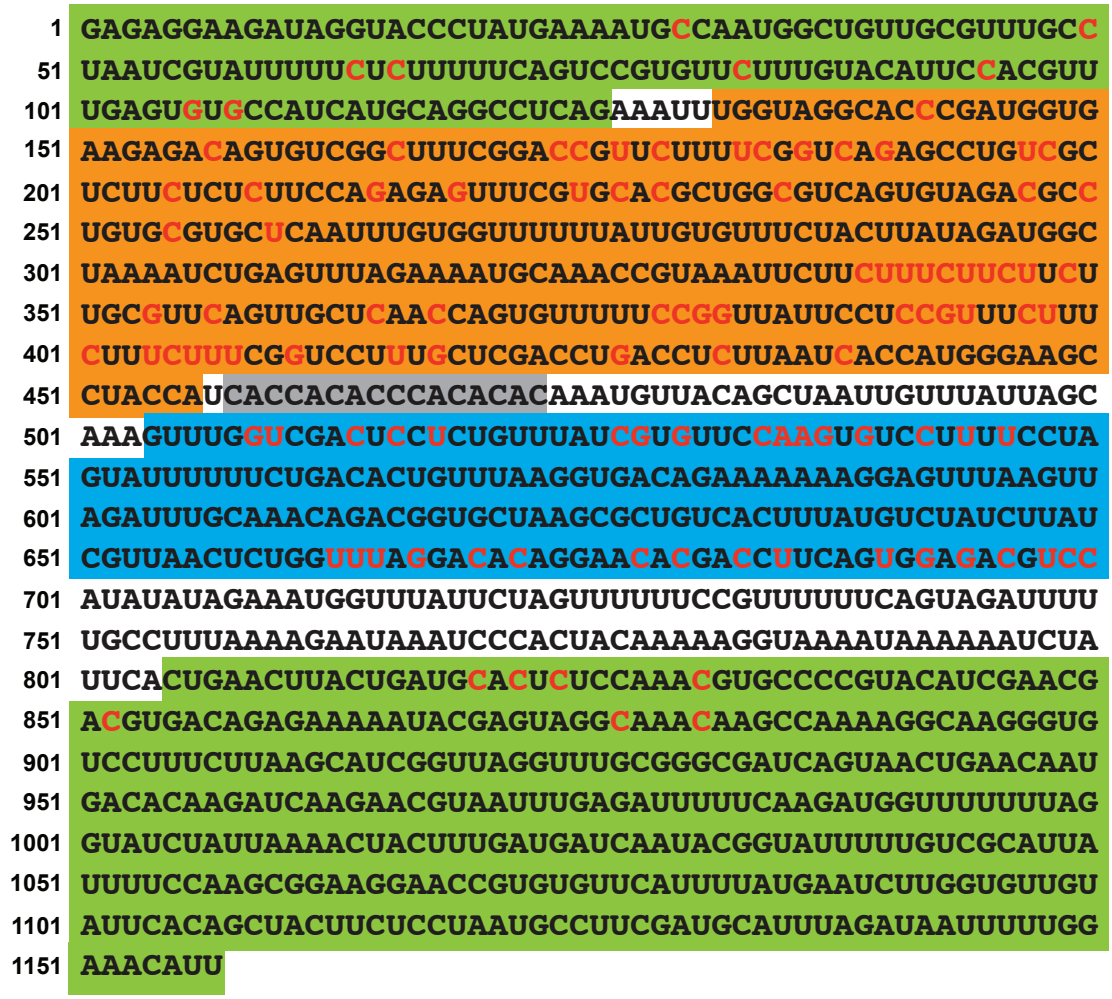

Figure 4.2: Lowest free energy *Mfold* secondary structure predictions for TLC1 and DA-TLC1. (**A**) *Mfold* secondary model for wild-type TLC1. Nucleotides are colored in the p-num format, with the most well determined nucleotides colored in red (Zuker and Jacobson, 1998). Note that *Mfold* in unable to predict the structure of the pseudoknot in the central core. The initial ∆G of folding was predicted to be −321 kcal/mol. (**B**) *Mfold* secondary model for DA-TLC1, with nucleotides colored in the p-num format. Increased redness in the three RNA arms indicates a higher confidence in the secondary structure. Note that the central core folds differently than in the *Mfold* prediction for wild-type TLC1, and is instead more similar to that of TSA-T (see Figure 2.2B). The determined Ku arm was designed to fold into the phylogenetically derived structure for the wild-type arm (Zappulla and Cech, 2004). The initial ∆G of folding was predicted to be −385 kcal/mol.

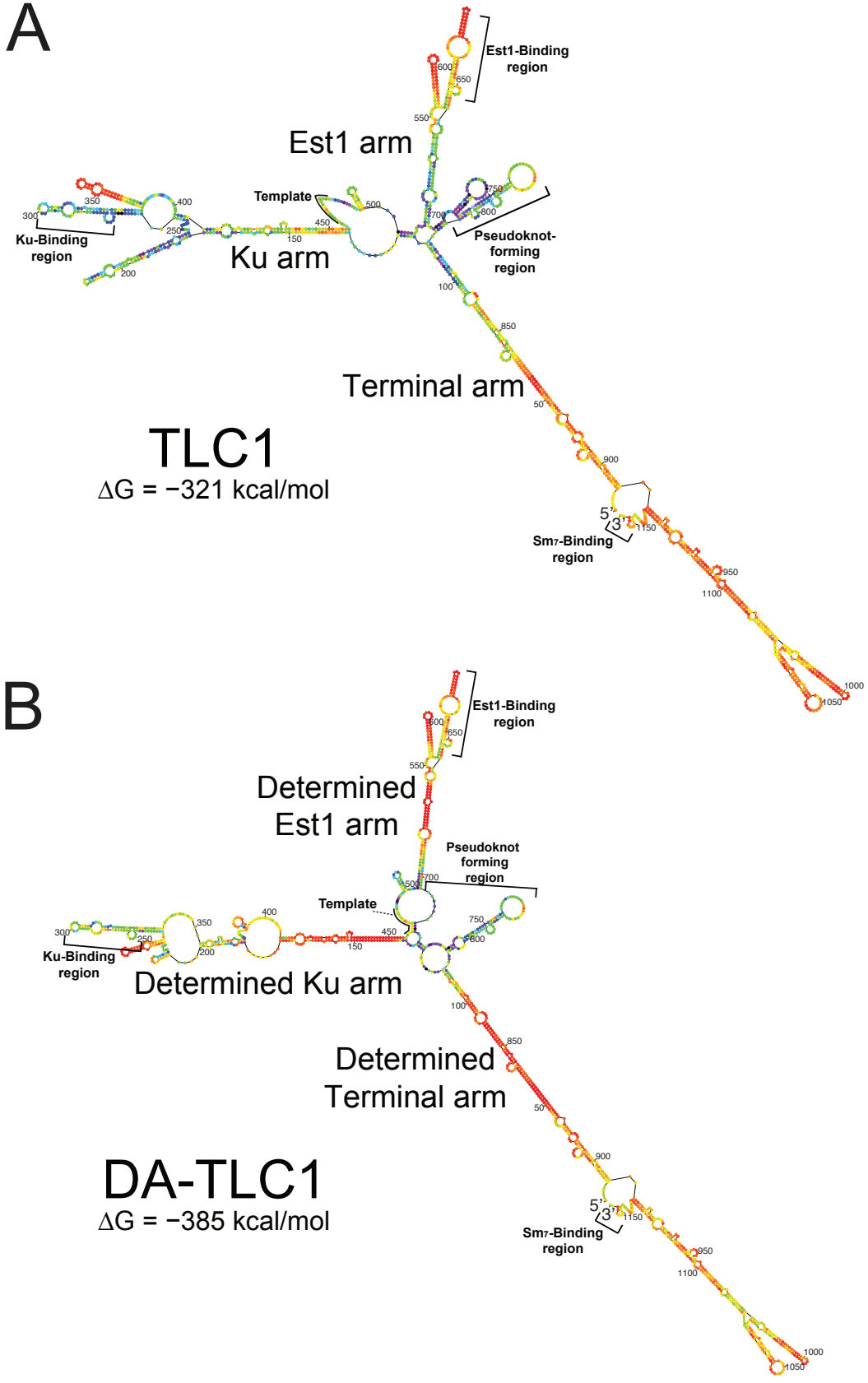
A
Est1-Binding region
Est1 arm
Template
Ku-Binding region
Ku arm
Pseudoknot-forming region
Terminal arm
TLC1
ΔG = −321 kcal/mol
Sm7-Binding region
B
Est1-Binding region
Determined Est1 arm
Pseudoknot forming region
Template
Ku-Binding region
Determined Ku arm
Determined Terminal arm
DA-TLC1
ΔG = −385 kcal/mol
Sm7-Binding region

central catalytic core is predicted to fold differently; rather than forming the two-hairpin structure seen in lieu of the pseudoknot in wild-type TLC1, the core of DA-TLC1 has only a single hairpin, and the template is partially paired with nucleotides from the opposite side of the core (Figure 4.2). The secondary structure predicted in the core of DA-TLC1 is also seen in the *Mfold* model for TSA-T (see Figure 2.2B), and therefore is likely to represent a functional structure. Additionally, the Ku arm is predicted by *Mfold* to fold differently in DA-TLC1 compared to TLC1 (Figure 4.2). This is because DA-TLC1 was designed to match the phylogenetically-derived model for TLC1 (Zappulla and Cech, 2004).

The *Mfold* model for DA-TLC1 also shows that each arm is energetically more "well determined" than those of wild-type TLC1. More nucleotides in each of the three arms of DA-TLC1 are colored red on the P-num scale than in wild-type TLC1, indicating a higher degree of confidence in the indicated folded conformation (Figure 4.2). The arms of DA-TLC1 are therefore more likely to fold into the predicted state than those in TLC1. Accordingly, DA-TLC1 is predicted to have a lower initial free energy of folding than TLC1 (Mfold predicts −385 kcal/mol compared to −321 kcal/mol for wild type).

DA-TLC1 is more functional than wild-type TLC1 *in vitro*

Wild-type TLC1 RNA is unable to support telomerase enzyme function in an *in vitro* reconstituted telomerase activity assay (Zappulla et al., 2005), presumably due to misfolding of the central core. To test whether the more well-determined structure of DA-TLC1 promotes telomerase function *in vitro*, I performed an *in vitro* assay. DA-TLC1 was expressed alongside ProA-tagged yeast TERT, Est2, in an *in vitro* transcription and translation system. Immunopurified telomerase RNP was incubated with a telomeric DNA primer and [α-^{32}P]-dGTP, and products were separated by urea-polyacrylamide gel electrophoresis.

DA-TLC1 supported telomerase function *in vitro* at levels similar to TSA-T (Figure 4.3). As previously reported, wild-type TLC1 was nearly nonfunctional *in vitro*. Miniaturized telomerase RNA, Mini-T, supported robust telomerase activity, while stiffened-arm telomerase, TSA-T, had slightly reduced levels of activity (Figure 4.3; Lebo and Zappulla, 2012; Zappulla et al., 2005). While DA-TLC1 telomerase activity was slightly lower than that of Mini-T, it was still many-fold higher than that of wild-type TLC1. These data indicate that the well-determined arms of DA-TLC1 improve telomerase catalytic core function *in vitro*.

Cells expressing DA-TLC1 do not senesce, but do have extremely short telomeres

Having demonstrated that the well-determined arms of DA-TLC1 support increased telomerase activity *in vitro*, I next tested DA-TLC1 function *in vivo*. DA-TLC1 RNA was expressed from a centromere-containing (*CEN*) plasmid, with sequences from upstream and downstream of the wild-type *TLC1* locus, in a *tlc1*Δ *rad52*Δ strain. Deletion of *rad52*Δ prevents alternative recombination-based survivor pathways for telomere lengthening, and ensures that all cellular telomere lengthening is telomerase dependent (Le et al., 1999; Li and Lustig, 1996; Lundblad and Blackburn, 1993; McEachern and Blackburn, 1996). Cells were then restreaked 10 times, representing approximately 250 generations of growth.

DA-TLC1-expressing cells survived without senescing through the course of the experiment (Figure 4.4A). In contrast, cells lacking a functional telomerase RNA senesced by 125 generations of growth. This demonstrates that the essential RNA domains in DA-TLC1, including the catalytic core and the Est1-binding arm, fold into functional structures *in vivo*.

However, DA-TLC1 maintains telomeres much shorter than wild type. To assess telomere length, I performed a telomere Southern blot on genomic DNA isolated from

Figure 4.3: DA-TLC1 supports telomerase function in an *in vitro* reconstituted telomerase assay. TLC1 variants were co-expressed with ProA-Est2 in an *in vitro* transcription and translation system, co-immunopurified, and reacted with a telomeric DNA primer (top). Addition of seven nucleotides to the primer was monitored by denaturing polyacrylamide gel electrophoresis (bottom). Products from two independent enzyme reactions from the same telomerase RNP are shown. Relative telomerase activity is indicated; ++++ for robust telomerase activity, +++ for strong activity, ++ for weak activity, + for trace activity, and − for no activity. Loading control, LC, is a [γ-^{32}P]-labeled primer.

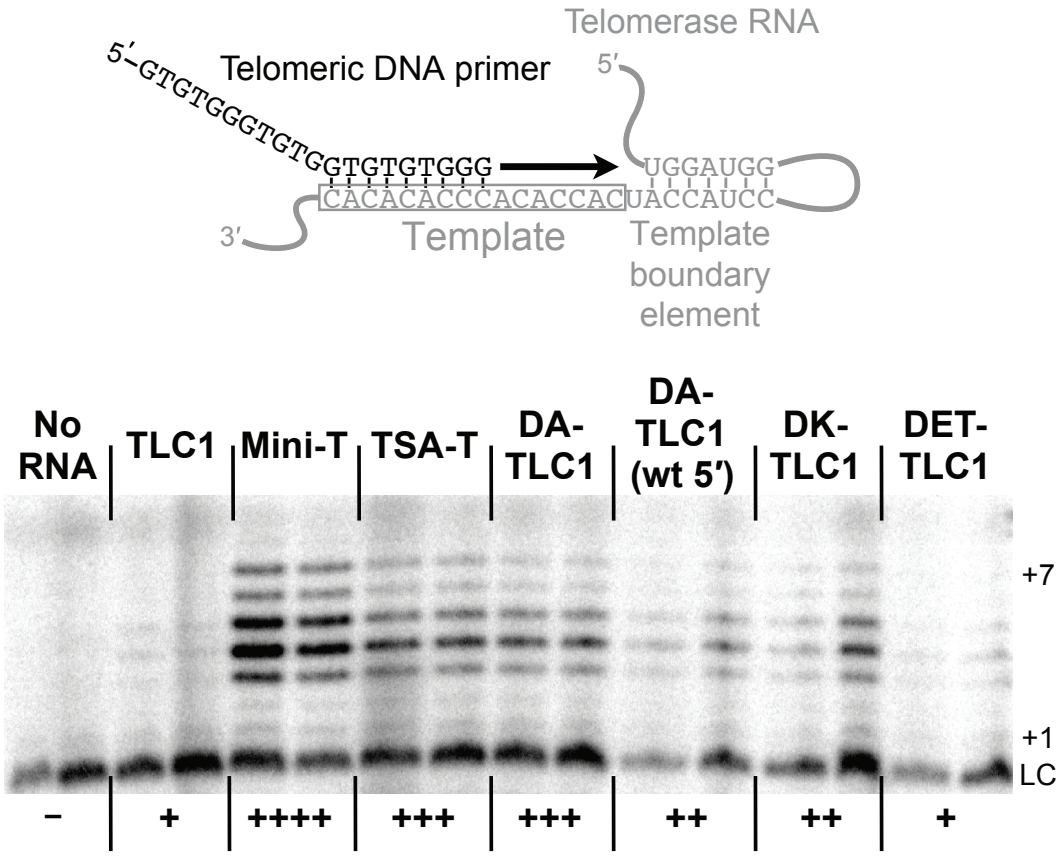

Figure 4.4: DA-TLC1 maintains shortened telomeres *in vivo*. (**A**) Cells expressing DA-TLC1 do not senesce. Each telomerase RNA allele was harbored on a low-copy *CEN* plasmid in a *tlc1*Δ *rad52*Δ yeast strain, and restreaked for over 250 generations. Growth shown at 250 generations. (**B**) Telomere Southern blot of *Xho*I-digested genomic DNA. Two independent isolates at 250 generations are shown. Change in telomere length relative to wild-type TLC1 is indicated for two isolates, ± S.D. (**C**) Dot blot of total RNA isolated from cells at 50 generations of growth, probed for the shared 3′ end of TLC1 common to all RNA variants and normalized to U1 snRNA control spots. Normalized telomerase RNA abundance relative to TLC1 from four isolates is indicated, ± S.D.

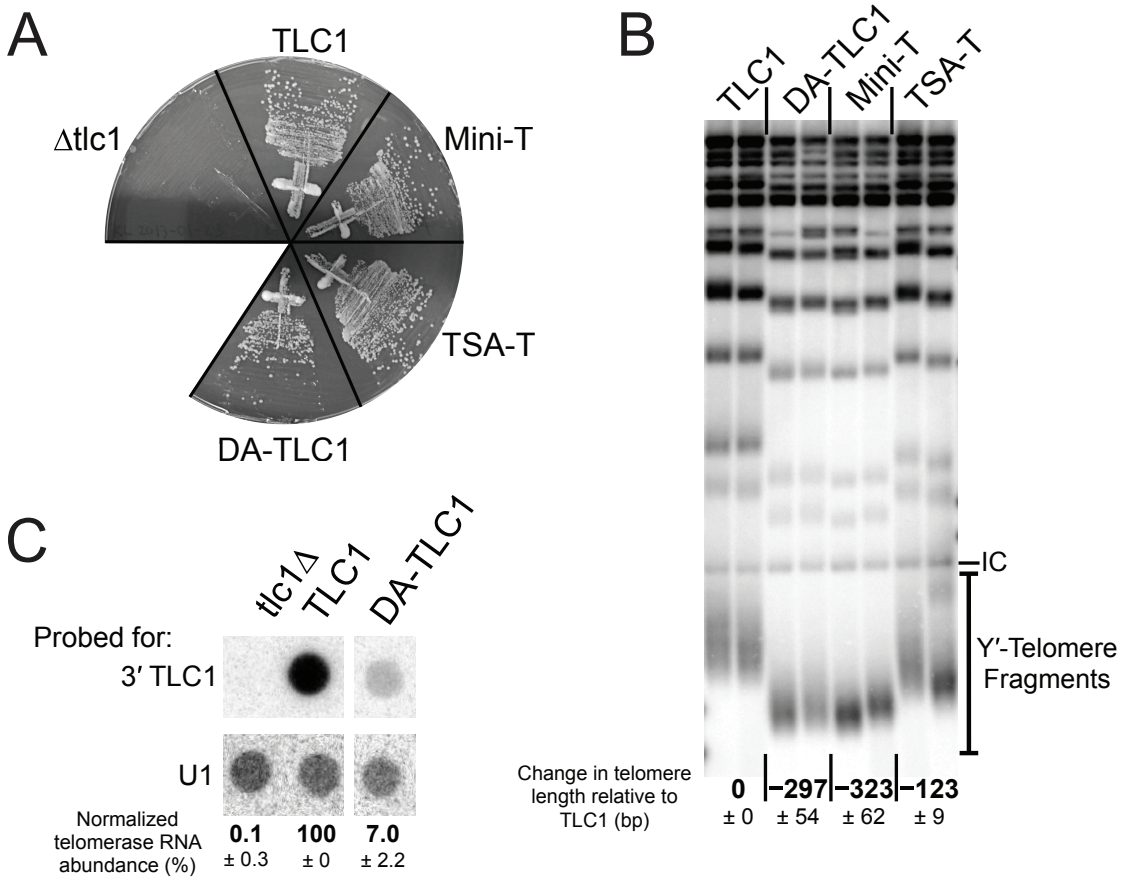

cells expressing DA-TLC1. Telomeres in these cells were approximately 300 bp shorter than wild type (Figure 4.4B). This length is similar to telomeres maintained by Mini-T, and much shorter than those maintained by TSA-T. The short telomeres are likely due to low DA-TLC1 RNA abundance; dot blots performed on total cellular RNA reveal that the cellular level of DA-TLC1 is ~7% that of wild-type TLC1 (Figure 4.4C). This level of accumulation *in vivo* is similar to — and perhaps even lower than — that of Mini-T and TSA-T (Lebo and Zappulla, 2012; Zappulla et al., 2005). Together, these data indicate a partial, but substantial, a defect in DA-TLC1 RNA accumulation *in vivo*.

The determined Ku arm has positive effects on *in vitro* telomerase RNA function, but negative effects on *in vivo* abundance

In order to identify which portion of DA-TLC1 causes the *in vivo* defects, I made several DA-TLC1 variants. First, I restored the 5′ side of the terminal arm (nts 1−117) to the wild-type sequence, which converts 8 of the substituted nucleotides back to wild type. This region of the terminal arm has been implicated in maintaining telomerase RNA abundance (see Chapter 5). *Mfold* predicts a similar secondary structure for "DA-TLC1(wt 5′)" compared to DA-TLC1 (Figure 4.5A). The "redness" of the p-num annotation is also similar to DA-TLC1, although the terminal arm is less well determined, and DA-TLC1(wt 5′) has slightly higher an initial ΔG of −364 kcal/mol. This construct supported slightly reduced telomerase activity *in vitro* compared to DA-TLC1 or TSA-T (Figure 4.3), and still resulted in low telomerase RNA abundance in the cell (Figure 4.6).

Next, I created a version of TLC1 with only the Ku arm mutated to be well determined. The Ku arm in this determined-Ku arm TLC1 (DK-TLC1) is predicted by *Mfold* to fold into the phylogenetically derived structure, similar to DA-TLC1 (Figure 4.5B). However, due to the wild-type Est1 and terminal arms in DK-TLC1, the predicted secondary structure of the central core is similar to that of wild-type TLC1 rather than

Figure 4.5: Lowest free energy *Mfold* secondary structure predictions for DA-TLC1 variants. (**A**) *Mfold* secondary model for DA-TLC1(wt 5′), with the wild-type 5′ end (nts 1−117). Nucleotides are colored in the p-num format, with the most well determined nucleotides colored in red (Zuker and Jacobson, 1998). The initial ∆G of folding was predicted to be −364 kcal/mol. (**B**) *Mfold* secondary model for DK-TLC1, with wild-type Est1 and terminal arms and only the Ku arm redesigned to be well-determined. The initial ∆G of folding was predicted to be −339 kcal/mol. (**C**) *Mfold* secondary model for DET-TLC1, with a wild-type Ku arm, but Est1 and terminal arms redesigned to be well-determined. The initial ∆G of folding was predicted to be −367 kcal/mol.

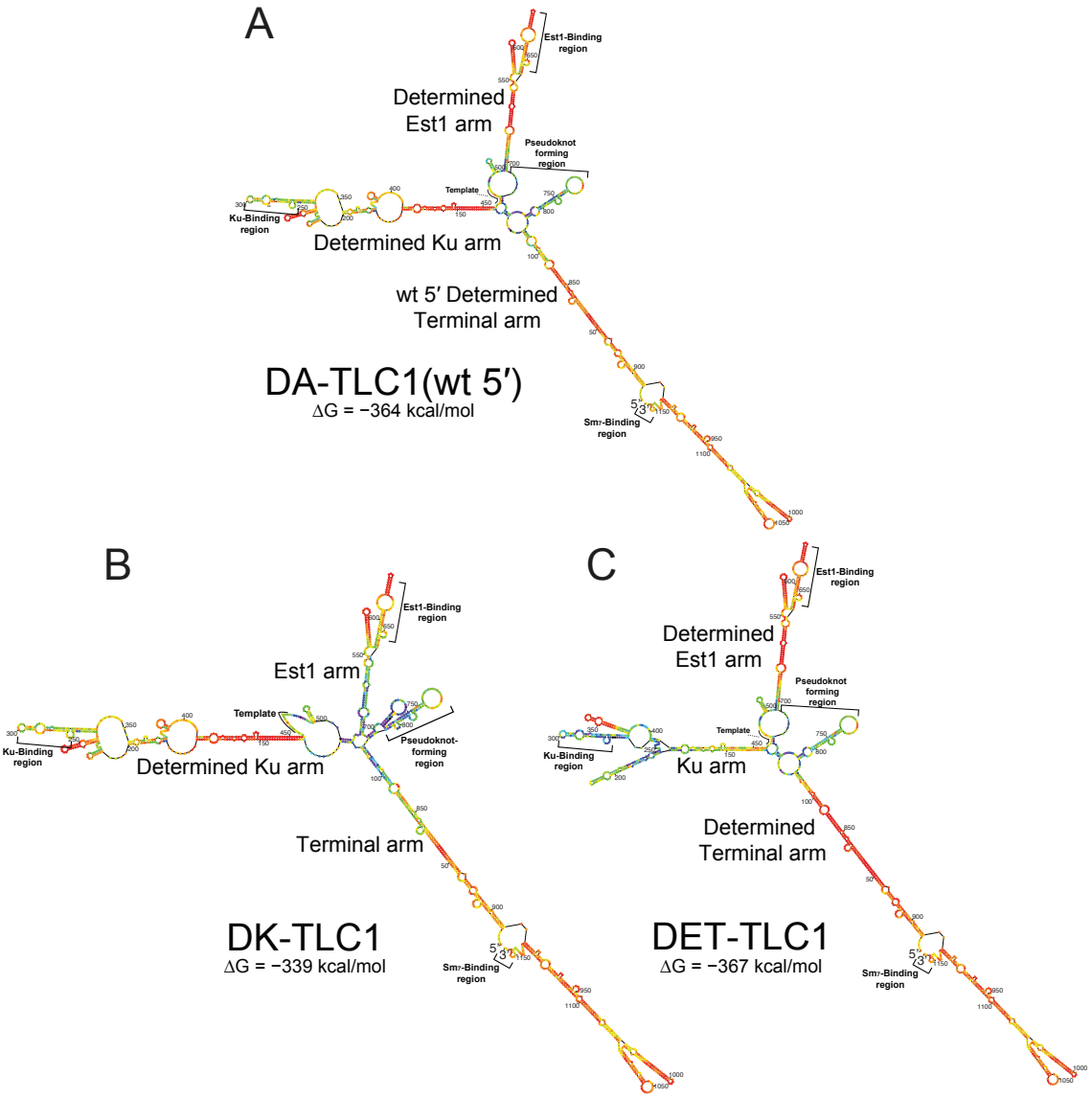
A
Est1-Binding region
Determined Est1 arm
Pseudoknot forming region
Template
Ku-Binding region
Determined Ku arm
wt 5′ Determined Terminal arm
DA-TLC1(wt 5′)
ΔG = −364 kcal/mol
Smƴ-Binding region
B
Est1-Binding region
Est1 arm
Template
Ku-Binding region
Pseudoknot-forming region
Determined Ku arm
Terminal arm
DK-TLC1
ΔG = −339 kcal/mol
Smƴ-Binding region
C
Est1-Binding region
Determined Est1 arm
Pseudoknot forming region
Template
Ku-Binding region
Ku arm
Determined Terminal arm
DET-TLC1
ΔG = −367 kcal/mol
Smƴ-Binding region

Figure 4.6: The determined Ku arm causes low telomerase RNA abundance *in vivo*. (**A**) Cells expressing determined-arm TLC1 variants do not senesce. Telomerase RNA alleles were expressed from *CEN* plasmids in a *tlc1*Δ, *rad52*Δ strain. Growth at 250 generations is shown. (**B**) TLC1 variants with the determined Ku arm have low *in vivo* RNA abundance. Graph of relative RNA abundance of telomerase RNA variants, determined by dot blot. Averages from two independent isolates are shown in % TLC1. Error bars represent S.D.

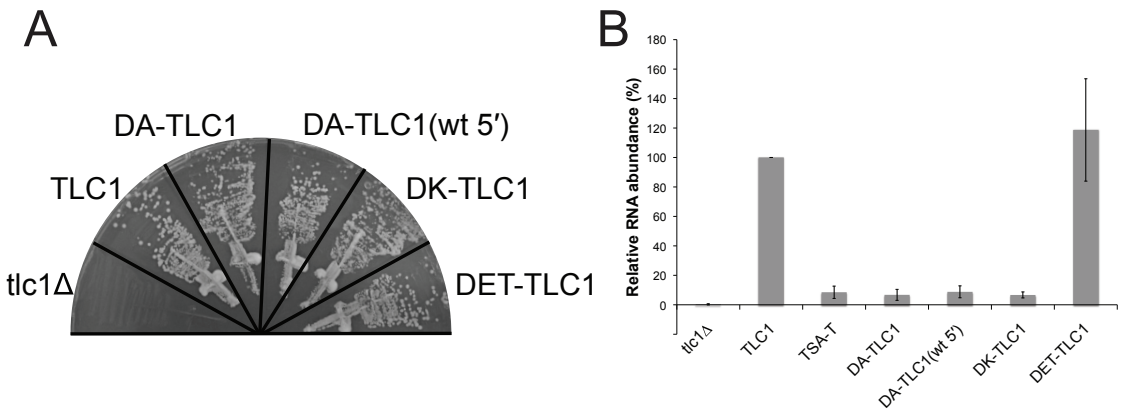

DA-TLC1 or TSA-T. DK-TLC1 also has a higher initial ∆G than DA-TLC1, −339 kcal/mol. DK-TLC1 supports *in vitro* telomerase function, although activity is slightly reduced compared to DA-TLC1 (Figure 4.3). Like DA-TLC1, DK-TLC1 has low RNA abundance when expressed from a *CEN* plasmid *in vivo* (Figure 4.6).

Finally, I made a TLC1 variant with a wild-type Ku arm, but determined Est1 and terminal arms (DET-TLC1). The *Mfold* prediction for the DET-TLC1 secondary structure has a wild-type Ku arm, but well-determined Est1 and terminal arms, with an initial ∆G of −367 kcal/mol (Figure 4.5C). DET-TLC1 was barely functional *in vitro*, supporting telomerase activity only slightly higher than wild-type TLC1 (Figure 4.3). However, DET-TLC1, with the wild-type Ku arm, had near-wild-type RNA levels *in vivo* (Figure 4.6B). Taken together, these data suggest that the determined Ku arm is responsible for both the increased *in vitro* activity of DA-TLC1 and for the reduced telomerase RNA abundance *in vivo*.

4.4: DISCUSSION

The budding yeast *Saccharomyces cerevisiae* has been a powerful model organism for studying the genetics and molecular mechanisms of telomerase function, leading to important discoveries, including the first telomerase subunit gene and genetic discovery of the TERT catalytic protein subunit (Lendvay et al., 1996; Lingner et al., 1997b; Singer and Gottschling, 1994). However, biochemical studies have been limited by the misfolding of full-length TLC1 *in vitro*, as evidenced by the failure to support telomerase enzyme function in an *in vitro* reconstituted telomerase assay. To bypass this problem, as series of miniaturized mutants of TLC1 have been designed that restore *in vitro* activity (Zappulla et al., 2005).

The minimally sized Micro-T RNAs have each of the three accessory-protein-binding arms entirely deleted, leaving just a 155-nt central catalytic core (Mefford et al., 2013; Qiao and Cech, 2008). However, although Micro-T is functional *in vitro*, it would be certainly unable to function *in vivo* because it lacks the important and essential accessory-protein-binding sites. The slightly larger Mini-T RNAs are functional both *in vitro* and *in vivo* (Zappulla et al., 2005). With 657 nts deleted from the RNA arms, Mini-T(500) is highly mutated in both sequence and structure, and the truncated arms draw the accessory-protein binding sites in much closer to the catalytic core. Additionally, Mini-T RNA abundance is ~15% of wild type *in vivo*, and telomeres maintained at a stable but much shorter length. Finally, TSA-T has the three accessory-protein-binding arms stiffened by the deletion of 201 nts and several nucleotide substitutions (see Chapter 2; Lebo and Zappulla, 2012). TSA-T is functional *in vitro*, although slightly less than Mini-T and Micro-T. TSA-T is also highly functional *in vivo*, despite low RNA abundance. On a per-RNA basis, TSA-T actually maintains longer telomeres than wild-type TLC1, despite the fact that the stiffened arms of TSA-T significantly alter the overall

architecture of the telomerase RNP. While the many heavily mutated TLC1 RNA mutants have helped make important advances in understanding the molecular mechanisms and organization of the yeast telomerase RNP, a minimally mutated RNA that folds into its native state *in vitro* would allow us to examine the most biologically accurate RNA conformation and, ultimately, assembly of the biologically relevant RNP complex. Being able to study such a minimally mutated TLC1 biochemically *in vitro* would advance our understanding of both telomerase and the growing field of long noncoding RNAs (lncRNAs).

To design a minimally mutated wild-type-length TLC1 RNA that folds into its biologically relevant conformation and functions both *in vivo* and *in vitro*, I employed *Mfold* RNA secondary structure prediction software (Zuker, 2003). Using the p-num output format to color nucleotides based on confidence in the local secondary structure modeling, I tested a series of nucleotide substitutions mutants in TLC1 to design a telomerase RNA with well-determined accessory-protein-binding arms. The resulting "Determined-Arm TLC1" (DA-TLC1) is wild-type length (1157 nts) with 110 nucleotide substitutions (Figure 4.1). With only 9.5% of the nucleotides mutated, DA-TLC1 is significantly less mutated that Mini-T, which has 657 nts deleted, or TSA-T, which has 201 nts deleted in addition to several other nucleotide substitutions. Furthermore, DA-TLC1 was designed to have a secondary structure based on the phylogenetically derived structure model for wild-type TLC1 (Figure 4.2).

Unlike wild-type TLC1, the catalytic core of DA-TLC1 folds into a catalytically competent state *in vitro*, supporting enzymatic activity in a reconstituted telomerase assay (Figure 4.3). This appears to be due primarily to stabilizing effects of the well-determined Ku arm in DA-TLC1; in fact, mutating only the Ku arm into the well-determined state in TLC1 was sufficient to promote *in vitro* telomerase activity, despite only a modest decrease in the ΔG for DK-TLC1 compared to wild type (see DK-TLC1 in

Figure 4.3). This is similar to variants of TLC1 with a stiffened Ku arm, which are also functional *in vitro* (see Figure 2.7B). Together, these data suggest that it is the primarily the Ku arm that causes wild-type TLC1 to misfold *in vitro*; stabilizing the folding of the arm is able to substantially prevent this misfolding, allowing the catalytic core to form properly.

Although engineering the Ku arm of TLC1 to fold into a more "well-determined" structure increases telomerase function *in vitro*, it appears to have the opposite effect *in vivo*. Cells expressing TLC1 variants with a well determined Ku arm did not senesce, but had extremely short telomeres, similar to Mini-T (Figure 4.4). This is likely an effect of very low DA-TLC1 RNA abundance in the cell. The telomeres are so short relative to the low RNA abundance that it is possible that the core-function of DA-TLC1 is compromised (unlike TSA-T, which maintains telomeres longer than wild-type TLC1 on a per RNA basis (see Figure 2.6; Lebo and Zappulla, 2012).

It is unclear why redesigning the Ku arm to fold into a more well-determined final state has a negative effect on telomerase function *in vivo*. It is possible that the secondary structure model I used to design the determined Ku arm was inaccurate. There are currently three different Ku arm models, including the *Mfold* lowest energy predicted structure, without any constraints on folding, and two phylogenetically determined models (Dandjinou et al., 2004; Zappulla and Cech, 2004). Due to rapid evolution in the Ku arm region, there is limited structural information in the phylogenetic analyses. Furthermore, the Ku arm is one of the most poorly determined regions in the Mfold model of the RNA. When designing DA-TLC1, I selected the model based on the four most closely related *Saccharomyces* species in order to reduce the influence from more divergent species (Zappulla and Cech, 2004). My findings suggest that this model is at least partially inaccurate in the Ku arm, and that the wild-type Ku arm may fold into a different secondary structure. It is possible that one of the other previously predicted

models for the Ku arm is correct instead. Alternatively, the determined Ku arm secondary structure may be accurate, but sequence mutations in the arm may disrupt an unknown important tertiary structure in the arm.

Another interesting possibility for why driving the Ku arm folding into a more well-determined final state has negative effects *in vivo* could be that the RNA requires heterogeneity in its secondary structure, either in the ensemble population or through dynamic restructuring within the same RNA. The Ku arm may need to be able to achieve multiple different secondary structures for optimal function in telomerase and organismal fitness, possibly switching to different folding states at different points in telomere lengthening. These different Ku-arm states could potentially regulate core function, or perhaps regulate the Ku-mediated secondary telomerase-recruitment activity. By favoring a specific folding state, I may have prevented the folding of a second important conformation. If such RNA secondary-structure heterogeneity is in fact important for telomerase function, it could represent data in support of a third tenet of the TLC1 flexible scaffold model, with a required flexibility in base pairing.

It is still not clear why putative misfolding in the Ku arm would cause very low RNA abundance *in vivo*. It is possible that the phenotype is related to some dysfunction in the role of the Ku heterodimer in telomerase. However, this seems unlikely, since the effects of the determined Ku arm on TLC1 abundance and telomere length is much more severe than deleting the Ku-binding site in TLC1Δ48 (Stellwagen et al., 2003; Zappulla et al., 2011). Furthermore, other Ku-binding-competent TLC1 variants with mutations in the Ku arm have reduced RNA levels, including TLC1(S−−), with a stiffened Ku arm (see Chapter 2, and Figure 2.8). Together, these data suggest an additional role for the Ku arm in TLC1 function, in addition to tethering the Ku heterodimer to the complex. The nature of the putative second function is not clear; it may be involved in regulating RNA

structure, abundance, or function, or it may help mediate previously unknown interactions with other protein components.

Overall, DA-TLC1 failed to provide robust function *in vivo*, despite supporting activity better than wild type *in vitro*. These results indicate that the determined Ku arm is responsible for the reduced *in vivo* function, and suggest previously unknown roles for the Ku arm in telomerase. While DA-TLC1 did not achieve the original goal, namely engineering a TLC1 RNA variant with maximal *in vitro* activity and maintaining full-length telomeres *in vivo*, I still think the goal is achievable. Promoting the arms folding into well-determined structures based on *Mfold* modeling did help to increase *in vitro* activity substantially. I think it is likely that a re-engineered Ku arm could help to complete the desired TLC1 RNA variant. This redesign would involve promoting the core-proximal region of the Ku arm to be well determined, while leaving the distal region unchanged. This may allow the distal portion of the arm to fold into any required functional conformations, while still stabilizing catalytic core formation by driving folding of the core-proximal region.

4.5: METHODS

Design of DA-TLC1

To engineer DA-TLC1, I made a series of nucleotides substitutions in the arms of TLC1 *in silico*, and submitted them to the *Mfold* RNA secondary structure prediction webserver (Zuker, 2003), with two goals: (1) to drive the final folding state into the phylogenetically predicted structure (Zappulla and Cech, 2004), and (2) to increase the "determinedness" of the three RNA arms, guided by the P-num output. Over thirty variations of TLC1 were examined bioinformatically, ultimately culminating in the reported DA-TLC1, with more well-determined arms than wild-type TLC1, and a lower predicted initial ΔG (−385 kcal/mol, compared to −321 kcal/mol in TLC1; see Figure 4.2). DA-TLC1 has 110 nucleotide substitutions over its 1157 nt length, or 9.5% of its nucleotides mutated (see Figure 4.1). 15 nts are substituted in the terminal arm, 62 in the Ku arm, and 33 in the Est1 arm. A gene-synthesis fragment for *DA-TLC1* was ordered (*GENEWIZ*), and ligated into a *CEN* vector harboring upstream and downstream sequences from genomic *TLC1*.

The DA-TLC1 variants in Figure 4.5 were cloned using restriction enzyme sites in TLC1. DA-TLC1 with wt 5′ end was created by cloning the *Stu*I to *Nsi*I fragment of *DA-TLC1* into a *TLC1*-harboring plasmid, effectively restoring nts 1−117 to wild type. DK-TLC1 was created by ligating the *Stu*I to *Nco*I fragment of *DA-TLC1* into *TLC1*, adding the determined Ku arm to wild-type TLC1. DET-TLC1 was created by ligating the *Stu*I to *Nco*I fragment of *TLC1* into *DA-TLC1*, restoring the wild-type Ku arm sequence to DA-TLC1.

Experiments in yeast

All telomerase RNA alleles were expressed from *TRP1*-marked centromeric (*CEN*) plasmids. These plasmids were transformed into strain TCy43 (*MAT-a ura3-53 lys2-801 ade2-101 trp1-Δ1 his3-Δ200 leu2-Δ1 VR::ADE2-TEL adh4::URA3-TEL tlc1Δ::LEU2 rad52Δ::HIS3 [pTLC1-LYS2-CEN]*) (Seto et al., 1999). After shuffling out *TLC1* (*LYS2/CEN*) on solid medium containing α-aminoadipate, colonies were restreaked 10 times on synthetic compete media plates lacking tryptophan, with each restreak representing approximately 25 generations of yeast growth.

Nucleic acid blots

Southern blots were performed as previously described (Lebo and Zappulla, 2012; Zappulla et al., 2005; Zappulla et al., 2011). Briefly, cell pellets for genomic DNA isolation were prepared from cultures made from serially restreaked plates, with each streak representing ~25 generations. Genomic DNA was isolated (Gentra Puregene system), equal amounts were digested with *Xho*I and electrophoresed through a 1.1% agarose gel at 70 V for 17 h, and transferred to Hybond-N+ Nylon membrane (GE). The blot was then probed for telomeric sequences and a 1627-bp non-telomeric fragment of chromosome IV. Average Y′ telomere fragment length was quantified using the weighted average mobility (WAM) method described previously (Zappulla et al., 2011).

RNA dot blots were performed as previously described (Lebo and Zappulla, 2012). Total cellular RNA was extracted from late log phase or early stationary phase yeast cultures by a slightly modified version of the hot phenol RNA isolation method (Kohrer and Domdey, 1991). After boiling, 5 µg of RNA was spotted twice onto Hybond-N+ Nylon Membrane (GE). The membrane was cut in half such that the two dots of each sample were separate membrane sections, air-dried, UV-crosslinked (SpectroLinker XL-1500 UV Crosslinker, using two runs of the “Optimal crosslink” setting), and pre-

hybridized in Church buffer at 55°C for 10 minutes. One membrane was probed for the 3′ region of TLC1 (nucleotides 906 to 1140), while the other was probed for the U1 snRNA (Friedman and Cech, 1999). Telomerase RNA levels were normalized to U1 levels.

Reconstituted telomerase activity assays

Linearized “run off” DNA templates for T7 transcription of telomerase RNAs were made using PCR products of the gene with a T7 promoter included at the 5′ end of the forward primer. *In vitro* telomerase activity assays were performed as described previously (Zappulla et al., 2005). Briefly, linear DNA template for telomerase RNA was mixed with plasmid containing T7-ProA-Est2 in an RRL transcription and translation system. Telomerase was immunopurified with IgG-Sephadex beads. Telomerase beads were then incubated with telomeric primer, dNTPs, and [α-^{32}P]-dGTP. Products were electrophoresed through a 10% polyacrylamide/TBE/urea gel, and imaged using phosphor screens and a Typhoon 9410 Variable Mode Imager. As an internal control for product recovery and loading, ~1 nM [γ-^{32}P]-labeled primer was added before the telomerase reaction. Activity levels were normalized to the internal control.

Chapter 5:

Identification of RNA abundance-regulating elements in the terminal arm of yeast telomerase RNA

5.1 ABSTRACT:

Large portions of the three long RNA arms of *S. cerevisiae* telomerase RNA, TLC1, can be deleted while retaining telomerase function. However, I have observed that deletions within the core-proximal half of the terminal arm, dubbed the Terminal Arm Humerus (TAH), result in TLC1 levels ~10% of wild type, causing shortened telomeres. Through precise mutations in the RNA, I have isolated potential RNA domains in the terminal arm with roles in telomerase RNA abundance. Furthermore, several putative protein-binding sites localize to these regions, suggesting a possible role for a protein factor in maintaining TLC1 abundance in the cell. Finally, my results suggest that the conserved three-way junction element in TLC1 may play a role in telomerase RNA abundance.

5.2 INTRODUCTION:

Telomerase RNA is critical for telomerase holoenzyme function, both *in vivo* and *in vitro*, due to its roles as both a template for reverse transcription and as a scaffold for RNP assembly (Greider and Blackburn, 1987, 1989; Shippen-Lentz and Blackburn, 1990; Zappulla and Cech, 2004). Because telomerase RNA is the limiting factor in RNP assembly, maintaining RNA abundance in the cell is very important and a reduction can cause defects in telomere maintenance (Greider, 2006; Hathcock et al., 2002; Mozdy and Cech, 2006; Tuzon et al., 2011). Telomerase haploinsufficiency has been associated with human disease (Armanios et al., 2005; Garcia et al., 2007). Therefore, understanding elements that control telomerase RNA abundance in the cell is important for studies of telomerase function.

The 1157-nt *Saccharomyces cerevisiae* telomerase RNA, TLC1, abundance *in vivo* is very low, with only 29 ± 7 copies per cell (Mozdy and Cech, 2006). Several elements within the *TLC1* promoter have been identified that regulate the low RNA abundance (Dionne et al., 2013). Within TLC1 RNA itself, many mutations have been identified that reduce RNA levels. The Ku- and Sm_7-binding sites on TLC1 are needed maintain the RNA. Deletion of the Ku-binding site in TLC1 reduces levels to approximately 50% of wild type, although the mechanism by which Ku affects TLC1 abundance is not known (Zappulla et al., 2011). The role of Sm_7 in TLC1 RNA abundance is better understood. TLC1 is initially transcribed as a 1251-nt precursor that is terminated by either a polyadenylation sequence or the non-coding RNA factors Nrd1 and Nab3 (Chapon et al., 1997; Noel et al., 2012). This precursor is later processed into the 1157-nt mature TLC1 by exonucleolytic digestion from the 3′ end. Sm_7 binds to the TLC1 precursor and blocks resection by the exonuclease, leaving the Sm_7 ring bound to the end of the mature RNA (Coy et al., 2013). Loss of Sm_7 binding to the RNA causes

TLC1 to be fully digested by the exonuclease, leaving only the low-abundance precursor form. The abundance of TLC1ΔSm$_7$ RNA is only approximately 5% of wild type (Seto et al., 1999).

Other abundance-regulating domains in TLC1 are not well understood. Mutations within the Ku-binding arm cause low TLC1 abundance through an unknown mechanism, although the RNA levels vary depending on the mutation (see Chapters 2 and 4). Mutations in the terminal arm, however, result in very similar RNA abundance phenotypes. In particular, the published TLC1ΔΔ, Mini-T, and TSA-T truncation mutants all have telomerase RNA levels 10−15% of wild type (Lebo and Zappulla, 2012; Zappulla and Cech, 2004; Zappulla et al., 2005). All of these TLC1 variants have deletions in the core-proximal region of the terminal arm, although they vary greatly in sequence and structure; TLC1ΔΔ and Mini-T have extensive nucleotide deletions resulting in a truncated terminal arm, while TSA-T has only the unpaired nucleotides in the arm deleted, creating a stiffened dsRNA helix. Building on the “arm” metaphor, this region was dubbed the “Terminal Arm Humerus” (TAH). I sought to understand how these different TAH mutants all produced the same RNA abundance phenotype.

Here, I show that deletions in the Terminal Arm Humerus cause low RNA abundance. In particular, mutating just nucleotides 21−30 in TLC1 result in a low RNA abundance phenotype, although not quite as low as the full TAH mutations. I provide evidence for a second domain in the middle of the TAH that has a moderate effect on RNA levels. Finally, I demonstrate that deleting the three-way junction of TLC1 reduces RNA abundance. Overall, these results identify important regions for TLC1 RNA maintenance within the cell.

5.3 RESULTS:

Mutations in the terminal arm of TLC1 result in low RNA abundance *in vivo*

Several published TLC1 RNA variants with mutations in the terminal arm have similarly low telomerase RNA levels in the cell. This includes RNAs with truncations in the terminal arm, such as Mini-T (Zappulla et al., 2005) and TLC1ΔΔ (Zappulla and Cech, 2004), and stiffened versions of the terminal arm with unpaired nucleotides deleted in TSA-T and TLC1(−−S) (see Chapter 2; Lebo and Zappulla, 2012). Each of these mutant RNAs was published to have RNA abundance ranging from 10 to 15% of wild type.

To show that the RNA levels of these terminal arm mutants were in fact similar, I analyzed them on the same dot blot. Centromere-containing (*CEN*) plasmids harboring the *TLC1* variants, in addition to upstream and downstream sequences from the *TLC1* genomic locus, were expressed in *tlc1*Δ, *rad52*Δ cells; deleting *RAD52* prevents an alternative recombination-based mechanism for telomere maintenance, ensuring that telomere length effects were the result of telomerase-mediated maintenance (Le et al., 1999; Li and Lustig, 1996; Lundblad and Blackburn, 1993; McEachern and Blackburn, 1996). Total cellular RNA was isolated after 50 generations of growth and spotted onto a membrane for a dot blot; Northern blotting was not used due to the strongly impeded migration of TSA-T RNA through polyacrylamide gels. Blots were probed for either the 3′ end of TLC1 (Lebo and Zappulla, 2012), or using a Mini-T-based probe (Zappulla et al., 2005), and normalized to a U1 probe. Note that the Mini-T variants lack the 3′ end of TLC1, and will not anneal to the 3′-end probe. Similarly, TSA-T is not recognized by the Mini-T probe, likely due to the stably-paired arms blocking access to the probe DNA.

Dot blot analysis confirmed that TSA-T, TLC1(−−S), TLC1ΔΔ, and Mini-T all have similar RNA abundances in the cell, ranging from 10 to 13% of wild-type TLC1 levels

(Figure 5.1). While TSA-T and Mini-T could not be analyzed using the same probe, using both probes in parallel allowed for direct comparison, since both were normalized to TLC1. Other RNA variants that could be analyzed with either probe, such as TLC1ΔΔ and TLC1(−−S), had similar RNA abundances regardless of which probe was used.

It is not immediately clear why these TLC1 mutants have similar RNA abundance phenotypes, since they vary greatly in both structure and sequence. However, they all have mutations in Terminal Arm Humerus (TAH) region of TLC1 (Figure 5.1C). The stiffened terminal arm in TSA-T and TLC1(−−S) has all unpaired nucleotides in the TAH deleted, in addition to several other point mutations; these mutations are all between nts 27−114 and 815−894 in wild-type TLC1 (Figure 5.1C). In Mini-T, nts 21−106 and 823−895 of the TAH are entirely deleted. Finally, in TLC1ΔΔ, nts 12−92 and 836−904 are deleted, and replaced with 10 CG base pairs. Based on these mutated regions, I reasoned that the minimal TAH mutated in all of the low-abundance TLC1 variants, nts 27−92 and 836−894, must contain a previously unknown important region (see blue rectangle in Figure 5.1C).

To test whether the TAH *per se* was causing the reduced RNA abundance in the mutants, I analyzed the RNA levels for a version of Mini-T with the TAH restored. Mini-T+TAH RNA was less than 36% as abundance as wild-type TLC1 (Figure 5.1A and B). However, this is approximately three times higher than Mini-T levels. This indicates that although there are other RNA-abundance regulating factors disrupted in Mini-T, the TAH plays a major role in telomerase RNA levels.

Figure 5.1: Mutations in the Terminal Arm Humerus (TAH) result in low RNA abundance. (**A**) TSA-T, TLC1(−−S), TLC1ΔΔ, and Mini-T have similar cellular telomerase RNA levels. Dot blot of total cellular RNA isolated from *tlc1*Δ, *rad52*Δ cells expressing *TLC1* variants from *CEN* plasmids, probed for the 3′ end of TLC1, Mini-T, or the U1 snRNA. Relative abundance from two independent isolates is shown indicated ±S.D. for the 3′ end of TLC1 and Mini-T probes, normalized to U1. Gray numbers indicate unreliable values due to RNAs that cannot be analyzed accurately by the specific probe (the 3′ TLC1 probe does not anneal to Mini-T or Mini-T+TAH, and the Mini-T probe does not anneal well to TSA-T). (**B**) Graph of RNA levels for TAH mutants determined by dot blot in **A**. Dark gray bars represent data from the 3′ TLC1 probe, light gray from the Mini-T probe. Error bars represent S.D. from two replicates. Asterisks indicate unreliable values due to RNAs that cannot be analyzed accurately by the specific probe. (**C**) The Terminal Arm Humerus. Secondary structure model for the TAH based on the phylogenetically-derived secondary structure (Zappulla and Cech, 2004). Regions mutated in the stiffened arms of TLC1(−−S) and TSA-T (nts 27−114 and 815−894) and the truncated arms of Mini-T (nts 21−106 and 823−895) and TLC1ΔΔ (nts 12−92 and 836−904) are indicated by dashed blue lines. The region of the TAH mutated in all of the variants (nts 27−92 and 836−894) is indicated by the blue rectangle.

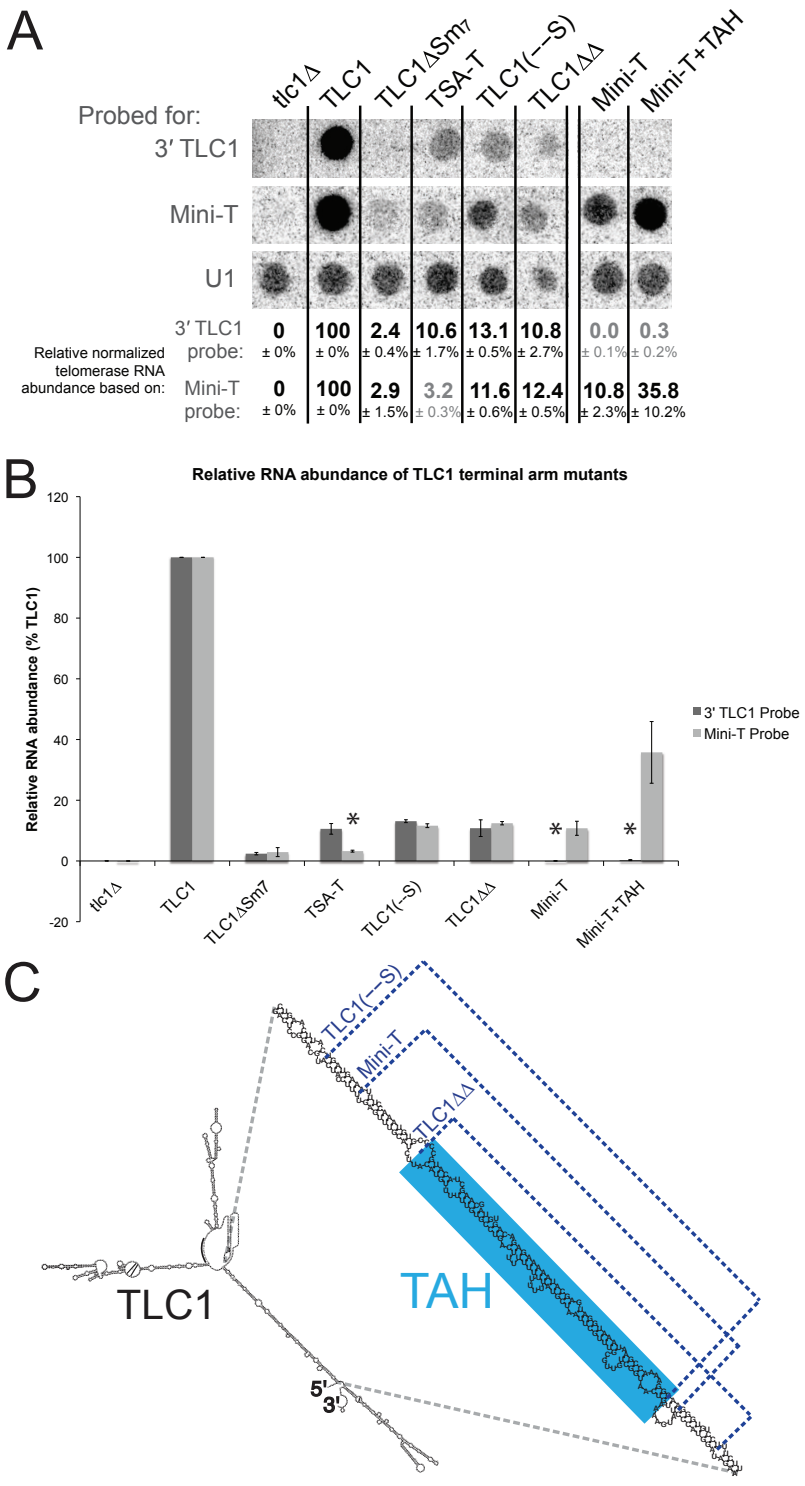
A
tlc1Δ
TLC1
TLC1ΔSm7
TSA-T
TLC1(−−S)
TLC1ΔΔ
Mini-T
Mini-T+TAH
Probed for:
3′ TLC1
Mini-T
U1
Relative normalized telomerase RNA abundance based on:
3′ TLC1 probe:
Mini-T probe:
0 ± 0%
100 ± 0%
2.4 ± 0.4%
10.6 ± 1.7%
13.1 ± 0.5%
10.8 ± 2.7%
0.0 ± 0.1%
0.3 ± 0.2%
0 ± 0%
100 ± 0%
2.9 ± 1.5%
3.2 ± 0.3%
11.6 ± 0.6%
12.4 ± 0.5%
10.8 ± 2.3%
35.8 ± 10.2%
B
Relative RNA abundance of TLC1 terminal arm mutants
Relative RNA abundance (% TLC1)
120
100
80
60
40
20
0
-20
3' TLC1 Probe
Mini-T Probe
tlc1Δ
TLC1
TLC1ΔSm7
TSA-T
TLC1(−S)
TLC1ΔΔ
Mini-T
Mini-T+TAH
C
TLC1(−−S)
Mini-T
TLC1ΔΔ
TAH
TLC1
5'
3'

Two regions of the Terminal Arm Humerus are important for RNA abundance

In order to further refine the region of the TAH responsible for the low RNA-abundance phenotype, I designed a series of truncation mutants in the terminal arm: ΔTAH-A, with nts 19−53 and 873−897 deleted; ΔTAH-B, with nts 53−76 and 855−873 deleted; and ΔTAH-C, with nts 77−95 and 835−855 deleted (Figure 5.2A). These subdomains were designed based on the phylogenetic structure of TLC1 (Zappulla and Cech, 2004), and *Mfold* secondary structure predictions were used to promote proper folding of the rest of the terminal arm and TLC1 (Zuker, 2003). All of the TAH mutants were tested *in vivo* in *tlc1*Δ *rad52*Δ cells, expressed from *CEN* plasmids. None of the RNA variants resulted in senescence (Figure 5.2B).

RNA abundance analysis by dot blots suggests that there are two regions of the TAH responsible for the low RNA level phenotype. A series of dot blot analyses were performed (for a typical dot blot result, see Figure 5.2C; for combined graphical analysis, see Figure 5.2D). TLC1ΔTAH-A reproducibly had the lowest RNA abundances, at 28% of wild type, although this was still higher than the TAH mutant phenotype observed for TLC1ΔΔ or TLC1(−−S). TLC1ΔTAH-B had less severe reductions in RNA levels, to 54% of wild type. TLC1ΔTAH-C had little effect on RNA levels, with an abundance 91% of wild-type TLC1. Together, these data suggest that the A and B regions of the TAH are responsible for the low RNA abundance phenotype.

To determine whether the 5′ or 3′ sides of the arm had different roles in the RNA abundance phenotype, I made versions the terminal arm based on TSA-T, but with nucleotides mutated from only the 5′ or 3′ (Figure 5.2A, bottom). These “5′ Stiff” and “3′ Stiff” TLC1 variants did not cause senescence (Figure 5.2B). TLC1-3′ Stiff did not result in low RNA abundance, and actually raised it to 141% of wild-type TLC1 (Figure 5.2C and D). TLC1-5′ Stiff RNA levels were 63% of wild type, similar to TLC1ΔTAH-B, suggesting that the 5′ side of the TAH may play a role in telomerase RNA abundance.

Figure 5.2: Regions within the TAH that effect RNA abundance. (**A**) TAH mutants structures based on the phylogenetically-derived secondary structure (Zappulla and Cech, 2004). TAH-A = nts 19−53 and 873−897, in red; TAH-B = nts 53−76 and 855−873, in green; and TAH-C = nts 77−95 and 835−855, in purple. "5′ Stiff" and "3′ Stiff" have the 5′ or 3′ sides of the terminal arm from TSA-T, with bulges and unpaired nucleotides deleted in addition to several substitution mutants, in orange. (**B**) Cells expressing the TAH mutations do not senesce. TLC1 variants were expressed from centromere-containing (*CEN*) plasmids in *tlc1*Δ, *rad52* cells, and grown for 250 generations. Growth at 150 generations is shown. TLC1ΔSm_7 maintains very short telomeres, sometimes resulting in senescence, as shown. (**C**) TAH-A contributes the most to the RNA abundance phenotype. Typical dot blot analysis of TAH mutant RNAs shown. Average relative normalized telomerase RNA abundances are indicated, ±S.E.M., for given n values based on dot blots probed for 3′ TLC1 or Mini-T. (**D**) Graph of RNA levels for TAH mutants, based on data in **C**.

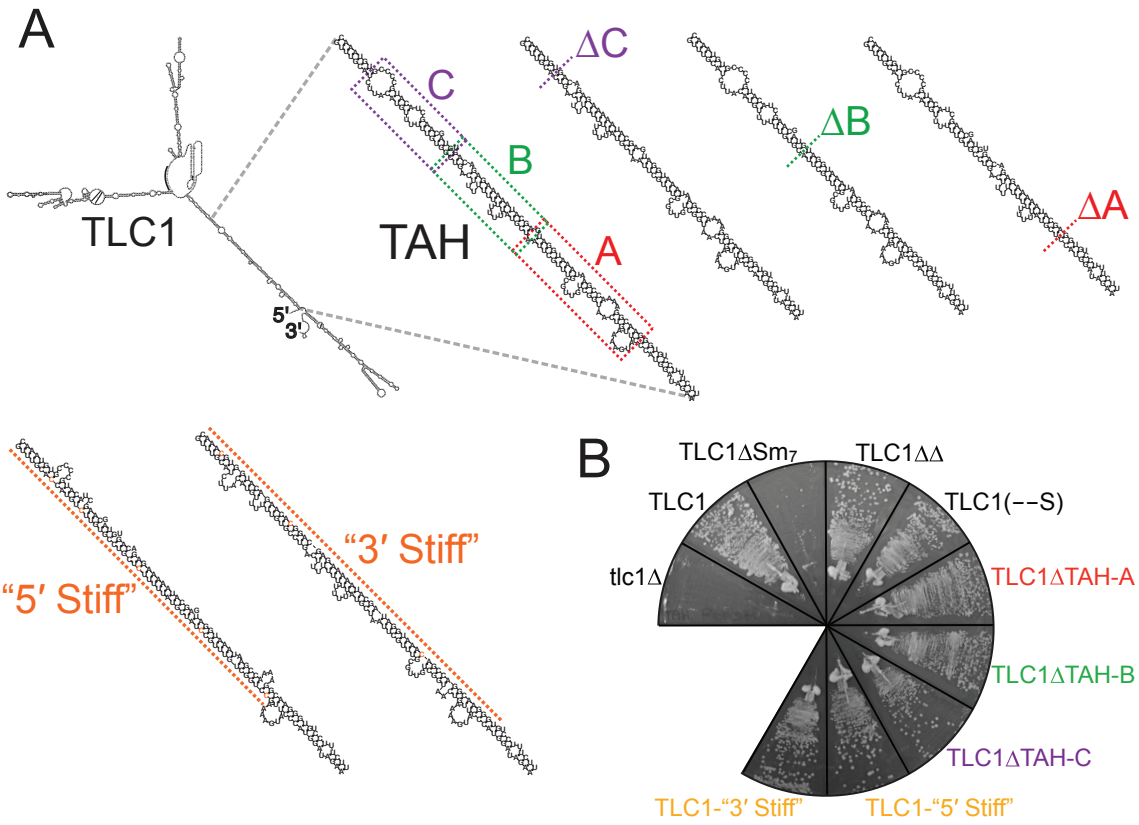
A
TLC1
TAH
5'
3'
C
B
A
ΔC
ΔB
ΔA
"5′ Stiff"
"3′ Stiff"
B
TLC1ΔSm7
TLC1ΔΔ
TLC1
TLC1(−−S)
tlc1Δ
TLC1ΔTAH-A
TLC1ΔTAH-B
TLC1ΔTAH-C
TLC1-"3′ Stiff"
TLC1-"5′ Stiff"

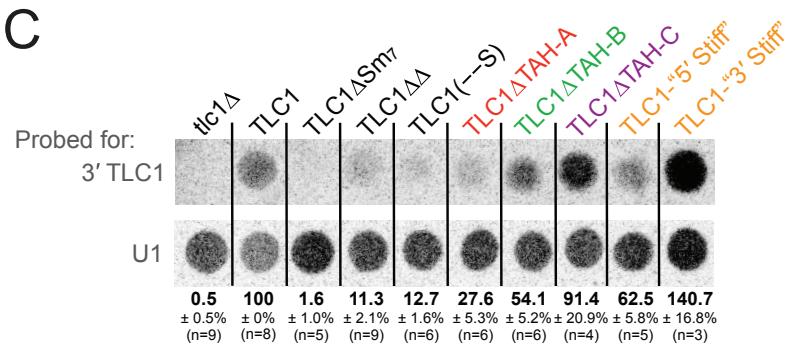
C
tlc1Δ
TLC1
TLC1ΔSm7
TLC1ΔΔ
TLC1(−−S)
TLC1ΔTAH-A
TLC1ΔTAH-B
TLC1ΔTAH-C
TLC1-"5′ Stiff"
TLC1-"3′ Stiff"
Probed for:
3′ TLC1
U1
0.5 ± 0.5% (n=9)
100 ± 0% (n=8)
1.6 ± 1.0% (n=5)
11.3 ± 2.1% (n=9)
12.7 ± 1.6% (n=6)
27.6 ± 5.3% (n=6)
54.1 ± 5.2% (n=6)
91.4 ± 20.9% (n=4)
62.5 ± 5.8% (n=5)
140.7 ± 16.8% (n=3)

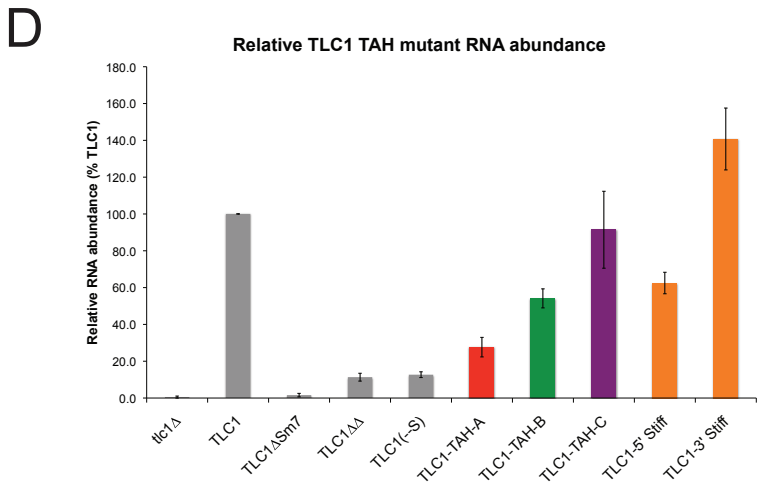
D
Relative TLC1 TAH mutant RNA abundance
Relative RNA abundance (% TLC1)
180.0
160.0
140.0
120.0
100.0
80.0
60.0
40.0
20.0
0.0
tlc1Δ
TLC1
TLC1ΔSm7
TLC1ΔΔ
TLC1(–S)
TLC1-TAH-A
TLC1-TAH-B
TLC1-TAH-C
TLC1-5' Stiff
TLC1-3' Stiff

Bulges on the 5′ side of the TAH are important in TAH-A, but not TAH-B

I next tested whether bulges in the 5′ side of the TAH-A and TAH-B regions were important for RNA abundance. I deleted all of the bulges from the TAH-A region to make TLC1-TAH-AΔbulge (Figure 5.3A, left). In addition, I designed a mutation of the largest bulge in TAH-A, TLC1-TAH-AΔlargebulge; this mutation deletes the majority of the large bulge, but also creates a new single nucleotide bulge, and has a second point substitution mutant (Figure 5.3A, center). Like TLC1ΔTAH-A, the two bulge mutants did not result in senescence *in vivo* (Figure 5.3B, left).

Deleting all of the bulges in the TAH-A a region resulted in low RNA abundance similar to deleting the entire TAH-A (Figure 5.3C, left). Furthermore, deleting just the largest bulge was sufficient to cause the low RNA abundance phenotype. These data strongly indicate that nucleotides in the large bulge near the 5′ end of TLC1 are required for maintaining telomerase RNA abundance in the cell.

I also tested deletion of the bulges in the TAH-B region (Figure 5.3A, right). Although the specific structure of the bulges in this region is not clear, and varies between the phylogenetic model and the *Mfold* prediction, the TLC1-TAH-BΔBulges construct should remove all of the bulges from either structure. Like the other TAH mutations, TLC1-TAH-BΔBulges did not cause senescence (Figure 5.3B, right). However, dot blot analysis of total cellular RNA, probed for telomerase RNA, indicated that TLC1-TAH-BΔBulges does not have a low RNA abundance, and in fact appears to be higher than wild-type TLC1 abundance (Figure 5.3C, right). This suggests that the nucleotides in the bulges of the TAH-B region are not required maintaining RNA abundance.

Figure 5.3: Nucleotides in the bulges of TAH-A are important for telomerase RNA abundance. (**A**) TAH mutants structures based on the phylogenetically-derived secondary structure (Zappulla and Cech, 2004). TAH-AΔBulges = Δ21−27, Δ32−33, and Δ39−43; TAH-AΔLargeBulge = nts 21−30::TGGC; TAH-BΔBulges = Δ66−71, Δ73. TAH-A mutants are indicated in red, TAH-B mutants are indicated in green. (**B**) TAH bulge deletion mutants do not cause senescence. TLC1 variants were expressed from centromere-containing (*CEN*) plasmids in *tlc1*Δ, *rad52* cells, and grown for 250 generations. Growth at 150 generations is shown. (**C**) TAH-A bulge mutants cause low RNA abundance, but TAH-B mutants do not. Graphs of relative telomerase RNA abundance from dot blots, probed for 3′ TLC1 (left) or Mini-T (right). Average RNA abundance from two independent isolates is graphed, ±S.D.

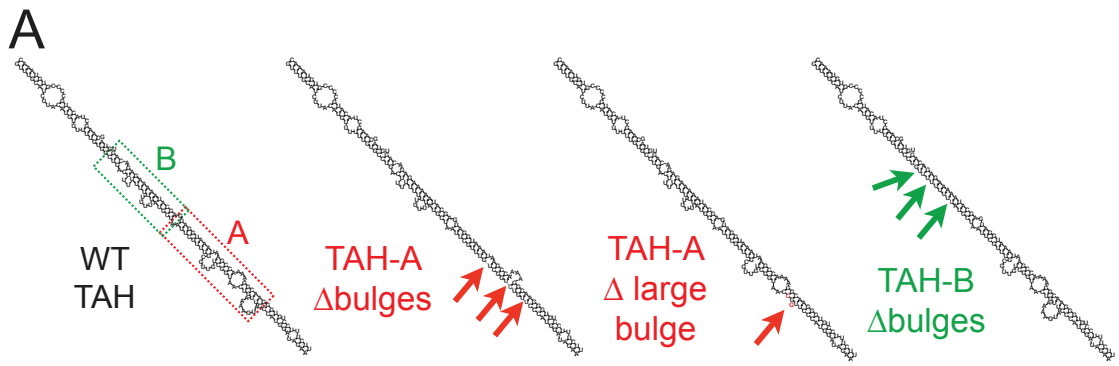
A
B
A
WT
TAH
TAH-A
Δbulges
TAH-A
Δ large
bulge
TAH-B
Δbulges

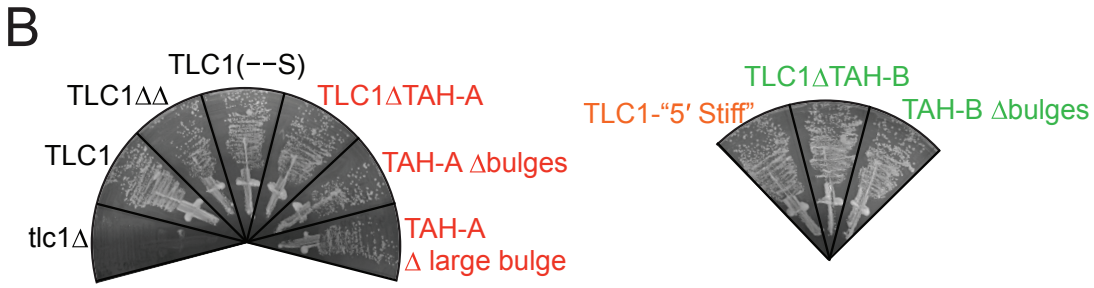
B
TLC1(−−S)
TLC1ΔΔ
TLC1ΔTAH-A
TLC1
TAH-A Δbulges
tlc1Δ
TAH-A
Δ large bulge
TLC1ΔTAH-B
TLC1-"5′ Stiff"
TAH-B Δbulges

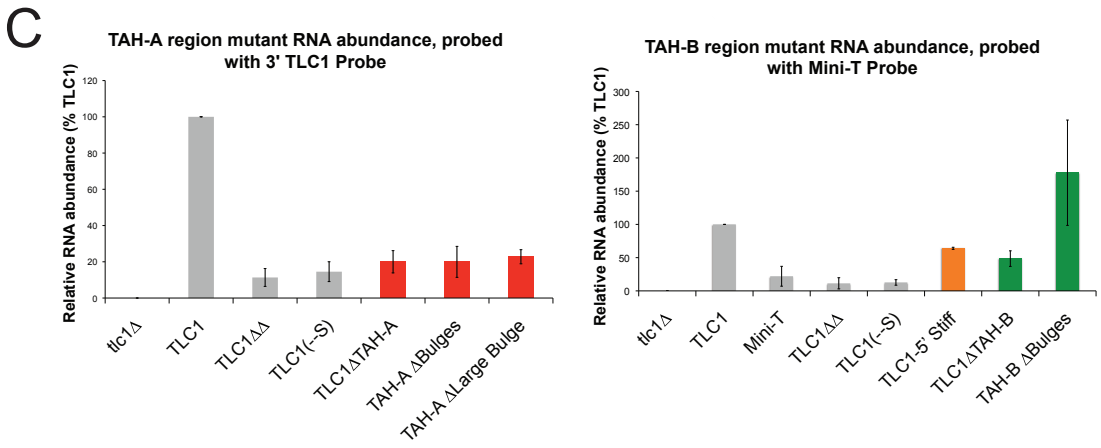
C
TAH-A region mutant RNA abundance, probed with 3' TLC1 Probe
Relative RNA abundance (% TLC1)
120
100
80
60
40
20
0
tlc1Δ
TLC1
TLC1ΔΔ
TLC1(-S)
TLC1ΔTAH-A
TAH-A ΔBulges
TAH-A ΔLarge Bulge
TAH-B region mutant RNA abundance, probed with Mini-T Probe
Relative RNA abundance (% TLC1)
300
250
200
150
100
50
0
tlc1Δ
TLC1
Mini-T
TLC1ΔΔ
TLC1(-S)
TLC1-5′ Stiff
TLC1ΔTAH-B
TAH-B ΔBulges

Mutations in the Three-Way Junction of TLC1 have reduced RNA abundance

In addition to the terminal-arm humerus, I tested mutations in the relatively well-conserved three-way junction at the apex of the TLC1 terminal arm (Figure 5.4A). In other species, including humans and fission yeast, a similar RNA element is required for TERT function, even *in vitro* (Brown et al., 2007; Mitchell and Collins, 2000; Tesmer et al., 1999). However, the *S. cerevisiae* three-way junction is not essential *in vivo* or *in vitro* (Livengood et al., 2002; Zappulla et al., 2005). Although it isn't essential, I sought to test whether the three-way junction plays any role in budding yeast telomerase function.

I designed two versions of TLC1 with a deleted three-way junction. The first deletes the entire distal region of the terminal arm after the terminal-arm humerus; in keeping with the arm-anatomy descriptions, I dubbed this region the "terminal forearm" (TFA; Figure 5.4A). This large deletion was designed based on the mature form of TLC1, but may cause structural problems in the polyadenylated precursor form. If TLC1ΔTFA disrupts Sm_7 function in RNA biogenesis, then it may adversely affect RNA abundance or telomerase function through in a non-three-way-junction specific manner. Therefore, I also designed a smaller three-way junction mutant, TLC1ΔTWJ, which deletes the three-way junction without being predicted to disrupt the structure of the mature or precursor forms of TLC1 (Figure 5.4A). In addition, I made Sm_7-binding mutants of both three-way junction deletions, to test for genetic interactions between the Sm_7 and three-way junction pathways (Seto et al., 1999).

Cells expressing TLC1ΔTFA or TLC1ΔTWJ did not senesce, confirming that the three-way junction is not essential in *S. cerevisiae* telomerase function (Figure 5.4B). However, RNA abundance for both mutants was lower than wild type, although it was still higher than that of Mini-T or TLC1ΔSm_7 (Figure 5.4C). Mutating the Sm_7-binding site in TLC1ΔTFA and TLC1ΔTWJ reduce RNA abundance further, to a level similar to

TLC1ΔSm$_7$. These data are the first to suggest that the three-way junction might play a role in telomerase RNA abundance in *S. cerevisiae*.

Figure 5.4: Mutations to the TLC1 three-way junction cause reduced RNA abundance. (**A**) TAH mutants structures based on the phylogenetically-derived secondary structure (Zappulla and Cech, 2004). TLC1ΔTFA = Δ912−1129; TLC1ΔTWJ = Δ937−1113. (**B**) Deletion of the three-way junction does not cause senescence. TLC1 variants were expressed from centromere-containing (*CEN*) plasmids in *tlc1*Δ, *rad52* cells, and grown for 250 generations. Growth at 125 generations is shown. (**C**) Three-way junction deletion results in reduced RNA abundance. Graph of average relative RNA abundances from two isolates, ±S.D., based on total RNA dot blots probed with a Mini-T probe.

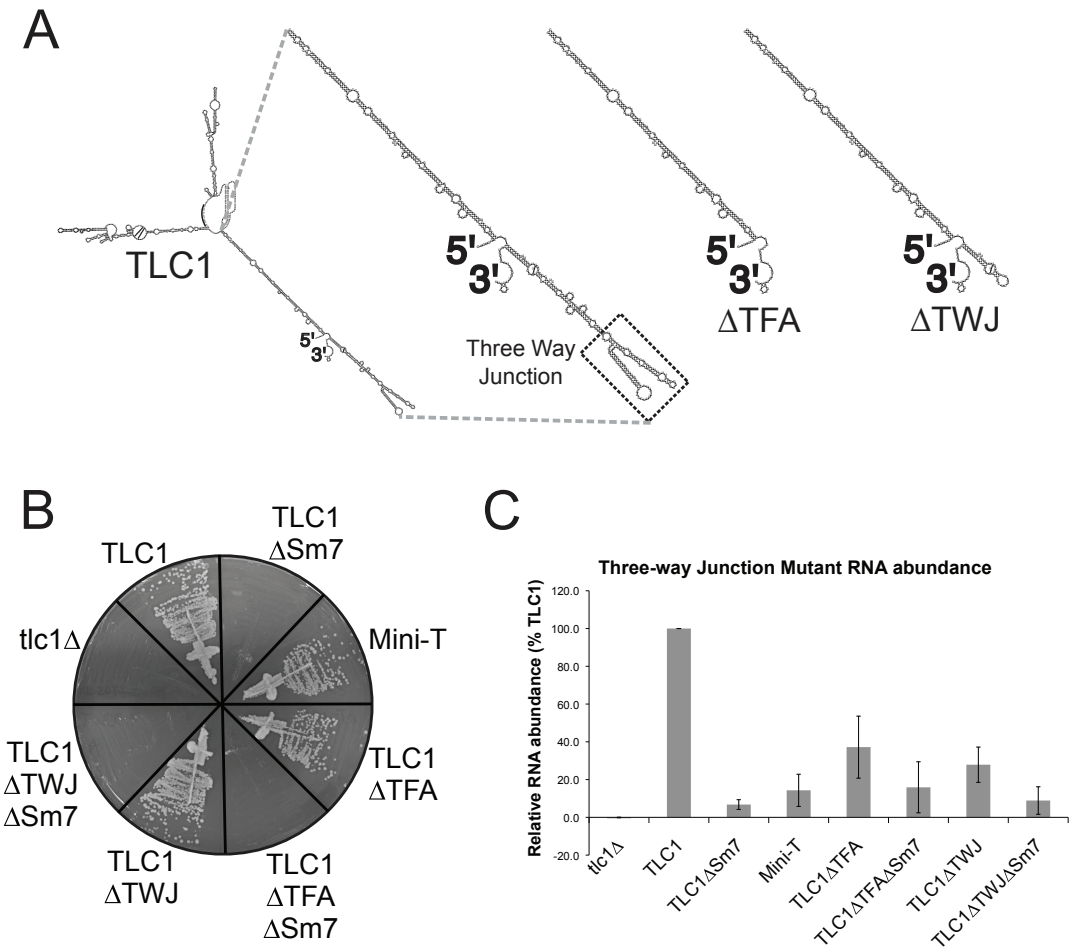

5.4 DISCUSSION:

Maintaining telomerase RNA abundance in the cell is important for proper telomere maintenance. Telomerase RNA has been shown to have a haploinsufficiency phenotype in organisms from yeast to humans, and low levels of telomerase has been associated with human disease (Armanios et al., 2005; Garcia et al., 2007; Hathcock et al., 2002; Mozdy and Cech, 2006). Previous research has demonstrated that some telomerase holoenzyme protein subunits have roles in maintaining telomerase RNA abundance. In particular, the Sm_7 complex plays an important role in RNA biogenesis. Sm_7 binds to the 3′ end of TLC1, in the terminal arm, and loss of Sm_7 binding to TLC1 results in very low RNA abundance (Seto et al., 1999).

Several TLC1 RNA variants with mutations in the "Terminal Arm Humerus" (TAH) have similar low RNA levels to each other, including the truncated armed Mini-T and TLC1ΔΔ, and the stiffened armed TSA-T and TLC1(−−S) (Lebo and Zappulla, 2012; Zappulla and Cech, 2004; Zappulla et al., 2005). However, the phenotype of these terminal arm mutants is different from Sm_7 mutants; the TAH mutations have RNA levels 10−15% of wild-type TLC1, whereas Sm_7 mutants have even lower RNA abundance, less than 5% of wild type (Figure 5.1A). This suggests that the TAH RNA abundance phenotype is either distinct from the Sm_7 pathway, or that it only partially disrupts Sm_7 function. Each of the published TAH mutants may have as few as 3−5 copies of TLC1 per cell (Mozdy and Cech, 2006).

It is important to note that these RNAs are very different from each other both in structure and sequence. The stiffened arms of TSA-T and TLC1(−−S) hold accessory proteins rigidly away from the core on long RNA struts, while the truncated arms in Mini-T and TLC1ΔΔ reel proteins closer in to the core. Furthermore, stability of the RNAs varies greatly; it is unlikely that mutations in the TAH cause a loss of global RNA folding,

since the long dsRNA arms of TSA-T should drive it to fold very stably. Therefore, it is likely that there is a previously unidentified RNA domain within the TAH that plays a role in telomerase RNA abundance regulation. This may be a function of the RNA alone, or may involve binding to previously unknown proteins. Interestingly, PAR-CLiP analysis of all polyadenylated RNAs within the cell revealed several potential protein-binding sites within the terminal arm of TLC1 (Freeberg et al., 2013). Furthermore, two of these potential binding sites are localized to the TAH-A and B regions, which I have shown to be important for RNA abundance (Figure 5.2).

My data indicate that nucleotides 21−30 in TLC1 are important for maintaining RNA abundance; mutation of these nucleotides, which localize to a large bulge in the TAH-A region, was sufficient to cause low RNA abundance (Figure 5.3). It is not clear whether other nucleotides in the region also contribute to the phenotype. However, TLC1-5′ Stiff, which deletes all of the bulges in the 5′ side of the TAH except the important large bulge, does not have the very low RNA abundance seen in TLC1ΔTAH-A. While this may suggest that the large bulge is both necessary and sufficient for the TAH-A role in telomerase RNA abundance regulation, it is still not clear why TSA-T and TLC1(−−S) have the very low RNA levels while still retaining wild-type nts 21−30.

Additionally, I have shown that deletion of the middle of the TAH results in moderately reduced RNA levels (see TLC1ΔTAH-B in Figure 5.2). A similar moderate reduction in RNA abundance occurs when deleting all of the bulges and unpaired nucleotides in the 5′ side of the TAH (see TLC1-5′ Stiff in Figure 5.2). This suggested that the two phenotypes might be related, and that the unpaired nucleotides in TAH-B might be important. However, deletion of these nucleotides in TLC1-TAH-BΔBulges did not cause low RNA abundance (Figure 5.3). It is possible that the remaining U to C mutation in the TAH-B section of TLC1-5′ Stiff, which is not present in TLC1-TAH-BΔBulges, disrupted a critical sequence. Alternatively, the two phenotypes may not be

directly related. It remains possible that there is no second RNA abundance domain in the TAH at all; both TLC1ΔTAH-B and TLC1-5′ Stiff may simply be causing partial disruptions of the RNA-abundance regulation function of the TAH-A region.

I hypothesize that the TAH may contain a binding site for an RNA chaperone that helps global folding of TLC1. Such a chaperone may be very important to ensure a functional core in the RNA, due to the large size of the 1157-nt TLC1 and the long-range interactions required for terminal formation. In fact, the lack of the specific chaperone in *in vitro* transcription and translation systems may be responsible for the inability of wild-type TLC1 to function when telomerase is reconstituted *in vitro* (Zappulla et al., 2005). I hypothesize that this chaperone would bind to the 5′ side of the TAH as it emerges from the RNA polymerase early during transcription, before the rest of TLC1 has been transcribed. This could prevent misfolding of the 5′ end of TLC1 before its binding partner near to the 3′ end has been made. After the Ku and Est1 arms have been transcribed and folded into their local structures, the protein chaperone could release from the 5′ end, allowing it to pair correctly with the 3′ side of the TAH. If TAH mutants disrupt binding of this RNA chaperone, it may cause the 5′ end to misfold, altering global TLC1 structure and causing loss of RNA stability. It remains to be seen what RNA chaperones, if any, actually do bind to TLC1.

In addition to studying the importance of the TAH in the TLC1 terminal arm, I also examined the relatively well-conserved three-way junction at the apex of the terminal arm (Figure 5.4A). This three-way junction, which is also found in other yeasts, is structurally analogous to the human CR4/5 domain, and is essential for TERT activity *in vitro* and *in vivo* (Brown et al., 2007; Mitchell and Collins, 2000; Tesmer et al., 1999; Theimer and Feigon, 2006). However, both previous published data and my findings indicate that the three-way junction in *S. cerevisiae* is not essential, either *in vivo* or *in vitro* (Figure 5.4B; Livengood et al., 2002; Zappulla et al., 2005). However, it remains

possible that the three-way junction of TLC1 plays an important, albeit nonessential, role in Est2 function.

My results indicate that deletion of the three-way junction results in low TLC1 abundance in the cell (Figure 5.4C). This may suggest that the three-way junction of TLC1 has an important function in regulating telomerase RNA abundance. Alternatively, the low RNA abundance of the three-way junction mutants may simply be disrupting function of the nearby Sm_7 site, possibly by causing misfolding of the precursor form of TLC1. To assess whether the three-way junction phenotype is genetically related to Sm_7 function, I also tested Sm_7-binding mutants of the three-way junction deletions. These RNAs had similar abundance to TLC1ΔSm_7 (Figure 5.4C), which may indicate that the three-way junction mutations are partially disrupting Sm_7 function. Assessing the ratio of precursor to mature TLC1 RNA in the three-way junction mutants by Northern blot will help determine whether Sm_7 function is affected. In addition, further studies of the three-way junction *in vivo*, particularly measuring telomere length by Southern blot, and *in vitro* through telomerase assays will give a more complete understanding of the role for the three-way junction in *S. cerevisiae* telomerase function.

Overall, I have identified several potential RNA-abundance regulating domains in the terminal arm of TLC1. In particular, I showed that nucleotides 21−30 are important for TLC1 RNA abundance in the cell. Additionally, I provide evidence that the middle section of the terminal arm humerus, particularly on the 5′ side, plays a role in RNA levels. I hypothesize that these sites may interact with RNA chaperone proteins, which could help fold the large TLC1 RNA into a functional structure *in vivo*. Finally, I demonstrate that deletions of the conserved three-way junction domain result in low telomerase RNA levels. These findings pave the way for future studies to identify important TLC1-binding proteins that regulate and maintain yeast telomerase RNA abundance.

5.5 METHODS:

TLC1 mutant design

TLC1 RNA variants were designed based on the phylogenetically predicted secondary structure (Zappulla and Cech, 2004), using the *Mfold* RNA secondary structure prediction webserver to guide the design (Zuker, 2003). Gene fragments were created using PCR, and ligated into a *TRP1*-marked centromeric *CEN* plasmid harboring *TLC1*. New TLC1 variants reported: TLC1ΔTAH-A = Δ19−53 and Δ873−897; TLC1ΔTAH-B = Δ53−76 and Δ855−873; TLC1ΔTAH-C = Δ77−95 and Δ835−855; TLC1-"5′ Stiff" and TLC1-"3′ Stiff" have the 5′ or 3′ sides of the terminal arm from TSA-T (see Chapter 2; Lebo and Zappulla, 2012); TAH-AΔBulges = Δ21−27, Δ32−33, and Δ39−43; TAH-AΔLargeBulge = nts 21−30::TGGC; TAH-BΔBulges = Δ66−71, Δ73; TLC1ΔTFA = Δ912−1129; TLC1ΔTWJ = Δ937−1113.

Experiments in yeast

All telomerase RNA alleles were expressed from *TRP1*-marked centromeric (*CEN*) plasmids. These plasmids were transformed into strain TCy43 (*MAT-a ura3-53 lys2-801 ade2-101 trp1-Δ1 his3-Δ200 leu2-Δ1 VR::ADE2-TEL adh4::URA3-TEL tlc1Δ::LEU2 rad52Δ::HIS3 [pTLC1-LYS2-CEN]*) (Seto et al., 1999). After shuffling out *TLC1* (*LYS2/CEN*) on solid medium containing α-aminoadipate, colonies were restreaked ten times on synthetic compete media plates lacking tryptophan, with each restreak representing approximately 25 generations of yeast growth.

Nucleic acid blots

Southern blots were performed as previously described (Lebo and Zappulla, 2012; Zappulla et al., 2005; Zappulla et al., 2011). Briefly, cell pellets for genomic DNA

isolation were prepared from cultures made from serially restreaked plates, with each streak representing ~25 generations. Genomic DNA was isolated (Gentra Puregene system), equal amounts were digested with *Xho*I and electrophoresed through a 1.1% agarose gel at 70 V for 17 h, and transferred to Hybond-N+ Nylon membrane (GE). The blot was then probed for telomeric sequences and a 1627-bp non-telomeric fragment of chromosome IV. Average Y′ telomere fragment length was quantified using the weighted average mobility (WAM) method described previously (Zappulla et al., 2011).

RNA dot blots were performed as previously described (Lebo and Zappulla, 2012). Total cellular RNA was extracted from late log phase or early stationary phase yeast cultures by a slightly modified version of the hot phenol RNA isolation method (Kohrer and Domdey, 1991). After boiling, 5µg of RNA was spotted twice onto Hybond-N+ Nylon Membrane (GE). The membrane was cut in half such that the two dots of each sample were separate membrane sections, air-dried, UV-crosslinked (SpectroLinker XL-1500 UV Crosslinker, using two runs of the “Optimal crosslink” setting), and pre-hybridized in Church buffer at 55°C for 10 minutes. One membrane was probed using either a probe for the 3′ region of TLC1 (nucleotides 906 to 1140), or a Mini-T probe (Zappulla et al., 2005), while the other was probed for the U1 snRNA (Friedman and Cech, 1999). Telomerase RNA levels were normalized to U1 levels.

Chapter 6:

Conclusions: The nature of flexible-scaffold RNAs

The telomerase ribonucleoprotein (RNP) holoenzyme is responsible for maintaining telomere lengths in most eukaryotes, counteracting the shortening that occurs during each round of DNA synthesis. The telomerase RNA plays a critical role in this process, acting as both a template for reverse transcription, and as a scaffold on which the protein subunits can assemble. In *S. cerevisiae*, the telomerase RNA is the 1157-nt TLC1, which forms a Y-shaped secondary structure with three long arms radiating out from a central core (Dandjinou et al., 2004; Singer and Gottschling, 1994; Zappulla and Cech, 2004). The yeast telomerase reverse transcriptase, Est2, binds to the central core of the RNA, while the important or essential accessory proteins or protein complexes Est1, Ku, and Sm_7 each bind near the tips of a different arm.

Interestingly, TLC1 has been shown to act as a functionally flexible scaffold, on which all known accessory-protein binding sites can be repositioned with retention of function (Mefford et al., 2013; Zappulla and Cech, 2004, 2006; Zappulla et al., 2011). These findings are further supported by the very low conservation in the RNA, particularly in the RNA arms between protein binding sites (Dandjinou et al., 2004; Zappulla and Cech, 2004). The rapidly evolving RNA in these arms can be deleted from the RNA without eliminating telomerase activity *in vivo* (Zappulla et al., 2005). Taken together, these data suggest that the TLC1 flexible scaffold RNA holds the RNP together without conferring a rigid structure. This contrasts with canonical RNPs, such as the ribosome (Ban et al., 2000; Moore and Steitz, 2002; Verschoor et al., 1998), which are highly structured with precise nucleotide positioning, and it has been proposed that yeast telomerase is the archetype for a new class of RNPs (Zappulla and Cech, 2004, 2006).

It has been hypothesized that other long noncoding RNAs (lncRNAs) may act as flexible scaffolds (Cech and Steitz, 2014; Guttman et al., 2011; Wang and Chang, 2011). Many lncRNAs have been discovered across different species, with nearly 10,000 found in humans alone (Bernstein et al., 2012). LncRNA functions vary (Johnsson et al., 2014;

Kung et al., 2013); many have been implicated in chromosome remodeling, like XIST and HOTAIR (Bergmann and Spector, 2014; Khalil et al., 2009; Penny et al., 1996; Tsai et al., 2010), while others may act as anti-sense regulators for mRNAs, such as PTENpg1 (Johnsson et al., 2013). These RNAs are long, and are often produced from introns or pseudogenes (Bekpen et al., 2009; Guil et al., 2012; Harrison et al., 2005; Kung et al., 2013). Like TLC1, lncRNAs tend to have low sequence conservation across the entire RNA, but have high conservation in smaller regions (Pang et al., 2006). This may suggest that these RNAs function as flexible scaffolds similar to TLC1, with poorly-conserved stretches of RNA tethering conserved protein regions or functional RNA domains together. Determining how the structure of such lncRNAs relates to their function is important for understanding their roles in the cell. Because *Saccharomyces cerevisiae* is such a tractable organism for genetics and molecular biology, TLC1 provides an opportunity to investigate the nature of lncRNAs.

My research has advanced our understanding of flexible scaffold RNPs. Previously it was unclear whether the RNA-bound accessory proteins needed to ultimately "dock" into active positions in the RNP, using physically flexible RNA to flex into the correct docking site. By stiffening the three long RNA arms of TLC1, I demonstrated that physical flexibility of the RNA was not required for function, and that the accessory proteins retained function when held away from the core on rigid struts (see Chapter 2; Lebo and Zappulla, 2012). This indicates that the flexible scaffold RNP acts as "beads on a string," with accessory proteins tethered together by intervening RNA without specific functional orientations.

Although the tethering function of the RNA is essential for telomerase function in the cell, the arms of TLC1 are more than passive tethers. By using a heterologous RNA-protein interaction system to tether the Est1 accessory protein to TLC1 RNA, I was able to separate the recruitment functions of the Est1-arm from other essential roles in

telomere maintenance. I found that there is a second essential Est1 arm domain (SEED) in TLC1 that has an unknown essential function independent of Est1 protein (see Chapter 3). In addition, my research provided evidence for an addition functional region in the Ku-binding arm, which may help regulate TLC1 structure or abundance (see Chapter 4). Furthermore, such functional RNA domains are also flexibly scaffolded to the RNP; the SEED can be relocated with the rest of the Est1-binding arm (Zappulla and Cech, 2004), and can even function from a separate RNA *in trans*. In other organisms, a secondary RNA domain that is essential for TERT function, such as the human CR4/5 (Mitchell and Collins, 2000) or the *S. pombe* three-way-junction (Qi et al., 2013), can provide function *in vitro* when provided *in trans*, suggesting that these essential domains may also be flexibly scaffolded. Together, these findings indicate that the RNA in a flexible scaffold RNP can have roles in holoenzyme function beyond passive tethering of accessory proteins.

The extent of "flexibility" in the flexible scaffold RNPs is still not fully known. It is clear that TLC1 is functionally flexible, in that the functional domains of the RNA can be relocated without loss of function. There is also some evidence for physical flexibility in the arms, allowing them to bend. Although stiffening the arms is tolerated, the low conservation in the arms would likely disfavor the formation of highly specific structures. However, other potential aspects of "flexibility" are less clear. It is possible that portions of the RNA require "flexibility" in base pairing interactions; i.e., regions of the RNA could separate and pair with different nucleotides in a different secondary structure. Such heterogeneity in the secondary structure may help to regulate RNA function in recruitment to the telomere or telomere elongation. This could be one explanation for why driving the Ku arm towards a single phylogenetically predicted model results in low RNA abundance and short telomeres (see Chapter 4). It is possible that Ku the arm may

need to sample multiple base pairings for full activity. Other forms of flexibility in TLC1 and other flexible scaffolds may yet be discovered.

Overall, my research has advanced the flexible scaffold model for telomerase RNA. I have shown that yeast telomerase accessory proteins do not require specific orientations for functions. However, the RNA is more than a passive tether, and can contribute to telomere maintenance beyond simply binding accessory proteins. Finally, I identified new regions of interest in both the Ku and terminal arms, which appear to aid in regulation of telomerase RNA abundance in the cell. My findings suggest that the flexible scaffold RNP may best be viewed as a series of functional modules, which include both proteins RNA domains, all tethered together by intervening segments of RNA in non-specific positions within the RNP holoenzyme.

REFERENCES:

Abdallah, P., Luciano, P., Runge, K.W., Lisby, M., Geli, V., Gilson, E., and Teixeira, M.T. (2009). A two-step model for senescence triggered by a single critically short telomere. Nat Cell Biol *11*, 988-993.

Abels, J.A., Moreno-Herrero, F., van der Heijden, T., Dekker, C., and Dekker, N.H. (2005). Single-molecule measurements of the persistence length of double-stranded RNA. Biophys J *88*, 2737-2744.

Adams Martin, A., Dionne, I., Wellinger, R.J., and Holm, C. (2000). The function of DNA polymerase alpha at telomeric G tails is important for telomere homeostasis. Mol Cell Biol *20*, 786-796.

Armanios, M., Chen, J.L., Chang, Y.P., Brodsky, R.A., Hawkins, A., Griffin, C.A., Eshleman, J.R., Cohen, A.R., Chakravarti, A., Hamosh, A*., et al.* (2005). Haploinsufficiency of telomerase reverse transcriptase leads to anticipation in autosomal dominant dyskeratosis congenita. Proc Natl Acad Sci U S A *102*, 15960-15964.

Autexier, C., and Greider, C.W. (1998). Mutational analysis of the Tetrahymena telomerase RNA: identification of residues affecting telomerase activity in vitro. Nucleic Acids Res *26*, 787-795.

Bachand, F., and Autexier, C. (2001). Functional regions of human telomerase reverse transcriptase and human telomerase RNA required for telomerase activity and RNA-protein interactions. Mol Cell Biol *21*, 1888-1897.

Ban, N., Nissen, P., Hansen, J., Moore, P.B., and Steitz, T.A. (2000). The complete atomic structure of the large ribosomal subunit at 2.4 A resolution. Science *289*, 905-920.

Beattie, T.L., Zhou, W., Robinson, M.O., and Harrington, L. (2001). Functional multimerization of the human telomerase reverse transcriptase. Mol Cell Biol *21*, 6151-6160.

Bekpen, C., Marques-Bonet, T., Alkan, C., Antonacci, F., Leogrande, M.B., Ventura, M., Kidd, J.M., Siswara, P., Howard, J.C., and Eichler, E.E. (2009). Death and resurrection of the human IRGM gene. PLoS Genet *5*, e1000403.

Bergmann, J.H., and Spector, D.L. (2014). Long non-coding RNAs: modulators of nuclear structure and function. Curr Opin Cell Biol *26*, 10-18.

Berman, A.J., Akiyama, B.M., Stone, M.D., and Cech, T.R. (2011). The RNA accordion model for template positioning by telomerase RNA during telomeric DNA synthesis. Nat Struct Mol Biol *18*, 1371-1375.

Bernstein, B.E., Birney, E., Dunham, I., Green, E.D., Gunter, C., and Snyder, M. (2012). An integrated encyclopedia of DNA elements in the human genome. Nature *489*, 57-74.

Bertuch, A.A., and Lundblad, V. (2003). The Ku heterodimer performs separable activities at double-strand breaks and chromosome termini. Mol Cell Biol *23*, 8202-8215.

Bhattacharyya, A., and Lilley, D.M. (1989). The contrasting structures of mismatched DNA sequences containing looped-out bases (bulges) and multiple mismatches (bubbles). Nucleic Acids Res *17*, 6821-6840.

Bianchi, A., Negrini, S., and Shore, D. (2004). Delivery of yeast telomerase to a DNA break depends on the recruitment functions of Cdc13 and Est1. Mol Cell *16*, 139-146.

Bianchi, A., and Shore, D. (2007). Early replication of short telomeres in budding yeast. Cell *128*, 1051-1062.

Blackburn, E.H., and Collins, K. (2011). Telomerase: an RNP enzyme synthesizes DNA. Cold Spring Harb Perspect Biol *3*.

Bley, C.J., Qi, X., Rand, D.P., Borges, C.R., Nelson, R.W., and Chen, J.J. (2011). RNA-protein binding interface in the telomerase ribonucleoprotein. Proc Natl Acad Sci U S A *108*, 20333-20338.

Bourns, B.D., Alexander, M.K., Smith, A.M., and Zakian, V.A. (1998). Sir proteins, Rif proteins, and Cdc13p bind Saccharomyces telomeres in vivo. Mol Cell Biol *18*, 5600-5608.

Brown, Y., Abraham, M., Pearl, S., Kabaha, M.M., Elboher, E., and Tzfati, Y. (2007). A critical three-way junction is conserved in budding yeast and vertebrate telomerase RNAs. Nucleic Acids Res *35*, 6280-6289.

Bryan, T.M., Goodrich, K.J., and Cech, T.R. (2000). Telomerase RNA bound by protein motifs specific to telomerase reverse transcriptase. Mol Cell *6*, 493-499.

Bryan, T.M., Goodrich, K.J., and Cech, T.R. (2003). Tetrahymena telomerase is active as a monomer. Mol Biol Cell *14*, 4794-4804.

Bustamante, C., Smith, S.B., Liphardt, J., and Smith, D. (2000). Single-molecule studies of DNA mechanics. Curr Opin Struct Biol *10*, 279-285.

Cech, T.R. (2004). Beginning to understand the end of the chromosome. Cell *116*, 273-279.

Cech, T.R., and Steitz, J.A. (2014). The noncoding RNA revolution-trashing old rules to forge new ones. Cell *157*, 77-94.

Cervantes, R.B., and Lundblad, V. (2002). Mechanisms of chromosome-end protection. Curr Opin Cell Biol *14*, 351-356.

Chai, W., Ford, L.P., Lenertz, L., Wright, W.E., and Shay, J.W. (2002). Human Ku70/80 associates physically with telomerase through interaction with hTERT. J Biol Chem *277*, 47242-47247.

Chan, A., Boule, J.B., and Zakian, V.A. (2008). Two pathways recruit telomerase to Saccharomyces cerevisiae telomeres. PLoS Genet *4*, e1000236.

Chandra, A., Hughes, T.R., Nugent, C.I., and Lundblad, V. (2001). Cdc13 both positively and negatively regulates telomere replication. Genes Dev *15*, 404-414.

Chanfreau, G., Buckle, M., and Jacquier, A. (2000). Recognition of a conserved class of RNA tetraloops by Saccharomyces cerevisiae RNase III. Proc Natl Acad Sci U S A *97*, 3142-3147.

Chang, M., Arneric, M., and Lingner, J. (2007). Telomerase repeat addition processivity is increased at critically short telomeres in a Tel1-dependent manner in Saccharomyces cerevisiae. Genes Dev *21*, 2485-2494.

Chapon, C., Cech, T.R., and Zaug, A.J. (1997). Polyadenylation of telomerase RNA in budding yeast. RNA *3*, 1337-1351.

Chappell, A.S., and Lundblad, V. (2004). Structural elements required for association of the Saccharomyces cerevisiae telomerase RNA with the Est2 reverse transcriptase. Mol Cell Biol *24*, 7720-7736.

Chen, J.L., Blasco, M.A., and Greider, C.W. (2000). Secondary structure of vertebrate telomerase RNA. Cell *100*, 503-514.

Chen, J.L., and Greider, C.W. (2003). Template boundary definition in mammalian telomerase. Genes Dev *17*, 2747-2752.

Chen, J.L., Opperman, K.K., and Greider, C.W. (2002). A critical stem-loop structure in the CR4-CR5 domain of mammalian telomerase RNA. Nucleic Acids Res *30*, 592-597.

Chu, C., Qu, K., Zhong, F.L., Artandi, S.E., and Chang, H.Y. (2011). Genomic maps of long noncoding RNA occupancy reveal principles of RNA-chromatin interactions. Mol Cell *44*, 667-678.

Cloutier, T.E., and Widom, J. (2004). Spontaneous sharp bending of double-stranded DNA. Mol Cell *14*, 355-362.

Cohn, M., and Blackburn, E.H. (1995). Telomerase in yeast. Science *269*, 396-400.

Coy, S., Volanakis, A., Shah, S., and Vasiljeva, L. (2013). The Sm complex is required for the processing of non-coding RNAs by the exosome. PLoS One *8*, e65606.

Dalby, A.B., Goodrich, K.J., Pfingsten, J.S., and Cech, T.R. (2013). RNA recognition by the DNA end-binding Ku heterodimer. RNA *19*, 841-851.

Dandjinou, A.T., Levesque, N., Larose, S., Lucier, J.F., Abou Elela, S., and Wellinger, R.J. (2004). A phylogenetically based secondary structure for the yeast telomerase RNA. Curr Biol *14*, 1148-1158.

Diede, S.J., and Gottschling, D.E. (1999). Telomerase-mediated telomere addition in vivo requires DNA primase and DNA polymerases alpha and delta. Cell *99*, 723-733.

Dionne, I., Larose, S., Dandjinou, A.T., Abou Elela, S., and Wellinger, R.J. (2013). Cell cycle-dependent transcription factors control the expression of yeast telomerase RNA. RNA *19*, 992-1002.

Evans, S.K., and Lundblad, V. (1999). Est1 and Cdc13 as comediators of telomerase access. Science *286*, 117-120.

Evans, S.K., and Lundblad, V. (2002). The Est1 subunit of Saccharomyces cerevisiae telomerase makes multiple contributions to telomere length maintenance. Genetics *162*, 1101-1115.

Fan, X., and Price, C.M. (1997). Coordinate regulation of G- and C strand length during new telomere synthesis. Mol Biol Cell *8*, 2145-2155.

Feng, J., Funk, W.D., Wang, S.S., Weinrich, S.L., Avilion, A.A., Chiu, C.P., Adams, R.R., Chang, E., Allsopp, R.C., Yu, J.*, et al.* (1995). The RNA component of human telomerase. Science *269*, 1236-1241.

Fisher, T.S., Taggart, A.K., and Zakian, V.A. (2004). Cell cycle-dependent regulation of yeast telomerase by Ku. Nat Struct Mol Biol *11*, 1198-1205.

Forstemann, K., Hoss, M., and Lingner, J. (2000). Telomerase-dependent repeat divergence at the 3' ends of yeast telomeres. Nucleic Acids Res *28*, 2690-2694.

Freeberg, M.A., Han, T., Moresco, J.J., Kong, A., Yang, Y.C., Lu, Z.J., Yates, J.R., and Kim, J.K. (2013). Pervasive and dynamic protein binding sites of the mRNA transcriptome in Saccharomyces cerevisiae. Genome Biol *14*, R13.

Friedman, K.L., and Cech, T.R. (1999). Essential functions of amino-terminal domains in the yeast telomerase catalytic subunit revealed by selection for viable mutants. Genes Dev *13*, 2863-2874.

Friedman, K.L., Heit, J.J., Long, D.M., and Cech, T.R. (2003). N-terminal domain of yeast telomerase reverse transcriptase: recruitment of Est3p to the telomerase complex. Mol Biol Cell *14*, 1-13.

Fulle, S., and Gohlke, H. (2009). Constraint counting on RNA structures: linking flexibility and function. Methods *49*, 181-188.

Gallardo, F., Laterreur, N., Cusanelli, E., Ouenzar, F., Querido, E., Wellinger, R.J., and Chartrand, P. (2011). Live cell imaging of telomerase RNA dynamics reveals cell cycle-dependent clustering of telomerase at elongating telomeres. Mol Cell *44*, 819-827.

Garcia, C.K., Wright, W.E., and Shay, J.W. (2007). Human diseases of telomerase dysfunction: insights into tissue aging. Nucleic Acids Res *35*, 7406-7416.

Geggier, S., Kotlyar, A., and Vologodskii, A. (2011). Temperature dependence of DNA persistence length. Nucleic Acids Res *39*, 1419-1426.

Geggier, S., and Vologodskii, A. (2010). Sequence dependence of DNA bending rigidity. Proc Natl Acad Sci U S A *107*, 15421-15426.

Gillis, A.J., Schuller, A.P., and Skordalakes, E. (2008). Structure of the Tribolium castaneum telomerase catalytic subunit TERT. Nature *455*, 633-637.

Gilman, M. (2001). Ribonuclease Protection Assay. Current Protocols in Molecular Biology *24*, 4.7.1-4.7.8.

Gomez, D.E., Armando, R.G., Farina, H.G., Menna, P.L., Cerrudo, C.S., Ghiringhelli, P.D., and Alonso, D.F. (2012). Telomere structure and telomerase in health and disease (review). Int J Oncol *41*, 1561-1569.

Grandin, N., and Charbonneau, M. (2008). Protection against chromosome degradation at the telomeres. Biochimie *90*, 41-59.

Grandin, N., Damon, C., and Charbonneau, M. (2001). Ten1 functions in telomere end protection and length regulation in association with Stn1 and Cdc13. EMBO J *20*, 1173-1183.

Greider, C.W. (2006). Telomerase RNA levels limit the telomere length equilibrium. Cold Spring Harb Symp Quant Biol *71*, 225-229.

Greider, C.W., and Blackburn, E.H. (1985). Identification of a specific telomere terminal transferase activity in Tetrahymena extracts. Cell *43*, 405-413.

Greider, C.W., and Blackburn, E.H. (1987). The telomere terminal transferase of Tetrahymena is a ribonucleoprotein enzyme with two kinds of primer specificity. Cell *51*, 887-898.

Greider, C.W., and Blackburn, E.H. (1989). A telomeric sequence in the RNA of Tetrahymena telomerase required for telomere repeat synthesis. Nature *337*, 331-337.

Guil, S., Soler, M., Portela, A., Carrere, J., Fonalleras, E., Gomez, A., Villanueva, A., and Esteller, M. (2012). Intronic RNAs mediate EZH2 regulation of epigenetic targets. Nat Struct Mol Biol *19*, 664-670.

Gunisova, S., Elboher, E., Nosek, J., Gorkovoy, V., Brown, Y., Lucier, J.F., Laterreur, N., Wellinger, R.J., Tzfati, Y., and Tomaska, L. (2009). Identification and comparative

analysis of telomerase RNAs from Candida species reveal conservation of functional elements. RNA *15*, 546-559.

Guttman, M., Donaghey, J., Carey, B.W., Garber, M., Grenier, J.K., Munson, G., Young, G., Lucas, A.B., Ach, R., Bruhn, L.*, et al.* (2011). lincRNAs act in the circuitry controlling pluripotency and differentiation. Nature *477*, 295-300.

Hagerman, P.J. (1988). Flexibility of DNA. Annu Rev Biophys Biophys Chem *17*, 265-286.

Hagerman, P.J. (1997). Flexibility of RNA. Annu Rev Biophys Biomol Struct *26*, 139-156.

Harrison, P.M., Zheng, D., Zhang, Z., Carriero, N., and Gerstein, M. (2005). Transcribed processed pseudogenes in the human genome: an intermediate form of expressed retrosequence lacking protein-coding ability. Nucleic Acids Res *33*, 2374-2383.

Hathcock, K.S., Hemann, M.T., Opperman, K.K., Strong, M.A., Greider, C.W., and Hodes, R.J. (2002). Haploinsufficiency of mTR results in defects in telomere elongation. Proc Natl Acad Sci U S A *99*, 3591-3596.

Herrero-Galan, E., Fuentes-Perez, M.E., Carrasco, C., Valpuesta, J.M., Carrascosa, J.L., Moreno-Herrero, F., and Arias-Gonzalez, J.R. (2013). Mechanical identities of RNA and DNA double helices unveiled at the single-molecule level. J Am Chem Soc *135*, 122-131.

Hughes, T.R., Evans, S.K., Weilbaecher, R.G., and Lundblad, V. (2000). The Est3 protein is a subunit of yeast telomerase. Curr Biol *10*, 809-812.

Jang, S.B., Hung, L.W., Chi, Y.I., Holbrook, E.L., Carter, R.J., and Holbrook, S.R. (1998). Structure of an RNA internal loop consisting of tandem C-A+ base pairs. Biochemistry *37*, 11726-11731.

Jiang, J., Miracco, E.J., Hong, K., Eckert, B., Chan, H., Cash, D.D., Min, B., Zhou, Z.H., Collins, K., and Feigon, J. (2013). The architecture of Tetrahymena telomerase holoenzyme. Nature *496*, 187-192.

Johnsson, P., Ackley, A., Vidarsdottir, L., Lui, W.O., Corcoran, M., Grander, D., and Morris, K.V. (2013). A pseudogene long-noncoding-RNA network regulates PTEN transcription and translation in human cells. Nat Struct Mol Biol *20*, 440-446.

Johnsson, P., Lipovich, L., Grander, D., and Morris, K.V. (2014). Evolutionary conservation of long non-coding RNAs; sequence, structure, function. Biochim Biophys Acta *1840*, 1063-1071.

Jones, M.H., and Guthrie, C. (1990). Unexpected flexibility in an evolutionarily conserved protein-RNA interaction: genetic analysis of the Sm binding site. EMBO J *9*, 2555-2561.

Khalil, A.M., Guttman, M., Huarte, M., Garber, M., Raj, A., Rivea Morales, D., Thomas, K., Presser, A., Bernstein, B.E., van Oudenaarden, A.*, et al.* (2009). Many human large intergenic noncoding RNAs associate with chromatin-modifying complexes and affect gene expression. Proc Natl Acad Sci U S A *106*, 11667-11672.

Kim, N.K., Theimer, C.A., Mitchell, J.R., Collins, K., and Feigon, J. (2010). Effect of pseudouridylation on the structure and activity of the catalytically essential P6.1 hairpin in human telomerase RNA. Nucleic Acids Res *38*, 6746-6756.

Kim, N.W., Piatyszek, M.A., Prowse, K.R., Harley, C.B., West, M.D., Ho, P.L., Coviello, G.M., Wright, W.E., Weinrich, S.L., and Shay, J.W. (1994). Specific association of human telomerase activity with immortal cells and cancer. Science *266*, 2011-2015.

Kohrer, K., and Domdey, H. (1991). Preparation of high molecular weight RNA. Methods Enzymol *194*, 398-405.

Kung, J.T., Colognori, D., and Lee, J.T. (2013). Long noncoding RNAs: past, present, and future. Genetics *193*, 651-669.

Lai, C.K., Miller, M.C., and Collins, K. (2002). Template boundary definition in Tetrahymena telomerase. Genes Dev *16*, 415-420.

Lai, C.K., Miller, M.C., and Collins, K. (2003). Roles for RNA in telomerase nucleotide and repeat addition processivity. Mol Cell *11*, 1673-1683.

Laterreur, N., Eschbach, S.H., Lafontaine, D.A., and Wellinger, R.J. (2013). A new telomerase RNA element that is critical for telomere elongation. Nucleic Acids Res *41*, 7713-7724.

Le, S., Moore, J.K., Haber, J.E., and Greider, C.W. (1999). RAD50 and RAD51 define two pathways that collaborate to maintain telomeres in the absence of telomerase. Genetics *152*, 143-152.

Lebo, K.J., and Zappulla, D.C. (2012). Stiffened yeast telomerase RNA supports RNP function in vitro and in vivo. RNA *18*, 1666-1678.

Lee, J., Mandell, E.K., Rao, T., Wuttke, D.S., and Lundblad, V. (2010). Investigating the role of the Est3 protein in yeast telomere replication. Nucleic Acids Res *38*, 2279-2290.

Lee, J., Mandell, E.K., Tucey, T.M., Morris, D.K., and Lundblad, V. (2008). The Est3 protein associates with yeast telomerase through an OB-fold domain. Nat Struct Mol Biol *15*, 990-997.

Lendvay, T.S., Morris, D.K., Sah, J., Balasubramanian, B., and Lundblad, V. (1996). Senescence mutants of Saccharomyces cerevisiae with a defect in telomere replication identify three additional EST genes. Genetics *144*, 1399-1412.

Leung, A.K., Nagai, K., and Li, J. (2011). Structure of the spliceosomal U4 snRNP core domain and its implication for snRNP biogenesis. Nature *473*, 536-539.

Levy, M.Z., Allsopp, R.C., Futcher, A.B., Greider, C.W., and Harley, C.B. (1992). Telomere end-replication problem and cell aging. J Mol Biol *225*, 951-960.

Li, B., and Lustig, A.J. (1996). A novel mechanism for telomere size control in Saccharomyces cerevisiae. Genes Dev *10*, 1310-1326.

Lin, J., Ly, H., Hussain, A., Abraham, M., Pearl, S., Tzfati, Y., Parslow, T.G., and Blackburn, E.H. (2004). A universal telomerase RNA core structure includes structured motifs required for binding the telomerase reverse transcriptase protein. Proc Natl Acad Sci U S A *101*, 14713-14718.

Lingner, J., Cech, T.R., Hughes, T.R., and Lundblad, V. (1997a). Three Ever Shorter Telomere (EST) genes are dispensable for in vitro yeast telomerase activity. Proc Natl Acad Sci U S A *94*, 11190-11195.

Lingner, J., Hughes, T.R., Shevchenko, A., Mann, M., Lundblad, V., and Cech, T.R. (1997b). Reverse transcriptase motifs in the catalytic subunit of telomerase. Science *276*, 561-567.

Liti, G., Haricharan, S., Cubillos, F.A., Tierney, A.L., Sharp, S., Bertuch, A.A., Parts, L., Bailes, E., and Louis, E.J. (2009). Segregating YKU80 and TLC1 alleles underlying natural variation in telomere properties in wild yeast. PLoS Genet *5*, e1000659.

Livengood, A.J., Zaug, A.J., and Cech, T.R. (2002). Essential regions of Saccharomyces cerevisiae telomerase RNA: separate elements for Est1p and Est2p interaction. Mol Cell Biol *22*, 2366-2374.

Longtine, M.S., McKenzie, A., 3rd, Demarini, D.J., Shah, N.G., Wach, A., Brachat, A., Philippsen, P., and Pringle, J.R. (1998). Additional modules for versatile and economical PCR-based gene deletion and modification in Saccharomyces cerevisiae. Yeast *14*, 953-961.

Lubin, J.W., Tucey, T.M., and Lundblad, V. (2012). The interaction between the yeast telomerase RNA and the Est1 protein requires three structural elements. RNA *18*, 1597-1604.

Lundblad, V., and Blackburn, E.H. (1993). An alternative pathway for yeast telomere maintenance rescues est1- senescence. Cell *73*, 347-360.

Lundblad, V., and Szostak, J.W. (1989). A mutant with a defect in telomere elongation leads to senescence in yeast. Cell *57*, 633-643.

Luo, K., Vega-Palas, M.A., and Grunstein, M. (2002). Rap1-Sir4 binding independent of other Sir, yKu, or histone interactions initiates the assembly of telomeric heterochromatin in yeast. Genes Dev *16*, 1528-1539.

Mason, D.X., Goneska, E., and Greider, C.W. (2003). Stem-loop IV of tetrahymena telomerase RNA stimulates processivity in trans. Mol Cell Biol *23*, 5606-5613.

Mastroianni, A.J., Sivak, D.A., Geissler, P.L., and Alivisatos, A.P. (2009). Probing the conformational distributions of subpersistence length DNA. Biophys J *97*, 1408-1417.

McClintock, B. (1942). The Fusion of Broken Ends of Chromosomes Following Nuclear Fusion. Proc Natl Acad Sci U S A *28*, 458-463.

McCormick-Graham, M., and Romero, D.P. (1995). Ciliate telomerase RNA structural features. Nucleic Acids Res *23*, 1091-1097.

McEachern, M.J., and Blackburn, E.H. (1996). Cap-prevented recombination between terminal telomeric repeat arrays (telomere CPR) maintains telomeres in Kluyveromyces lactis lacking telomerase. Genes Dev *10*, 1822-1834.

Mefford, M.A., Rafiq, Q., and Zappulla, D.C. (2013). RNA connectivity requirements between conserved elements in the core of the yeast telomerase RNP. EMBO J *32*, 2980-2993.

Miller, M.C., and Collins, K. (2002). Telomerase recognizes its template by using an adjacent RNA motif. Proc Natl Acad Sci U S A *99*, 6585-6590.

Mitchell, J.R., and Collins, K. (2000). Human telomerase activation requires two independent interactions between telomerase RNA and telomerase reverse transcriptase. Mol Cell *6*, 361-371.

Mitton-Fry, R.M., Anderson, E.M., Hughes, T.R., Lundblad, V., and Wuttke, D.S. (2002). Conserved structure for single-stranded telomeric DNA recognition. Science *296*, 145-147.

Moore, P.B., and Steitz, T.A. (2002). The involvement of RNA in ribosome function. Nature *418*, 229-235.

Mozdy, A.D., and Cech, T.R. (2006). Low abundance of telomerase in yeast: implications for telomerase haploinsufficiency. RNA *12*, 1721-1737.

Mumberg, D., Muller, R., and Funk, M. (1995). Yeast vectors for the controlled expression of heterologous proteins in different genetic backgrounds. Gene *156*, 119-122.

Nakamura, T.M., and Cech, T.R. (1998). Reversing time: origin of telomerase. Cell *92*, 587-590.

Nakayashiki, H., Kadotani, N., and Mayama, S. (2006). Evolution and diversification of RNA silencing proteins in fungi. J Mol Evol *63*, 127-135.

Noel, J.F., Larose, S., Abou Elela, S., and Wellinger, R.J. (2012). Budding yeast telomerase RNA transcription termination is dictated by the Nrd1/Nab3 non-coding RNA termination pathway. Nucleic Acids Res *40*, 5625-5636.

Nugent, C.I., Hughes, T.R., Lue, N.F., and Lundblad, V. (1996). Cdc13p: a single-strand telomeric DNA-binding protein with a dual role in yeast telomere maintenance. Science *274*, 249-252.

Olovnikov, A.M. (1973). A theory of marginotomy. The incomplete copying of template margin in enzymic synthesis of polynucleotides and biological significance of the phenomenon. J Theor Biol *41*, 181-190.

Osterhage, J.L., Talley, J.M., and Friedman, K.L. (2006). Proteasome-dependent degradation of Est1p regulates the cell cycle-restricted assembly of telomerase in Saccharomyces cerevisiae. Nat Struct Mol Biol *13*, 720-728.

Pang, K.C., Frith, M.C., and Mattick, J.S. (2006). Rapid evolution of noncoding RNAs: lack of conservation does not mean lack of function. Trends Genet *22*, 1-5.

Penny, G.D., Kay, G.F., Sheardown, S.A., Rastan, S., and Brockdorff, N. (1996). Requirement for Xist in X chromosome inactivation. Nature *379*, 131-137.

Peterson, S.E., Stellwagen, A.E., Diede, S.J., Singer, M.S., Haimberger, Z.W., Johnson, C.O., Tzoneva, M., and Gottschling, D.E. (2001). The function of a stem-loop in telomerase RNA is linked to the DNA repair protein Ku. Nat Genet *27*, 64-67.

Pfingsten, J.S., Goodrich, K.J., Taabazuing, C., Ouenzar, F., Chartrand, P., and Cech, T.R. (2012). Mutually exclusive binding of telomerase RNA and DNA by ku alters telomerase recruitment model. Cell *148*, 922-932.

Popenda, M., Szachniuk, M., Antczak, M., Purzycka, K.J., Lukasiak, P., Bartol, N., Blazewicz, J., and Adamiak, R.W. (2012). Automated 3D structure composition for large RNAs. Nucleic Acids Res *40*, e112.

Prescott, J., and Blackburn, E.H. (1997). Telomerase RNA mutations in Saccharomyces cerevisiae alter telomerase action and reveal nonprocessivity in vivo and in vitro. Genes Dev *11*, 528-540.

Putnam, C.D., Jaehnig, E.J., and Kolodner, R.D. (2009). Perspectives on the DNA damage and replication checkpoint responses in Saccharomyces cerevisiae. DNA Repair (Amst) *8*, 974-982.

Qi, H., and Zakian, V.A. (2000). The Saccharomyces telomere-binding protein Cdc13p interacts with both the catalytic subunit of DNA polymerase alpha and the telomerase-associated est1 protein. Genes Dev *14*, 1777-1788.

Qi, X., Li, Y., Honda, S., Hoffmann, S., Marz, M., Mosig, A., Podlevsky, J.D., Stadler, P.F., Selker, E.U., and Chen, J.J. (2013). The common ancestral core of vertebrate and fungal telomerase RNAs. Nucleic Acids Res *41*, 450-462.

Qiao, F., and Cech, T.R. (2008). Triple-helix structure in telomerase RNA contributes to catalysis. Nat Struct Mol Biol *15*, 634-640.

Rao, T., Lubin, J.W., Armstrong, G.S., Tucey, T.M., Lundblad, V., and Wuttke, D.S. (2014). Structure of Est3 reveals a bimodal surface with differential roles in telomere replication. Proc Natl Acad Sci U S A *111*, 214-218.

Russo, P., and Sherman, F. (1989). Transcription terminates near the poly(A) site in the CYC1 gene of the yeast Saccharomyces cerevisiae. Proc Natl Acad Sci U S A *86*, 8348-8352.

Sabourin, M., Tuzon, C.T., Fisher, T.S., and Zakian, V.A. (2007). A flexible protein linker improves the function of epitope-tagged proteins in Saccharomyces cerevisiae. Yeast *24*, 39-45.

Sauerwald, A., Sandin, S., Cristofari, G., Scheres, S.H., Lingner, J., and Rhodes, D. (2013). Structure of active dimeric human telomerase. Nat Struct Mol Biol *20*, 454-460.

Seto, A.G., Livengood, A.J., Tzfati, Y., Blackburn, E.H., and Cech, T.R. (2002). A bulged stem tethers Est1p to telomerase RNA in budding yeast. Genes Dev *16*, 2800-2812.

Seto, A.G., Umansky, K., Tzfati, Y., Zaug, A.J., Blackburn, E.H., and Cech, T.R. (2003). A template-proximal RNA paired element contributes to Saccharomyces cerevisiae telomerase activity. RNA *9*, 1323-1332.

Seto, A.G., Zaug, A.J., Sobel, S.G., Wolin, S.L., and Cech, T.R. (1999). Saccharomyces cerevisiae telomerase is an Sm small nuclear ribonucleoprotein particle. Nature *401*, 177-180.

Shay, J.W., and Bacchetti, S. (1997). A survey of telomerase activity in human cancer. Eur J Cancer *33*, 787-791.

Shcherbakova, D.M., Sokolov, K.A., Zvereva, M.I., and Dontsova, O.A. (2009). Telomerase from yeast Saccharomyces cerevisiae is active in vitro as a monomer. Biochemistry (Mosc) *74*, 749-755.

Shi, T., Bunker, R.D., Mattarocci, S., Ribeyre, C., Faty, M., Gut, H., Scrima, A., Rass, U., Rubin, S.M., Shore, D.*, et al.* (2013). Rif1 and Rif2 shape telomere function and architecture through multivalent Rap1 interactions. Cell *153*, 1340-1353.

Shippen-Lentz, D., and Blackburn, E.H. (1990). Functional evidence for an RNA template in telomerase. Science *247*, 546-552.

Singer, M.S., and Gottschling, D.E. (1994). TLC1: template RNA component of Saccharomyces cerevisiae telomerase. Science *266*, 404-409.

Stellwagen, A.E., Haimberger, Z.W., Veatch, J.R., and Gottschling, D.E. (2003). Ku interacts with telomerase RNA to promote telomere addition at native and broken chromosome ends. Genes Dev *17*, 2384-2395.

Stone, M.D., Mihalusova, M., O'Connor C, M., Prathapam, R., Collins, K., and Zhuang, X. (2007). Stepwise protein-mediated RNA folding directs assembly of telomerase ribonucleoprotein. Nature *446*, 458-461.

Szostak, J.W., and Blackburn, E.H. (1982). Cloning yeast telomeres on linear plasmid vectors. Cell *29*, 245-255.

Taggart, A.K., Teng, S.C., and Zakian, V.A. (2002). Est1p as a cell cycle-regulated activator of telomere-bound telomerase. Science *297*, 1023-1026.

Tang, W., Kannan, R., Blanchette, M., and Baumann, P. (2012). Telomerase RNA biogenesis involves sequential binding by Sm and Lsm complexes. Nature.

ten Dam, E., van Belkum, A., and Pleij, K. (1991). A conserved pseudoknot in telomerase RNA. Nucleic Acids Res *19*, 6951.

Teng, S.C., and Zakian, V.A. (1999). Telomere-telomere recombination is an efficient bypass pathway for telomere maintenance in Saccharomyces cerevisiae. Mol Cell Biol *19*, 8083-8093.

Tesmer, V.M., Ford, L.P., Holt, S.E., Frank, B.C., Yi, X., Aisner, D.L., Ouellette, M., Shay, J.W., and Wright, W.E. (1999). Two inactive fragments of the integral RNA cooperate to assemble active telomerase with the human protein catalytic subunit (hTERT) in vitro. Mol Cell Biol *19*, 6207-6216.

Theimer, C.A., and Feigon, J. (2006). Structure and function of telomerase RNA. Curr Opin Struct Biol *16*, 307-318.

Ting, N.S., Yu, Y., Pohorelic, B., Lees-Miller, S.P., and Beattie, T.L. (2005). Human Ku70/80 interacts directly with hTR, the RNA component of human telomerase. Nucleic Acids Res *33*, 2090-2098.

Tsai, M.C., Manor, O., Wan, Y., Mosammaparast, N., Wang, J.K., Lan, F., Shi, Y., Segal, E., and Chang, H.Y. (2010). Long noncoding RNA as modular scaffold of histone modification complexes. Science *329*, 689-693.

Tucey, T.M., and Lundblad, V. (2013). A yeast telomerase complex containing the Est1 recruitment protein is assembled early in the cell cycle. Biochemistry *52*, 1131-1133.

Tuzon, C.T., Wu, Y., Chan, A., and Zakian, V.A. (2011). The Saccharomyces cerevisiae telomerase subunit Est3 binds telomeres in a cell cycle- and Est1-dependent manner and interacts directly with Est1 in vitro. PLoS Genet *7*, e1002060.

Tzfati, Y., Fulton, T.B., Roy, J., and Blackburn, E.H. (2000). Template boundary in a yeast telomerase specified by RNA structure. Science *288*, 863-867.

Tzfati, Y., Knight, Z., Roy, J., and Blackburn, E.H. (2003). A novel pseudoknot element is essential for the action of a yeast telomerase. Genes Dev *17*, 1779-1788.

Vafabakhsh, R., and Ha, T. (2012). Extreme bendability of DNA less than 100 base pairs long revealed by single-molecule cyclization. Science *337*, 1097-1101.

Verschoor, A., Warner, J.R., Srivastava, S., Grassucci, R.A., and Frank, J. (1998). Three-dimensional structure of the yeast ribosome. Nucleic Acids Res *26*, 655-661.

Walker, J.R., Corpina, R.A., and Goldberg, J. (2001). Structure of the Ku heterodimer bound to DNA and its implications for double-strand break repair. Nature *412*, 607-614.

Wang, K.C., and Chang, H.Y. (2011). Molecular mechanisms of long noncoding RNAs. Mol Cell *43*, 904-914.

Wang, K.C., Yang, Y.W., Liu, B., Sanyal, A., Corces-Zimmerman, R., Chen, Y., Lajoie, B.R., Protacio, A., Flynn, R.A., Gupta, R.A*., et al.* (2011). A long noncoding RNA maintains active chromatin to coordinate homeotic gene expression. Nature *472*, 120-124.

Wang, S.S., and Zakian, V.A. (1990). Sequencing of Saccharomyces telomeres cloned using T4 DNA polymerase reveals two domains. Mol Cell Biol *10*, 4415-4419.

Waterhouse, A.M., Procter, J.B., Martin, D.M., Clamp, M., and Barton, G.J. (2009). Jalview Version 2--a multiple sequence alignment editor and analysis workbench. Bioinformatics *25*, 1189-1191.

Webb, C.J., and Zakian, V.A. (2012). Schizosaccharomyces pombe Ccq1 and TER1 bind the 14-3-3-like domain of Est1, which promotes and stabilizes telomerase-telomere association. Genes Dev *26*, 82-91.

Weinert, T.A., and Hartwell, L.H. (1988). The RAD9 gene controls the cell cycle response to DNA damage in Saccharomyces cerevisiae. Science *241*, 317-322.

Weinrich, S.L., Pruzan, R., Ma, L., Ouellette, M., Tesmer, V.M., Holt, S.E., Bodnar, A.G., Lichtsteiner, S., Kim, N.W., Trager, J.B.*, et al.* (1997). Reconstitution of human telomerase with the template RNA component hTR and the catalytic protein subunit hTRT. Nat Genet *17*, 498-502.

Wenz, C., Enenkel, B., Amacker, M., Kelleher, C., Damm, K., and Lingner, J. (2001). Human telomerase contains two cooperating telomerase RNA molecules. EMBO J *20*, 3526-3534.

Wiggins, P.A., and Nelson, P.C. (2006). Generalized theory of semiflexible polymers. Phys Rev E Stat Nonlin Soft Matter Phys *73*, 031906.

Wiggins, P.A., van der Heijden, T., Moreno-Herrero, F., Spakowitz, A., Phillips, R., Widom, J., Dekker, C., and Nelson, P.C. (2006). High flexibility of DNA on short length scales probed by atomic force microscopy. Nat Nanotechnol *1*, 137-141.

Wu, Y., and Zakian, V.A. (2011). The telomeric Cdc13 protein interacts directly with the telomerase subunit Est1 to bring it to telomeric DNA ends in vitro. Proc Natl Acad Sci U S A *108*, 20362-20369.

Zacharias, M., and Hagerman, P.J. (1996). The influence of symmetric internal loops on the flexibility of RNA. J Mol Biol *257*, 276-289.

Zappulla, D.C., and Cech, T.R. (2004). Yeast telomerase RNA: a flexible scaffold for protein subunits. Proc Natl Acad Sci U S A *101*, 10024-10029.

Zappulla, D.C., and Cech, T.R. (2006). RNA as a flexible scaffold for proteins: yeast telomerase and beyond. Cold Spring Harb Symp Quant Biol *71*, 217-224.

Zappulla, D.C., Goodrich, K., and Cech, T.R. (2005). A miniature yeast telomerase RNA functions in vivo and reconstitutes activity in vitro. Nat Struct Mol Biol *12*, 1072-1077.

Zappulla, D.C., Goodrich, K.J., Arthur, J.R., Gurski, L.A., Denham, E.M., Stellwagen, A.E., and Cech, T.R. (2011). Ku can contribute to telomere lengthening in yeast at multiple positions in the telomerase RNP. RNA *17*, 298-311.

Zappulla, D.C., Roberts, J.N., Goodrich, K.J., Cech, T.R., and Wuttke, D.S. (2009). Inhibition of yeast telomerase action by the telomeric ssDNA-binding protein, Cdc13p. Nucleic Acids Res *37*, 354-367.

Zhang, Q., Kim, N.K., Peterson, R.D., Wang, Z., and Feigon, J. (2010). Structurally conserved five nucleotide bulge determines the overall topology of the core domain of human telomerase RNA. Proc Natl Acad Sci U S A *107*, 18761-18768.

Zuker, M. (2003). Mfold web server for nucleic acid folding and hybridization prediction. Nucleic Acids Res *31*, 3406-3415.

Zuker, M., and Jacobson, A.B. (1998). Using reliability information to annotate RNA secondary structures. RNA *4*, 669-679.

CURRICULUM VITAE:

Kevin J. Lebo

Department of Biology
Johns Hopkins University
Baltimore, MD 21218
(410) 516-7316 (L), (201) 981-1327 (C)
KevinLebo@jhu.edu

EDUCATION:

2008–2014 **Ph.D., Cellular, Molecular, Developmental Biology and Biophysics**
Johns Hopkins University, Baltimore, Maryland

2004–2008 **B.S., Biochemistry**
Boston College, Chestnut Hill, Massachusetts

RESEARCH EXPERIENCE:

2009–2014 **Ph.D. Thesis Research – Advisor: Dr. David C. Zappulla**
Department of Biology
Johns Hopkins University, Baltimore, MD
Research focus: *S. cerevisiae* telomerase RNA structure and function

2007–2008 **Undergraduate Research – Advisor: Dr. Jianmin Gao**
Department of Chemistry
Boston College, Chestnut Hill, MA
Research focus: Driving forces of peptide aggregation

2006, Spring **Undergraduate Research – Advisor: Dr. Amir H. Hoveyda**
Department of Chemistry
Boston College, Chestnut Hill, MA
Research focus: Enantioselective conjugate addition

PUBLICATIONS:

Kevin J. Lebo and David C. Zappulla. (2012) Stiffened yeast telomerase RNA supports RNP function *in vitro* and *in vivo*. *RNA 18*, 1666-1678

Kevin J. Lebo, Rachel O. Niederer, and David C. Zappulla. A second essential function of the Est1-binding arm of yeast telomerase RNA. *(Under Review at* Cell Reports*)*

Kevin J. Lebo and David C. Zappulla. Synthetic design of a more stably folding TLC1 RNA that functions *in vivo* and *in vitro*. *(In preparation)*

Kevin J. Lebo, Caitlyn E. Cennamo, and David C. Zappulla. Identification of RNA abundance-regulating elements in the terminal arm of yeast telomerase RNA. *(In preparation)*

CONFERENCES AND COLLOQUIA:

2013 **"Telomeres and Telomerase,"** Cold Spring Harbor Laboratory, Cold Spring Harbor, NY (**Talk**, selected from the abstracts)

2011 **"Telomeres and Telomerase,"** Cold Spring Harbor Laboratory, Cold Spring Harbor, NY (Poster presentation)

2010 **"Telomerase and Retrotransposons: Reverse Transcriptases that Shaped Genomes,"** National Academy of Sciences Arthur M. Sackler Colloquium, Irvine, CA (Poster presentation)

2009−2013 **Annual Biology Department Retreats** (Johns Hopkins University) St. Michaels, MD and Flintstone, MD (Poster presentations each year)

AWARDS AND RECOGNITION:

2013, Fall **Johns Hopkins CMDB graduate program's nominee for the Harold M. Weintraub Graduate Student Award**, Fred Hutchinson Cancer Research Center, Seattle, WA

2013, Fall **Poster Presentation Award**, CMDB Graduate Program retreat, Johns Hopkins University, Baltimore, MD

2010, Fall **Merit-based travel award** for attendance at National Academy of Sciences Telomerase and Retrotransposons meeting, Irvine, CA

2010, Spring **DuPont Teaching Award** for contributions to Cell Biology Laboratory, Department of Biology, Johns Hopkins University, Baltimore, MD

TEACHING EXPERIENCE:

2013, Fall **Teaching Assistant**, "Advanced Molecular Biology" graduate course, Department of Biology, Johns Hopkins University, Baltimore, MD

2012–2014 **Teaching Assistant**, Biochemistry (Fall 2012) and Cell Biology (Spring 2013 and 2014) courses, Department of Biology, Johns Hopkins University, Baltimore, MD

2009-2010 **Laboratory Teaching Assistant**, Biochemistry (18 students; Fall 2009) and Cell Biology (15 students; Spring 2010) Laboratory, Department of Biology, Johns Hopkins University, Baltimore, MD